

DYNAMIC MODELING, SIMULATION AND CONTROL
OF A SMALL WIND-FUEL CELL HYBRID ENERGY
SYSTEM FOR STAND-ALONE APPLICATIONS

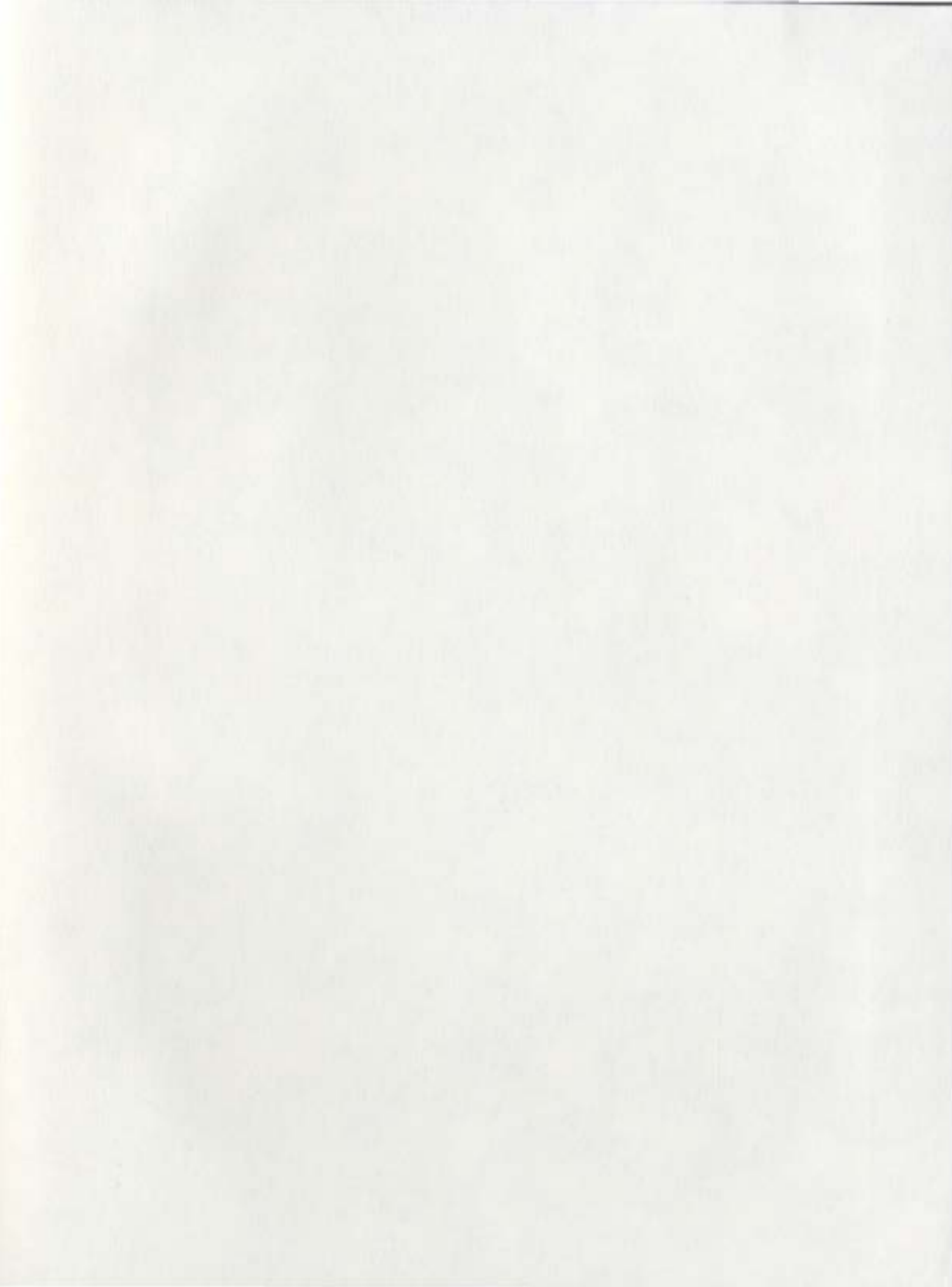
CENTRE FOR NEWFOUNDLAND STUDIES

TOTAL OF 10 PAGES ONLY
MAY BE XEROXED

(With Author's Permission)

MOHAMMAD JAHANGIR ALAM KHAN





DYNAMIC MODELING, SIMULATION AND CONTROL OF A
SMALL WIND-FUEL CELL HYBRID ENERGY SYSTEM
FOR STAND-ALONE APPLICATIONS

by

© Mohammad Jahangir Alam Khan

A thesis submitted to the School of Graduate Studies
in partial fulfillment of the requirements for the
degree of Master of Engineering

Faculty of Engineering and Applied Science
Memorial University of Newfoundland

June 2004

St. John's

Newfoundland

Canada



Library and
Archives Canada

Bibliothèque et
Archives Canada

Published Heritage
Branch

Direction du
Patrimoine de l'édition

395 Wellington Street
Ottawa ON K1A 0N4
Canada

395, rue Wellington
Ottawa ON K1A 0N4
Canada

Your file *Votre référence*

ISBN: 0-494-02350-3

Our file *Notre référence*

ISBN: 0-494-02350-3

NOTICE:

The author has granted a non-exclusive license allowing Library and Archives Canada to reproduce, publish, archive, preserve, conserve, communicate to the public by telecommunication or on the Internet, loan, distribute and sell theses worldwide, for commercial or non-commercial purposes, in microform, paper, electronic and/or any other formats.

The author retains copyright ownership and moral rights in this thesis. Neither the thesis nor substantial extracts from it may be printed or otherwise reproduced without the author's permission.

AVIS:

L'auteur a accordé une licence non exclusive permettant à la Bibliothèque et Archives Canada de reproduire, publier, archiver, sauvegarder, conserver, transmettre au public par télécommunication ou par l'Internet, prêter, distribuer et vendre des thèses partout dans le monde, à des fins commerciales ou autres, sur support microforme, papier, électronique et/ou autres formats.

L'auteur conserve la propriété du droit d'auteur et des droits moraux qui protègent cette thèse. Ni la thèse ni des extraits substantiels de celle-ci ne doivent être imprimés ou autrement reproduits sans son autorisation.

In compliance with the Canadian Privacy Act some supporting forms may have been removed from this thesis.

Conformément à la loi canadienne sur la protection de la vie privée, quelques formulaires secondaires ont été enlevés de cette thèse.

While these forms may be included in the document page count, their removal does not represent any loss of content from the thesis.

Bien que ces formulaires aient inclus dans la pagination, il n'y aura aucun contenu manquant.


Canada

To My Parents

Abstract

In this thesis, a detailed analysis of a wind-fuel cell hybrid energy system for stand-alone applications is carried out. Initially, a pre-feasibility study for such a system is conducted and for a given load, the sizes of various components are determined. Dynamic models of these components are developed based on empirical and physical relationships. The hybrid system is then integrated and simulated for investigating the transient behaviors during sudden load variation, wind speed change and hydrogen pressure drop. Optimization software tool HOMER is used for the pre-feasibility study and MATLAB-Simulink[®] is employed for dynamic system modeling. Finally, results of this analysis are summarized and scope for future works are indicated.

Acknowledgements

The author wishes to thank the Faculty of Engineering and Applied Science for providing the opportunity and necessary support towards completion of this work. In particular, the advice, guidance and support of Dr. M. T. Iqbal and his suggestion of a challenging research topic is gratefully acknowledged. The author is appreciative to Dr. J. E. Quaiocoe, Dr. B. Jeyasurya, Dr. V. Masek, and Dr. M. A. Rahman for their continued interest and encouragement. The administrative cooperation of Ms. Moya Crocker is also highly appreciated.

The author is thankful for the financial supports in the forms of (1) School of Graduate Studies Fellowship (2) Natural Sciences and Engineering Research Council (NSERC) Grant through Dr. M. T. Iqbal, and (3) Faculty of Engineering and Applied Sciences teaching assistantship duties.

The author appreciates the Meteorological Service of Canada's - Atlantic Climate Centre for providing wind and solar data recorded at St. John's airport.

A special word of thanks goes to the author's wife Sadia for her loving, caring and painstaking support. Finally, the Supreme Being is gratefully remembered for bestowing all the courage and strength throughout the course of this work.

Table of Contents

Abstract			i
Acknowledgements			ii
Table of Contents			iii
List of Tables			vii
List of Figures			viii
List of Abbreviations			xi
List of Symbols			xiii
Chapter	1	Introduction	1
	1.1	Research Rationale	3
	1.2	Literature Review	3
	1.3	Scope of Thesis	7
	1.4	Thesis Organization	9
Chapter	2	Pre-feasibility Study of Hybrid Energy System	10
	2.1	Hybrid Energy System	11
	2.1.1	Electrical load	12
	2.1.2	Renewable Resources	14
	2.1.2.1	Wind Energy Resource	14
	2.1.2.2	Solar Energy Resource	15
	2.1.3	Hybrid System Energy Components	15
	2.1.3.1	Diesel Generator	17
	2.1.3.2	Photovoltaic Array	17

	2.1.3.3	Wind Energy Conversion System (WECS)	18
	2.1.3.4	Fuel Cell System	19
	2.1.3.5	Electrolyzer	20
	2.1.3.6	Battery	20
	2.1.3.7	Power Converter	21
	2.1.4	Economics and Constraints	22
2.2		Sensitivity Results	22
2.3		Optimization results	28
2.4		Summary	31
Chapter	3	Modeling of Wind-Fuel Cell Hybrid Energy System	33
3.1		Wind Energy Conversion Systems (WECS)	34
	3.1.1	Small WECS Systems	36
	3.1.2	Small WECS Model Formulation	39
		3.1.2.1 Wind Field	41
		3.1.2.2 Rotor Aerodynamics	42
		3.1.2.2.1 Spatial Filtering	42
		3.1.2.2.2 Induction Lag	43
		3.1.2.3 Permanent Magnet DC Generator	44
	3.1.3	Controller Design	45
		3.1.3.1 Determination of Reference Rotor Speed	46
		3.1.3.2 Design of Fuzzy Logic Controller	49
	3.1.4	Summary	52
3.2		Fuel Cell System	53
	3.2.1	PEM Fuel Cell Systems	55
	3.2.2	PEM Fuel Cell Model Formulation	58
		3.2.2.1 Electrochemical Model	58
		3.2.2.1.1 Thermodynamic Potential	60
		3.2.2.1.2 Activation Overvoltage	61
		3.2.2.1.3 Ohmic Overvoltage	63

	3.2.2.2	Thermal Model	65
	3.2.2.3	Reactant Flow Model	69
	3.2.2.4	Air Flow Controller	72
	3.2.3	Summary	73
3.3		Electrolyzer	73
	3.3.1	Alkaline Electrolyzer Systems	74
	3.3.2	Alkaline Electrolyzer System Model Formulation	76
	3.3.2.1	Electrochemical Model	76
	3.3.2.2	Thermal Model	79
	3.3.3	Summary	82
3.4		Power Converter	83
	3.4.1	Power Converter Model Formulation	83
	3.4.1.1	WECS Buck-Boost Converter	84
	3.4.1.2	Fuel Cell Boost Converter	85
	3.4.1.3	Electrolyzer Converter	86
	3.4.1.4	Load Inverter	87
	3.4.2	Summary	89
3.5		System Integration	90
Chapter 4		System Integration and Simulation	93
	4.1	WECS Model	95
	4.2	PEM Fuel Cell System Model	95
	4.3	Electrolyzer Model	96
	4.4	Power Converter Model	97
	4.5	System Integration	97
Chapter 5		Results and Discussion	98
	5.1	Simulation with Randomly Varying Wind Component	99
	5.2	Simulation with Step Inputs	102
	5.3	Summary	109
Chapter 6		Conclusions	110

6.1	General Summary	110
6.2	Contributions	111
6.3	Conclusions	112
6.4	Further work	113
References		115
Appendix A: MATLAB-Simulink® Subsystem Blocks		130
Appendix B: List of Research Papers Based on this Research		137

List of Tables

Table 2.1:	Wind data for St. John's Airport	14
Table 2.2:	Search space alternatives	22
Table 3.1:	Hybrid energy system component sizes and models	33
Table 3.2:	Typical aspects of small and large WECS	35
Table 3.3:	Small wind turbine design parameters (BWC Excel-R type)	38
Table 3.4:	Small wind turbine model parameters	42
Table 3.5:	Fuzzy associative memory (FAM)	51
Table 3.6:	Fuel cell stack design parameters (Ballard MK5-E type)	57
Table 3.7:	Fuel cell model parameters	64
Table 3.8:	Parameters for the thermal model of Ballard MK5-E type system	68
Table 3.9:	Parameters for the reactant flow models	71
Table 3.10:	Alkaline electrolyzer design parameters (PHOEBUS type).	76
Table 3.11:	Electrolyzer electrochemical model parameters	79
Table 3.12:	Parameters for the thermal model of electrolyzer stack	82
Table 3.13:	Power converter parameters	89
Table 5.1:	Simulation event chart	99

List of Figures

Figure 1.1:	Transforming the global energy mix: The exemplary path until 2050/2100, German Advisory Council on Global Change (WBGU)	1
Figure 1.2:	Conceptual block diagram of a wind-fuel cell hybrid energy system	7
Figure 2.1:	General scheme of a stand-alone hybrid power system	11
Figure 2.2:	HOMER implementation of the hybrid energy system	12
Figure 2.3:	Daily load profile for a year	13
Figure 2.4:	Wind speed probability distribution function	15
Figure 2.5:	Average hourly wind speed for one year	15
Figure 2.6:	Average daily solar irradiation	16
Figure 2.7:	Diesel generator cost curves	17
Figure 2.8:	Cost of photovoltaic units	18
Figure 2.9:	BWC Excel-R Cost curves	18
Figure 2.10:	Fuel cell cost curves	19
Figure 2.11:	Electrolyzer cost curves	20
Figure 2.12:	Cost of battery	21
Figure 2.13:	Converter cost curves	21
Figure 2.14:	OST with diesel price = \$0.35/L and FC cost = 100%	24
Figure 2.15:	OST with diesel price = \$0.65/L and FC cost = 100%	24
Figure 2.16:	OST with diesel price = \$0.35/L and FC cost = 65%	25
Figure 2.17:	OST with diesel price = \$0.35/L and FC cost = 15%	26
Figure 2.18:	OST with solar irradiation = 3.15 kWh/m ² /d and wind speed = 6.64 m/s	27

Figure 2.19:	OST with solar irradiation = 3.15 kWh/m ² /d and diesel price = \$0.35/L	27
Figure 2.20:	Optimization results for wind speed = 6.64m/s, solar irradiation = 3.15 kWh/m ² /d, and diesel price = \$0.35/L	28
Figure 2.21:	Wind-fuel cell system cost analysis (HOMER Screenshot)	29
Figure 2.22:	Primary load and unmet load	30
Figure 2.23:	Wind power and fuel cell power	30
Figure 3.1:	Diversity of wind turbine design concepts	34
Figure 3.2:	Power curve and furling mechanism	37
Figure 3.3:	Power curve of BWC Excel-R type wind turbine	39
Figure 3.4:	Small WECS in a hybrid application	40
Figure 3.5:	Equivalent circuit of a permanent magnet DC generator	44
Figure 3.6:	Rotor torque and reference rotor speed	48
Figure 3.7:	Fuzzy variables and membership functions	51
Figure 3.8:	Fuzzy rule surface view	52
Figure 3.9:	Single PEM fuel cell cross sections	55
Figure 3.10:	Reactions in anode and cathode	55
Figure 3.11:	Schematic of PEM fuel cell system (Ballard MK5-E type)	57
Figure 3.12:	Polarization curve of a PEM fuel cell	59
Figure 3.13:	Circuit model of a single cell	62
Figure 3.14:	Energy balance model for a PEM fuel cell stack	66
Figure 3.15:	Single cell reaction in an alkaline electrolyzer	74
Figure 3.16:	Schematic of an electrolyzer system	75
Figure 3.17:	Current-voltage characteristics of an electrolyzer cell	77
Figure 3.18:	Efficiency parameters of an electrolyzer stack	78
Figure 3.19:	Electrolyzer energy balance	80
Figure 3.20:	Power converters in wind-fuel cell hybrid energy system	84
Figure 3.21:	Inverter load arrangement	87
Figure 3.22:	Hybrid energy system interconnections	90

Figure 3.23:	Flow chart of power flow controller	91
Figure 4.1:	MATLAB-Simulink [®] Implementation of Wind-Fuel cell hybrid energy systems	94
Figure 5.1:	Power balance under randomly varying wind	100
Figure 5.2:	Hydrogen consumption and production	101
Figure 5.3:	Power conversion at the load	101
Figure 5.4:	Wind energy converter performance	103
Figure 5.5:	Power balance with step changes in inputs	104
Figure 5.6:	Fuel cell system performance	105
Figure 5.7:	Electrolyzer performance	107
Figure 5.8:	Power converter performance	108
Figure A.1:	Subsystem ' <i>SS: Wind Field</i> '	130
Figure A.2:	Subsystem ' <i>SS: Aerodynamics</i> '	130
Figure A.3:	Subsystem ' <i>SS: PMDC Gen</i> '	131
Figure A.4:	Subsystem ' <i>SS: WT Controller</i> '	131
Figure A.5:	Subsystem ' <i>SS: Fuel Cell</i> '	132
Figure A.6:	Subsystem ' <i>SS: Fuel Cell Energy Balance</i> '	132
Figure A.7:	Subsystem ' <i>SS: Anode H2 Flow</i> '	133
Figure A.8:	Subsystem ' <i>SS: Cathode O2 Flow</i> '	133
Figure A.9:	Subsystem ' <i>SS: Electrolyzer</i> '	133
Figure A.10:	Subsystem ' <i>SS: Electrolyzer Energy Balance</i> '	134
Figure A.11:	Subsystem ' <i>SS: Buck-boost</i> '	134
Figure A.12:	Subsystem ' <i>SS: Boost</i> '	134
Figure A.13:	Subsystem ' <i>SS: PWM Inverter</i> '	135
Figure A.14:	Subsystem ' <i>SS: LC Filter</i> '	135
Figure A.15:	Subsystem ' <i>SS: Inverter Controller</i> '	135
Figure A.16:	Subsystem ' <i>SS: R-L Load</i> '	136
Figure A.17:	Subsystem ' <i>SS: Power Controller</i> '	136

List of Abbreviations

AC	Alternating Current
BPR	Back Pressure Regulator
BWC	Bergey Wind Company
COE	Cost of Energy
DC	Direct Current
DOF	Degree Of Fulfillment
ERU	Energy Research Unit
FAM	Fuzzy Associative Memory
FLC	Fuzzy Logic Controller
GDL	Gas Diffusion Layer
HAWT	Horizontal Axis Wind Turbines
HES	Hybrid Energy System
HOMER	Hybrid Optimization Model for Electric Renewables
HRI	Hydrogen Research Institute
KOH	Potassium Hydroxide
LMTD	Log Mean Temperature Difference
MEA	Membrane-Electrode Assembly
NPC	Net Present Cost
NREL	National Renewable Energy Laboratory
OST	Optimal System Types
PD	Proportional Derivative
PEM	Polymer Electrolyte Membrane

PID	Proportional Integral Derivative
PMA	Permanent Magnet Alternator
PMDC	Permanent Magnet DC
PR	Pressure Regulator
PV	Photovoltaic
PWM	Pulse Width Modulated
slpm	Standard Liter Per Minute
SS	Subsystem
TRS	Tip Speed Ratio
VAWT	Vertical Axis Wind Turbine
WECS	Wind Energy Conversion System
WT	Wind Turbine

List of Symbols

Wind Energy Conversion System

<i>Symbol</i>	<i>Parameter</i>	<i>Unit</i>
β	Spatial filter empirical parameter	s
λ	Tip speed ratio (TSR)	-
λ_o	Optimum Tip speed ratio (TSR)	-
ω_r	Rotor speed	rad.s ⁻¹
ω_{ref}	Reference rotor speed	rad.s ⁻¹
ω_{ro}	Rated rotor speed	rad.s ⁻¹
ϕ	Magnetic flux	V.rad ⁻¹ .s ⁻¹
ϕ_d	Decay factor over blade surface	-
ρ	Air density	Kg.m ⁻³
τ_l	Induction lag time constant	s
a	Spatial filter empirical parameter	s ⁻¹
a_i	Induction lag empirical parameter	-
A_{wt}	Wind turbine blade swept area	m ²
B	Damping constant	N.m.rad.s ⁻¹
C_p	Power coefficient	-
C_{pb}	Betz constant	-
C_{po}	Optimum Power coefficient	-
C_t	Torque coefficient	-

E_a	DC generator induced voltage	V
I_a	DC generator armature current	A
J	Moment of inertia	Kg.m ²
K	Generator constant	-
k_T	WECS controller parameter (depends on C_{p0} and λ_0)	-
k_w	WECS controller parameter (depends k_T)	-
L_a	DC generator armature inductance	mH
m_{wind}	Random white noise (wind field)	m.s ⁻²
P_a	Extractable aerodynamic power	W
P_{dump}	Power dissipated in the dump load	W
P_{max_wt}	Wind turbine maximum power	W
P_{r_wt}	Wind turbine rated power	W
P_{wind}	Available power in the wind	W
P_{wt}	Effective power output of wind turbine	W
R_a	DC generator armature resistance	Ω
R_{dump}	Dump load	Ω
R_{wt}	Wind turbine rotor radius	m
t	Time	s
T_a	Actual rotor torque	N.m
T_a'	Estimated rotor torque	N.m
T_l	Load torque	N.m
T_{max}	Maximum rotor torque	N.m
T_r	Rated rotor torque	N.m
T_v	Wind field time constant	s
V_{avg}	Mean wind speed	m.s ⁻¹
V_{cutin}	Cut-in wind speed	m.s ⁻¹
V_{cutout}	Cut-out wind speed	m.s ⁻¹
V_{eff}	Effective wind speed	m.s ⁻¹
V_{filt}	Filtered wind speed	m.s ⁻¹

V_o	Median wind speed	m.s^{-1}
V_{rated}	Rated wind speed	m.s^{-1}
V_{surv}	Survival wind speed	m.s^{-1}
V_{to_wt}	Wind turbine rated terminal voltage	V
V_{turb}	Wind turbulence component	m.s^{-1}
V_{wf}	Wind field average wind speed	m.s^{-1}
V_{wind}	Actual wind speed	m.s^{-1}
V_{wt}	Wind turbine terminal voltage	V
z	Turbine hub height	m

Fuel Cell System

<i>Symbol</i>	<i>Parameter</i>	<i>Unit</i>
$\xi_1 \dots \xi_4$	Activation overvoltage parametric coefficients	V or V.K^{-1}
ΔH	Hydrogen enthalpy of combustion	kJ.mol^{-1}
λ_{mem}	Membrane resistivity parameter	-
η_{act}	Activation overvoltage	V
η_{ohmic}	Ohmic overvoltage	V
τ_{fc}	Fuel cell thermal time constant	s
A_{fc}	Fuel cell area	cm^2
c'_{o_2}	Oxygen concentration at the cathode/membrane interface	mol.cm^{-3}
c'_{H_2}	Hydrogen concentration at the cathode/membrane interface	mol.cm^{-3}
C_{dl}	Double layer capacitance	F
C_{t_fc}	Fuel cell thermal capacitance	$\text{kJ.}^\circ\text{C}^{-1}$
$e_{p_{o_2}}$	Error in oxygen pressure level	atm
E^o	Reference potential at unity activity	V

E_{Nemst}	Thermodynamic potential	V
F	Faraday constant	C.mole ⁻¹
hA	Stack heat transfer coefficient	W.K ⁻¹
h_{cond_fc}	Heat exchanger conduction index	W.°C ⁻¹
h_{conv_fc}	Heat exchanger convection index	W.°C ⁻¹ .A ⁻¹
I_{fc}	Cell/stack current	A
k_a	Fuel cell anode flow constant	mol.s ⁻¹ .atm ⁻¹
k_c	Fuel cell cathode flow constant	mol.s ⁻¹ .atm ⁻¹
K_{pfc}	Air flow controller proportional gain	-
K_{dfc}	Air flow controller differential gain	-
K_{ifc}	Air flow controller integral gain	-
l_{mem}	Membrane thickness	μm
$LMTD_{fc}$	Log Mean Temperature Difference	°C
$\dot{m}_{H_2,used}$	Rate of hydrogen consumption	mol.s ⁻¹
$\dot{m}_{H_2,in}$	Hydrogen inlet flow-rate	mol.s ⁻¹
$\dot{m}_{H_2,out}$	Hydrogen outlet flow-rate	mol.s ⁻¹
$\dot{m}_{O_2,in}$	Oxygen inlet flow-rate	mol.s ⁻¹
$\dot{m}_{O_2,out}$	Oxygen outlet flow-rate	mol.s ⁻¹
$\dot{m}_{O_2,used}$	Rate of oxygen consumption	mol.s ⁻¹
MC	Product of stack mass and average specific heat	kJ.K ⁻¹
n	Number of electrons involved in per mole of a electrolyzed component	-
N_{fc}	Number of cells	-

p'_{H_2}	Hydrogen partial pressure	atm
p'_{O_2}	Oxygen partial pressure	atm
p_{BPR}	Oxygen pressure at the outlet (back regulator)	atm
p_{refO_2}	Reference oxygen pressure in cathode	atm
p_{tank}	Hydrogen pressure at the inlet (tank pressure)	atm
P_{fc}	Fuel cell electrical power output	W
P_{tot_fc}	Total power delivery into the stack	W
P_{r_fc}	Fuel cell rated power	kW
\dot{Q}_{stack_fc}	Fuel cell stack heat absorption rate	J.s ⁻¹
\dot{Q}_{cool_fc}	Heat flow rate through cooling water	J.s ⁻¹
\dot{Q}_{loss_fc}	Heat flow rate through the stack surface	J.s ⁻¹
r_M	Membrane resistivity	Ω.cm
R	Universal gas constant	J.mole ⁻¹ .K ⁻¹
R_{t_fc}	Fuel cell thermal resistance	°C.W ⁻¹
R_{act}	Activation resistance	Ω
R_{int}	Cell internal resistance/Membrane resistance	Ω
$T_{cw,in}$	Inlet cooling water temperature	°C
$T_{cw,out}$	Outlet cooling water temperature	°C
T_{amb}	Ambient temperature	°C
T_{fc}	Stack overall temperature	K
T'_{fc}	Stack overall temperature	°C
UA_{HX_fc}	Measure of the fuel cell heat exchanger size	W.°C ⁻¹
V_{act}	Absolute value of activation overvoltage	V

V_{cell}	Single PEM fuel cell voltage	V
V_a	Fuel cell anode volume	m^3
V_c	Fuel cell cathode volume	m^3
V_{stack}	Stack voltage	V

Electrolyzer Stack

<i>Symbol</i>	<i>Parameter</i>	<i>Unit</i>
η_e	Electrolyzer energy efficiency	-
η_F	Faraday efficiency	-
τ_{elz}	Electrolyzer thermal time constant	s
A_{elz}	Electrolyzer electrode surface area	m^2
$C_{t_{elz}}$	Electrolyzer thermal capacitance	$KJ.C^{-1}$
f_1	Parameter related to Faraday efficiency	$m.A^2.cm^{-4}$
f_2	Parameter related to Faraday efficiency	-
F	Faraday constant	$C.mole^{-1}$
$h_{cond_{elz}}$	Electrolyzer heat exchanger conduction index	$W.^{\circ}C^{-1}$
$h_{conv_{elz}}$	Electrolyzer heat exchanger convection index	$W.^{\circ}C^{-1}.A^{-1}$
I_{elz}	Electrolyzer current	A
$LMTD_{elz}$	Log Mean Temperature Difference	$^{\circ}C$
\dot{n}_{H_2}	Molar hydrogen flow rate (production)	$mol.s^{-1}$
N_{elz}	Number of cells in electrolyzer stack	-
$P_{ava_{elz}}$	Electrolyzer available power	W
P_{elz}	Electrolyzer consumed power	W
$P_{r_{elz}}$	Electrolyzer rated power	kW

\dot{Q}_{stack_elz}	Electrolyzer stack heat dissipation rate	$J.s^{-1}$
\dot{Q}_{gen_elz}	Heat generation rate inside the electrolyzer stack	$J.s^{-1}$
\dot{Q}_{cool_elz}	Heat flow rate through cooling water	$J.s^{-1}$
\dot{Q}_{loss_elz}	Heat flow rate through the stack surface	$J.s^{-1}$
r_1	Parameter related to ohmic resistance	$\Omega.m^2$
r_2	Parameter related to ohmic resistance	$\Omega.m^2.^{\circ}C^{-1}$
R_{t_elz}	Electrolyzer thermal resistance	$^{\circ}C.W^{-1}$
s	Coefficient of overvoltage on electrode	V
t_1	Overyoltage coefficient	$A^{-1}.m^2$
t_2	Overyoltage coefficient	$A^{-1}.m^2.^{\circ}C$
t_3	Overyoltage coefficient	$A^{-1}.m^2.^{\circ}C^2$
$T_{cw,in}$	Inlet cooling water temperature	$^{\circ}C$
$T_{cw,out}$	Outlet cooling water temperature	$^{\circ}C$
T_{amb}	Ambient temperature	$^{\circ}C$
T_{elz}	Electrolyzer stack temperature	$^{\circ}C$
UA_{HX_elz}	Measure of the heat exchanger size	$W.C^{-1}$
U_{rev}	Reversible cell voltage	V
U_{in}	Thermo-neutral cell voltage	V
U_{cell}	Alkaline electrolyzer single cell voltage	V
z	Number of electrons transferred per reaction	-

Power Converters

<i>Symbol</i>	<i>Parameter</i>	<i>Unit</i>
θ	Power factor angle between load voltage and current	rad
C_f	Filter capacitance	F
D_{wt}	Wind turbine buck-boost converter duty ratio	-
D_{fc}	Fuel cell boost converter duty ratio	-
e_{vwt}	Wind turbine buck-boost converter error	V
e_{vout}	Inverter controller error signal	V
e_{vfc}	Fuel cell boost converter error	V
e_{pelz}	Electrolyzer power error signal	W
I_L	Current through filter inductor	A
I_{out}	Output current at the load	A
I_{L_out}	Difference in inductor and load current	A
K_{pwt}	Buck-boost controller proportional gain	-
K_{dwt}	Buck-boost controller differential gain	-
K_{iwt}	Buck-boost controller integral gain	-
K_{pfc}	Boost controller proportional gain	-
K_{dfc}	Boost controller differential gain	-
K_{ifc}	Boost controller integral gain	-
K_{pelz}	Electrolyzer controller proportional gain	-
K_{delz}	Electrolyzer controller differential gain	-
K_{ielz}	Electrolyzer controller integral gain	-
K_{pinv}	Inverter PWM controller proportional gain	-

K_{dinv}	Inverter PWM controller differential gain	-
K_{iinv}	Inverter PWM controller integral gain	-
L_f	Filter inductance	mH
L_{out}	Inductive load at the output	mH
m_{inv}	Modulation index (PWM)	-
P_{out}	Power output at the load	W
R_C	Resistance in filter capacitor	Ω
R_L	Resistance in filter inductor	Ω
R_{out}	Resistive Load at the output	Ω
S_1, S_2, S_3, S_4	Full bridge inverter switches	-
V_{bus}	DC bus voltage	V
V_{inv}	Inverter output voltage	V
V_{out}	Load voltage at the output	V
V_{inv_out}	Difference in inverter and load voltage	V
V_{ref_out}	Reference output voltage (AC)	V
V_{bus_ref}	DC bus reference voltage	V

Chapter 1

Introduction

With persistent environmental, political and socio-economic quandary surrounding fossil fuel based energy system, renewed interest has been seen in researching alternative sources of energy. At present, 79.6 % of worldwide consumption is based on fossil energy sources whereas nuclear power generation is around 6.5 %. With a view to ensuring sustainable development and reducing green house gas emission, the proportion of renewable energies in the global energy mix is expected to rise from its current level of 13.9 % to 20 % by 2020, with a long term goal of achieving more than 50 % by 2050 (Figure 1.1) [1,2].

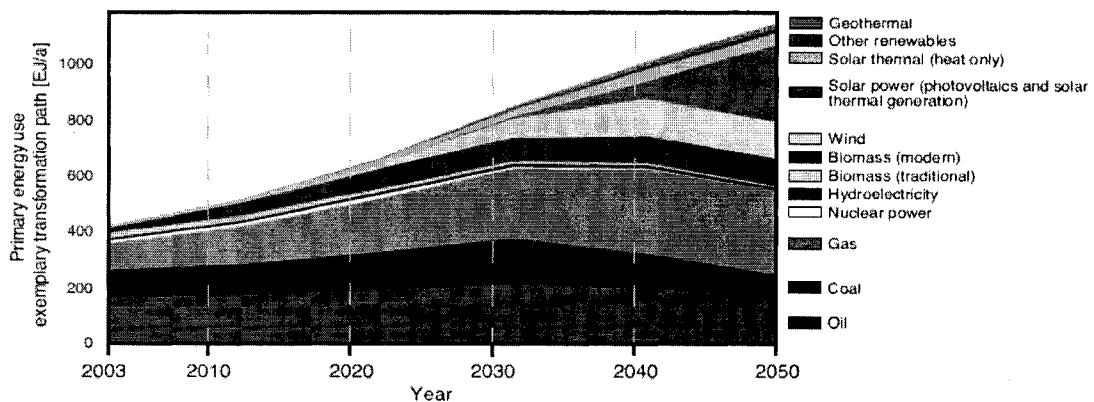


Figure 1.1: Transforming the global energy mix: The exemplary path until 2050, German Advisory Council on Global Change (WBGU) [1].

In Canada, about 61 % of total consumption is generated by hydroelectric sources and most of the remaining demand is met by fossil energy (19 % from coal, 12 % from nuclear, 5 % from natural gas, 2 % from oil, and only 1 % from other sources) [3,4]. Although the wind potential in Canada is immense, utilization of this renewable resource has remained mostly unexplored [2-5].

Large-scale grid-connected wind turbines have proven to be economically viable in many parts of the world [4, 5]. However, design of small-scale, stand-alone power sources for use in remote or off-grid locations is yet to reach a commercially feasible stage. With expected reduction in the component cost and gain in the system performance, attention towards wind energy alternatives for electric power generation in stand-alone applications is gaining momentum. Such small-scale systems also have the potential of integration with a large distributed energy infrastructure [5,6].

In a wind energy conversion system (WECS), available energy in the wind is typically converted to electricity by electro-mechanical means. Due to the intermittent nature of wind availability, the energy from a wind turbine is not continuous. In a hybrid energy system (HES), continuity in power flow is attempted by storing excess energy from the renewable source. Although, battery technology has reached a very mature stage, size, cost and disposal are the constraining factors for its use in remote stand-alone applications. Battery maintenance and self-discharge is a major issue in cold Canadian environment. Recent advancements in fuel cell and electrolyzer technology have opened up the option for using hydrogen as an energy storage medium [7,8]. Excess energy from the wind could be utilized in electrolyzers for hydrogen production by electrolysis of water. This stored hydrogen can be used for electricity generation by a fuel cell system whenever wind energy is insufficient. A hybrid energy system based on such alternative technologies operating in parallel with a renewable source may prove to be a solution for small-scale power generation for remote applications [9-17].

1.1 Research Rationale

Energy yield of a renewable source is highly dependent on geographical, climatic and environmental conditions. There exist a number of technology alternatives (such as, wind, solar, micro-hydro, geothermal etc.) with varying degrees of cost, performance and reliability indices. Successful operation of a wind-fuel cell hybrid energy system requires a comparative analysis amongst various other alternatives and their costs. At present, fossil fuel based systems are much cheaper than the emerging technologies. However, it is expected that the cost of wind, solar and hydrogen systems would reduce in the long run and might become cost-competitive against conventional sources. A site-specific pre-feasibility study is the essential first step towards determining the suitable technology option. For a remote application, this investigation should also include resource availability, energy consumption, and long-term projection.

Typically renewable energy systems are used in remote locations in autonomous mode where rapidly varying environmental conditions affect the performance of the systems. Variations in wind speed, power demand and hydrogen availability may restrict the reliability and operational limits of a wind-fuel cell system. Electrical and mechanical elements within the system could also face abnormal stress during rapidly changing conditions. Therefore, investigation of transient response is an important aspect in system integration, controller design and reliability analysis.

Computer based optimization, modeling, and simulation tools are useful methods in hybrid energy system design. This allows one to make important decision in component sizing, cost prediction and performance analysis.

1.2 Literature Review

To date, a comprehensive investigation of wind-fuel cell hybrid energy system with emphasis on system optimization, dynamic component modeling and transient analysis is almost nonexistent [8-28]. With rapid advancements in hydrogen energy research, a good number of reports are emerging for fuel cell and electrolyzer systems. However, research

in small wind energy technology is yet to gain favorable attention and availability of literature is scarce. Most of the pioneering works in wind-fuel cell hybrid systems are being done at two research institutions. The Hydrogen Research Institute (HRI) located at the Université du Québec à Trois-Rivières, Quebec, Canada has reported a number of analytical and experimental results [10-13]. The Energy Research Unit (ERU) at CLRC Rutherford Appleton Laboratory, Oxon, UK in association with ENEA, Casaccia Research Center, Italy is also engaged in similar research and has published some reports [7,14]. Several brief analyses of wind energy based hydrogen production schemes are discussed in references [15-18]. A good number of articles relating solar-hydrogen hybrid systems can also be found in [19-24]. Sizing and optimization methods for relevant renewable systems are reported in references [25,26]. Transient analysis and simplified dynamic models are outlined in references [27,28].

A stand-alone renewable system that uses hydrogen as an energy carrier has been designed, developed, optimized and tested at the Hydrogen Research Institute (HRI). The details of system integration, control strategies, and operational performance of the system have been reported in references [10-13]. The major system components are: a wind turbine (10 kW, Bergey-BWC Excel), a photovoltaic array (1 kW peak), a fuel cell system (5 kW, Ballard MK5-E), an electrolyzer (5 kW), a hydrogen tank (3.8 m³), a Battery system (42.240 kWh) and a power converter (5 kW). A two-year test result has indicated successful operation of the system with electrolyzer, battery and fuel cell efficiency of 50 %, 90 % and 45 %, respectively [13]. This research establishes the fact that a wind-hydrogen system could perform satisfactorily with additional elements such as photovoltaic arrays and battery systems. A systematic approach for component sizing, cost indication, mathematical modeling and pre-feasibility analysis was not reported.

At the ENEA, Casaccia Research Center, a wind-hydrogen demonstration plant has been designed, procured, and constructed, and initial test results have been reported in reference [14]. This prototype contained a wind turbine (5.2 kW), a battery storage system (330 Ah), an electrolyzer (2.25 kW) and several auxiliary equipment. The system is primarily designed for hydrogen production with excess wind and not configured for

stand-alone power generation. Although several important conclusions on the system's performance are outlined, a complete analysis is absent.

In references [15-17] conceptual analysis of wind driven hydrogen production units have been outlined. Yang *et al.* [15] surveyed various methods of system optimization and considered a set of steady-state equations for component modeling. Grimsmo *et al.* [16] have done similar analyses with emphasis on stochastic wind variations. A simplified dynamic model for wind turbine and electrolyzer were considered in the wind-hydrogen system described in [17]. Implications and qualitative comparisons of grid connected large wind-fuel cell power generation systems are highlighted in [18].

Øystein Ulleberg's Ph.D. dissertation [19] provides a comprehensive insight into various concepts of stand-alone power generation. This work is based on a solar-hydrogen experimental plant (PHOEBUS) installed in Jülich, Germany. Fundamental concepts of energy engineering, mathematical modeling and system optimization methods are described with great details in this work. However, this research focuses on solar energy aspects of a remote power system. Most of the modeling is done with steady-state equations for long-term (monthly/yearly) performance analysis. Issues raised about the solar-hydrogen system in the Ph.D. dissertation have some relevance with the research in wind-hydrogen system. However, a dynamic analysis and optimization problem for a wind energy based hybrid system needs more specific considerations.

A solar-hydrogen-biogas-fuel cell system for domestic applications has been built and tested by Hedström in Stockholm, Sweden [20]. The analysis in the thesis includes semi-empirical steady state simulation models. It is recognized in the thesis that further dynamic modeling is necessary in order to investigate the transient features of the system.

Prerequisites of a stand-alone fuel cell system for use in domestic buildings in Swedish environment have been discussed in good details by Wallmark *et al.* [21]. An analytical approach was applied for system sizing, and cost analysis. This report concludes that fuel cell systems are not cost-competitive against existing grid supply.

However, with reduction of fuel cell cost to 43 %, an autonomous fuel cell system might become feasible.

A solar-hydrogen stand-alone system for a residential home in Zollbrück, Switzerland has been built and tested by Hollmuller *et al.* [22]. The system consisted of a solar array (5 kW), a power converter, an electrolyzer (5 kW), hydrogen storage and other peripherals. Simulation of yearly production potential was carried out and need for proper controller design and better storage device was stressed.

Santarelli *et al.* [23] have reported a comparative analysis of a set of two hypothetical stand-alone energy systems for use in remote houses in Italy. A solar-fuel cell and a solar-hydro-fuel cell system were considered for steady state modeling, plant design and long term performance evaluation. Various cost and energy indices were discussed and the need for cost-reducing schemes for such systems was emphasized. Similar analysis for the Mexican environment has been reported by Torres *et al.* [24].

Cortell *et al.* [25] carried out a feasibility study of using various emerging alternatives in two remote applications. A small radio repeater station (336 W) in Prineville, Oregon and a village power system (148 kW) in Wales, Alaska were considered in that regard. National Renewable Energy Laboratory (NREL)'s optimization software HOMER [29] was used in this analysis. It was concluded that a fuel cell system would be cost effective if the associated cost reduces to 40 % of its present value.

A detailed pre-feasibility analysis of using solar-hydrogen-battery based stand-alone system in Arizona, USA was conducted by Vosen *et al.* [26]. This study focuses on various control strategies and their effects on system cost, resource sensitivity, power delivery and energy storage. It was concluded that significant reduction in component cost is required in order to make a stand-alone system cost-competitive.

In reference [27] transient analysis of a solar-diesel-battery based hybrid system is carried out. The scheme uses a custom-built simulation tool and investigates various combinations of energy sources. However, dynamic models of the components are not provided. Similar analysis for a wind-fuel cell-diesel system is reported in reference [28]. MATLAB-Simulink[®] [30] is used in simulating the hybrid system. The models

contained first order dynamics of the energy components and only a set of approximated time constants is accounted for. Since a number of interrelated issues complicate the operation of a complete hybrid energy system (HES), such a simplified method of transient analysis is not accurate and lacks reliability.

The bulk of published information highlights qualitative analysis of various hybrid energy systems and these reports are very useful in understanding the practical scenarios. However, a systematic approach for optimization, cost evaluation, dynamic modeling, and transient analysis of a wind-fuel cell system remains unrealized.

1.3 Scope of Thesis

In this thesis a hybrid energy system based on wind power and hydrogen storage is researched. Availability of wind energy is of intermittent nature and any shortage needs to be met by secondary power source or energy storage to ensure a continuous operation. Conventionally batteries have been widely used as storage devices. On the other hand, flexibility of hydrogen production, storage and usage has shown many favorable prospects over traditional energy systems. Such a method of energy conversion might possess some promising prospects in stand-alone applications.

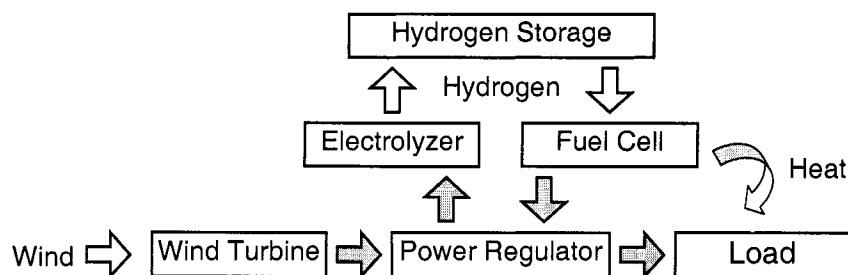


Figure 1.2: Conceptual block diagram of a wind-fuel cell hybrid energy system

A conceptual operating principle and configuration of a wind-fuel cell hybrid energy system is shown in Figure 1.2. A wind turbine works as the renewable energy

source delivering power to the load. Excess energy from the wind could be diverted by a control mechanism for hydrogen production using an electrolyzer. In case of insufficient power from the wind turbine, the stored hydrogen can be used for electricity generation by a fuel cell system. Radiated heat might be used for space heating or other applications.

To ensure economic operation of a hybrid energy system, it is required to size its various components and analyze the cost and performance indices. Investigation of dynamic behaviors is also important to understand the transient features and design the control systems. To date, thorough investigation of the hybrid system under consideration is almost non-existent. In this thesis a detailed investigation is attempted and the results are discussed.

Initially, a pre-feasibility study of using hybrid energy systems with hydrogen as an energy carrier for applications in Newfoundland, Canada is explained. Various renewable and non-renewable energy sources, energy storage methods and their applicability in terms of cost and performance are discussed. HOMER [29] is used as a sizing and optimization tool. Sensitivity analysis with varying wind speed data, solar radiation level, diesel price and fuel cell cost is done. A remote house having a specific energy demand is considered as the stand-alone load. Based on the findings of this analysis, suitable technology options and their sizes are identified.

In the latter sections, various components of a wind-fuel cell system are mathematically modeled with empirical and physical expressions. In the absence of a readily available model of the wind turbine and fuel cell, several novel schemes are provided. Suitable dynamic features are incorporated within the wind turbine, fuel cell and electrolyzer systems. Various controllers are designed and integrated with the energy elements for continuous operation in the stand-alone mode. Simplified models of the power converters are taken into account. The wind-fuel cell system is simulated in MATLAB-Simulink[®] and the results of the transient analyses are explained. Finally, the limitations of the investigation, practical considerations and indications for future research are summarized.

1.4 Thesis Organization

This work is broadly divided into two sections. Following the introductory remarks in Chapter 1, a pre-feasibility study of stand-alone hybrid energy systems for use in Newfoundland, is carried out in Chapter 2. In the chapters that follow, dynamic modeling, simulation and control of a wind-fuel cell hybrid energy system are delineated. In Chapter 3, the individual components of the hybrid system are modeled and integrated using suitable controllers. Simulation methods using MATLAB-Simulink[®] are explained in Chapter 4. The results of the transient analysis is presented and discussed in Chapter 5. The conclusions, contributions and scope for further investigation are highlighted in Chapter 6.

The reference section contains the sources of information along with available up to-date web links. The MATLAB-Simulink[®] models are organized in Appendix A for easy reference. A list of papers generated through this research is given in the Appendix B.

Chapter 2

Pre-feasibility Study of Hybrid Energy System

The performance of a hybrid energy system largely depends on the environmental conditions. Therefore, a site-specific analysis is required to investigate the associated cost, component size and overall economics. In this chapter, a pre-feasibility study is carried out for St. John's, Newfoundland, Canada. A search for accurate wind speed and solar irradiation data yielded St. John's Airport (47°37'N-52°44'W) region to be an ideal place for investigation. The sub-urban site considered here might not be feasible for a stand-alone system. However, sensitivity analysis is done with the wind and solar data and the output parameters are expressed as functions of these variables. It makes the results suitable for identifying technology alternatives for almost all parts of Newfoundland. Such stand-alone hybrid energy systems may find applications in remote lodges, telecommunication installations, recreational facilities etc.

National Renewable Energy Laboratory (NREL)'s, Hybrid Optimization Model for Electric Renewables (HOMER version 2.09) is used for this analysis [29]. It contains a number of energy component models and evaluates suitable technology options based on cost and availability of resources. Analysis with HOMER requires information on resources, economic constraints, and control methods. It also requires inputs on component types, their numbers, costs, efficiency, longevity etc. Sensitivity analysis

could be done with variables having a range of values instead of a specific number. This allows one to ascertain the effects of change in a certain parameter on the overall system.

Various combinations of diesel generator, wind turbine, PV array, fuel cell, electrolyzer, battery, and power converter modules are taken into account towards identifying an economic solution that would meet a given load. In addition to renewable primary sources (wind and solar), a more conventional fossil fuel based system (diesel generators) is considered. The use of other renewable sources such as, micro-hydro, geothermal, biomass was considered beyond the scope of the present work.

Although mostly unexplored, wind resource in Newfoundland is generally categorized as high [31]. On the other hand, it is expected that fuel cell technology would become cheaper and pragmatic in the near future [7,14]. Therefore, emphases are given in analyzing the size, cost and performance of a wind-fuel cell hybrid system. To widen the search space, each of these components is allowed to have more than one unit for inclusion in the optimum solution. Along with wind speed and solar irradiation data, fuel cell cost and diesel price are taken as sensitivity variables. Care is taken not to consider additional sensitivity parameters, as this causes the simulation time to increase greatly.

2.1 Hybrid Energy System

A general hybrid energy system generally consists of a primary renewable source (e.g.: PV array, wind generator etc.) working in parallel with a standby secondary non-renewable module and storage units (e.g.: fuel cell, battery etc.) as shown in Figure 2.1.

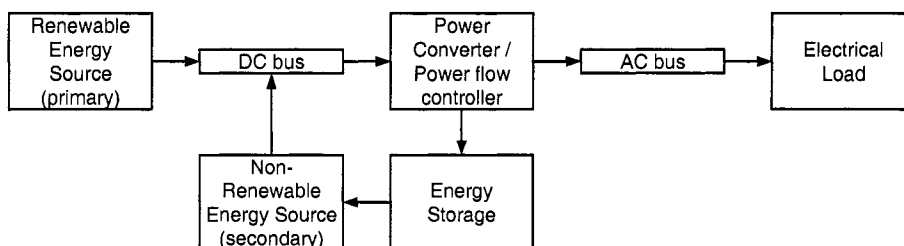


Figure 2.1: General scheme of a stand-alone hybrid power system

Figure 2.2 shows the proposed scheme as implemented in the HOMER simulation tool. The hydrogen storage tank is considered within the electrolyzer model. Supply of hydrogen to the fuel cell is set such that only stored hydrogen in the tank is used, without requiring additional fuel supply. Several additional units such as, compressors in fuel cell and hydrogen storage, DC-DC converters in PV modules and fuel cell, are assumed lumped within each corresponding model.

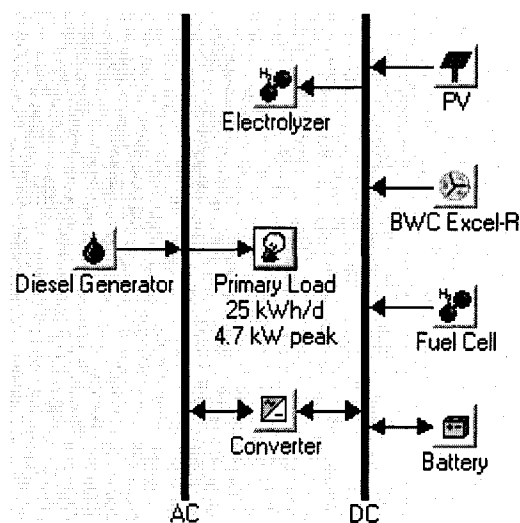


Figure 2.2: HOMER implementation of the hybrid energy system

The general scheme outlined in Figure 2.1 is reflected in the HOMER model (Figure 2.2). Additional information for load, resources etc. are described in the following sections.

2.1.1 Electrical load

A survey was conducted to identify energy consumption in a typical grid-connected house in Newfoundland against various off-grid installations around Canada [32-36]. An ordinary house in St. John's, Newfoundland may consume around 50 kWh/d with a peak demand of nearly 11 kW [32]. Meeting such a load by only renewable or hybrid energy

source is not practical, especially in a city area. Various energy saving schemes and housing standards [37], need to be considered when building an off-grid house. Remote houses, lodges or resorts built with such attributes may use as low as 10~15 kWh/d with 1~5 kW peak demand [33,34,36]. For a telecommunication installation, 21 kWh/d with 1 kW peak power may prove to be sufficient [35].

A set of energy consumption data for a typical grid connected house in St. John's is collected from [38]. This data was sampled every 15 minutes for 365 days of a year. For this study, the total energy consumption is scaled down to 25 kWh/d (with a 4.73 kW peak) to realize the off-grid nature of a remote house.

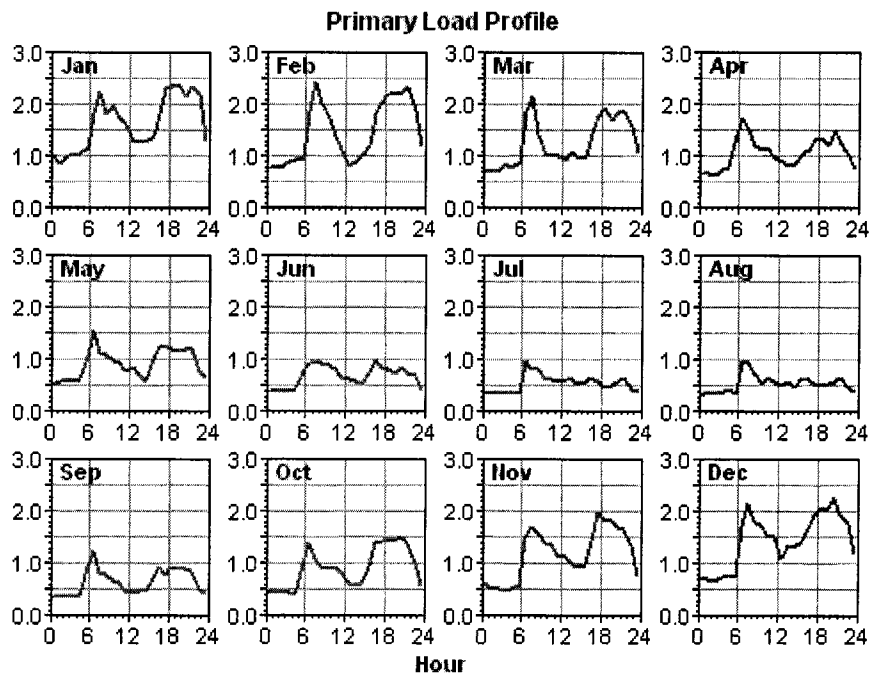


Figure 2.3: Daily load profile for a year

For a typical day, energy consumption is higher in the morning and evening hours (Figure 2.3). On the other hand, winter months (November to March) show an elevated power demand in comparison with the summer months (April to September). For this given load profile, hourly and daily variations are 42.7 % and 16.45 %, respectively.

2.1.2 Renewable Resources

Wind and solar energy resources of St. John's are considered for this study. Sensitivity analysis is done to make the results suitable for other places in Newfoundland.

2.1.2.1 Wind Energy Resource

A monthly average wind dataset for St. John's Airport (47°37'-N 52°44'-W) is collected from Environment Canada Climate normals [39]. This is an average of 49 years (from 1942 to 1990) and indicates that the annual average wind speed in St. John's is around 6.64 m/s.

Table 2.1: Wind data for St. John's Airport [39]

	<i>Jan</i>	<i>Feb</i>	<i>Mar</i>	<i>Apr</i>	<i>May</i>	<i>Jun</i>	<i>Jul</i>	<i>Aug</i>	<i>Sep</i>	<i>Oct</i>	<i>Nov</i>	<i>Dec</i>	<i>Year</i>
Speed (m/s)	7.78	7.5	7.22	6.67	6.11	6.11	5.83	5.83	5.83	6.39	6.95	7.5	6.64
Most Frequent Direction	W	W	W	W	W	SW	SW	SW	W	W	W	W	W

For implementation in HOMER, 8760 data points for each hour in one year is required. Therefore, another set of data containing hourly average wind speed for 365 days of a year (1998-1999) is collected from the Environment Canada's Regional office. Proper scaling is done to match the long-term average (Table 2.1) with this one-year data.

For this given data, Weibull distribution factor (a measure of the distribution of wind speeds over a year) is 1.961 (Figure 2.4).

The autocorrelation factor (randomness in wind speed) is found to be 0.86. The diurnal pattern strength (wind speed variation over a day) is 0.07435 and the hours of peak wind speed is 13.

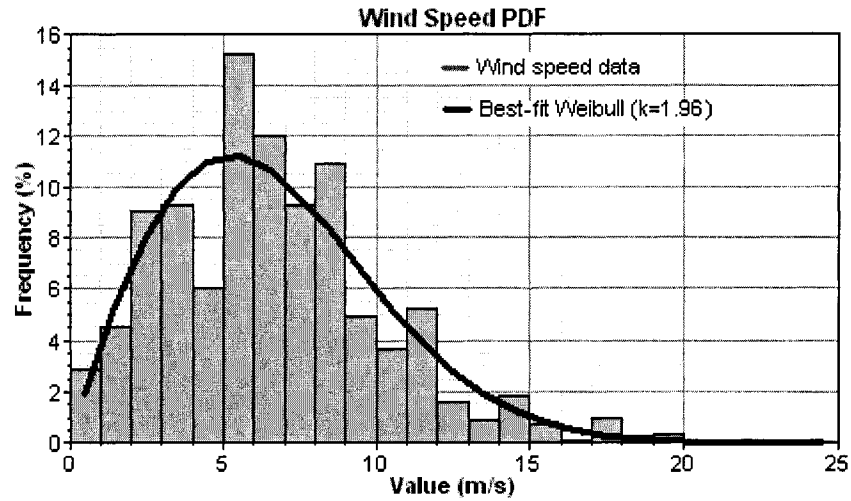


Figure 2.4: Wind speed probability distribution function

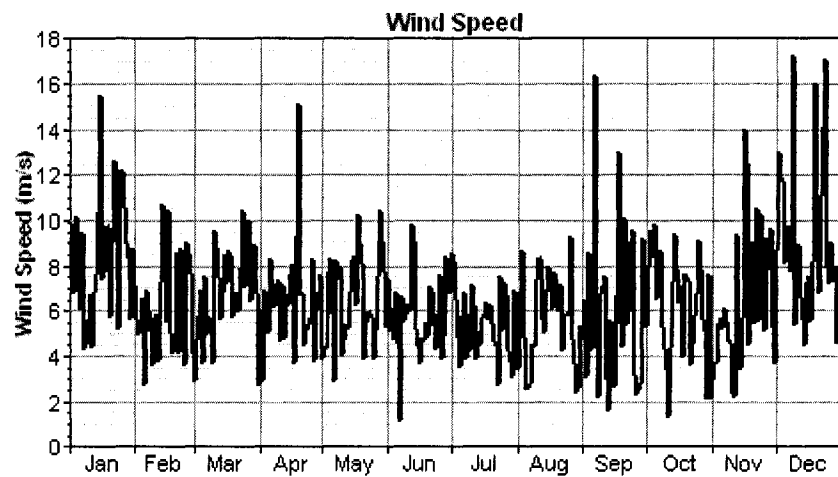


Figure 2.5: Average hourly wind speed for one year

Average wind speed in the winter season is slightly higher than the summer as shown in Figure 2.5. For sensitivity analysis, 4 levels of wind speed data are introduced around the annual average monthly wind speed of 6.64 m/s. These are: 3 m/s, 4.5 m/s, 6.64 m/s and 8 m/s. This range of variation appeared sufficient to consider wind power classes almost anywhere in Newfoundland [31].

2.1.2.2 Solar Energy Resource

Hourly solar irradiation data for the year of 1998-1999 is collected from Environment Canada's regional office. Scaling is done on this data to consider the long-term average annual resource (3.15 kWh/m²/d) for St. John's [39]. HOMER introduces the clearness index from the latitude information of the site under investigation (Figure 2.6).

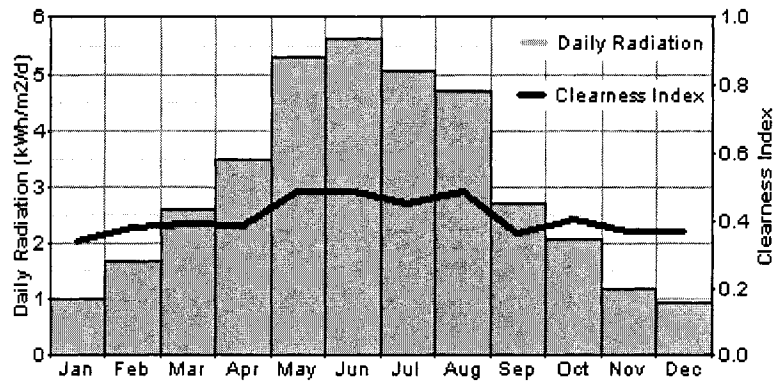


Figure 2.6: Average daily solar irradiation

Sensitivity analysis is done with 3 values around the mean, which are: 1.5 kWh/m²/d, 3.15 kWh/m²/d, and 5.0 kWh/m²/d.

2.1.3 Hybrid System Energy Components

The energy system components are diesel generator, PV module, wind turbine, battery, fuel cell, electrolyzer and power converter. Cost, number of units to be used, operating hours etc. need to be specified in HOMER for each of these equipment. The descriptions of these components are given in the sections below.

2.1.3.1 Diesel Generator

The cost of a commercially available diesel generator may vary from \$250/kW to \$500/kW [25]. For larger units, the per-kW cost is lower and smaller units cost more. Since the peak power demand is less than 5 kW, the diesel generator cost is taken as \$450/kW in this analysis. Replacement and operational costs are assumed to be \$400/kW and \$0.150/hr, respectively.

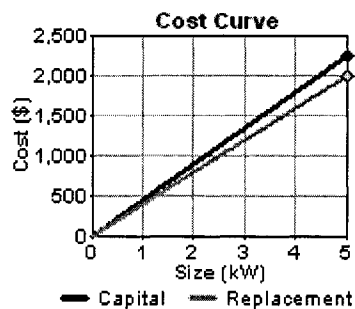


Figure 2.7: Diesel generator cost curves

Options for considering no diesel generator (0 kW) or a 5 kW unit are employed in HOMER. Operating lifetime is taken to be 10,000 hours [25]. Diesel price is used for sensitivity analysis, and three discrete values (\$0.20/L, \$0.35/L, \$0.65/L) are introduced. At present, diesel price is around \$0.35/L [40] and for a very remote location this could increase up to \$0.65/L [34,35].

2.1.3.2 Photovoltaic Array

The installation cost of PV arrays may vary from \$6.00/W to \$10.00/W [25,41]. Considering a more optimistic case, a 1 kW solar energy system's installation, and replacement costs are taken as \$7000, \$6000 respectively [25].

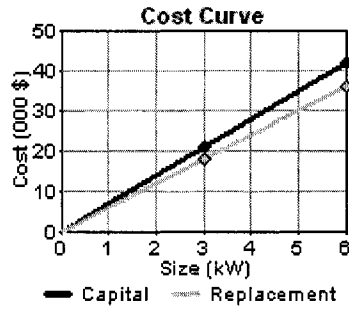


Figure 2.8: Cost of photovoltaic units

Three different sizes are considered, which are 0 kW (no PV module), 2 kW and 6 kW. The lifetime of the PV arrays are taken as 20 years and no tracking system is included in the PV system.

2.1.3.3 Wind Energy Conversion System (WECS)

Wind turbine size is generally considered much higher compared to the average electrical load. In this analysis, Bergey Wind Power's BWC Excel-R model is considered [42]. It has a rated capacity of 7.5 kW and provides 24 V, 48 V, 120 V or 240 V DC as output.

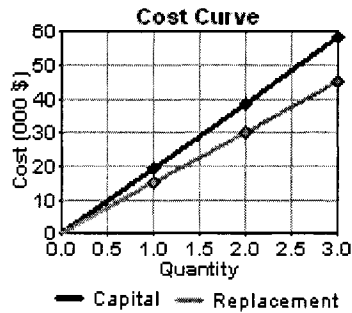


Figure 2.9: BWC Excel-R Cost curves

The cost of one unit is considered to be \$19,400 while replacement and maintenance costs are taken as \$15,000 and \$75/year [42]. To allow the simulation

program to find an optimum solution, provision for using 0 (no turbine), 1 or 2 units is given. Lifetime of a turbine is taken to be 20 years.

2.1.3.4 Fuel Cell System

The cost of fuel cell varies greatly depending on the type of technology, reformer, auxiliary equipment and power converters. At present, fuel cell costs vary from \$3,000/kW to \$6,000/kW [25,43,44,45]. However, current research and thrust for developing low-cost electric vehicles could reduce the price to \$195-325/kW in near future [45]. Considering these factors, the capital, replacement and operational costs are taken as \$3,000, \$2,500 and \$0.02/hour for a 1 kW system, respectively.

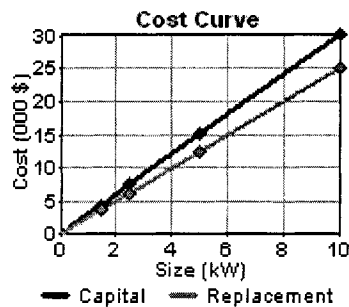


Figure 2.10: Fuel cell cost curves

Four different sizes of fuel cells are taken in the search space: 0 kW (no fuel cell used), 1.5 kW, 3.5 kW, and 5 kW. Fuel cell lifetime and efficiency are considered to be 40,000 hours and 50 %, respectively. Since the cost of fuel cell is one of the most significant issues in commercializing a hybrid energy system with hydrogen storage, a sensitivity analysis with varying cost is necessary. Here, a set of cost multiplying factors for fuel cell is taken into account (0.05, 0.15, 0.65, and 1.0).

2.1.3.5 Electrolyzer

Current production cost of electrolyzers is \$1,500/kW to \$3,000/kW [25,46]. With improvements in polymer technology, control systems and power electronics it is expected that costs would be significantly reduced in ten years [25]. In this analysis, a 1 kW system is associated with \$2000 capital, \$1500 replacement and \$20 maintenance cost.

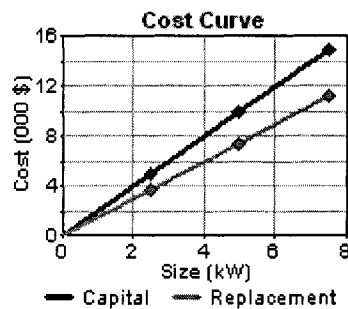


Figure 2.11: Electrolyzer cost curves

Different sizes of electrolyzers (0 kW, 2.5 kW, 5 kW, 7.5 kW) are considered in the model. Lifetime is considered as 25 years with an efficiency of 75 %. Hydrogen storage tanks are also included in the electrolyzer model. The cost of a tank with 1 kg capacity is assumed to be \$1,300. The replacement and operational costs are taken as \$1,200 and \$15/year [25]. Five different sizes (from 0 to 15 kg) are included, to widen the search space for a cost effective configuration.

2.1.3.6 Battery

To compare the energy storage capability of the electrolyzer-tank systems, conventional batteries are included in this analysis. Commercially available models, such as, Surrrette Battery Engineering's Surrrette™-6CS25P models (6 V, 1156 Ah, 9645 kWh) are considered in the scheme [47].

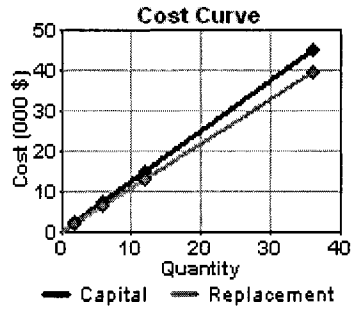


Figure 2.12: Cost of battery

Cost of one battery is \$1,250 with a replacement cost of \$1,100. The battery stack may contain a number of batteries (0, 2, 6, 12, or 36).

2.1.3.7 Power Converter

A power electronic converter system is needed to maintain flow of energy between the AC and DC components. For a 1 kW system the installation and replacement costs are taken as \$800 and \$750 respectively.

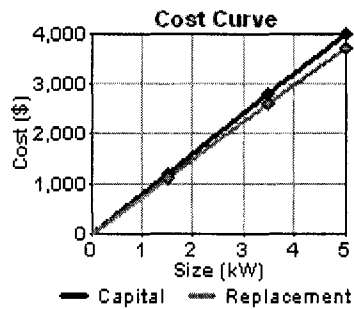


Figure 2.13: Converter cost curves

Three different sizes of converter (1.5 kW, 3.5 kW, and 5.0 kW) are considered in the model. Lifetime of a unit is considered to be 15 years with an efficiency of 90%.

2.1.4 Economics and Constraints

Considering the project lifetime to be 25 years, the annual real interest rate is taken as 8 %. For a small sized system, the fixed capital cost is less and it is assumed to be \$1500. Since operations and maintenance costs are given for the individual components, a nominal value (\$100) is used for this parameter. The maximum annual capacity shortage is 1% and operating reserve, as percentage of hourly load is 6.5 %. For renewable output, this reserve is 25 % and 50 % for solar and wind energy, respectively. These percentages are assumed quantities, which are typical to similar analyses [29]. No cost subsidy available from Canadian government is considered in this study.

2.2 Sensitivity Results

Four sensitivity variables (wind speed, solar irradiation, diesel price and fuel cell cost) are considered in this analysis. To keep provisions for finding suitable system type (combination of technologies) and system configuration (size and numbers of each component), the search space is widened by introducing various alternatives (Table 2.2).

Table 2.2: Search space alternatives

<i>Components</i>	<i>PV (kW)</i>	<i>BWC Excel R (Nos.)</i>	<i>Fuel Cell (kW)</i>	<i>Battery (Nos.)</i>	<i>Converter (kW)</i>	<i>Electrolyzer (kW)</i>	<i>H₂ Tank (kg)</i>
	0	0	0	0	1.5	0	0
Sizes/	2	1	1.5	2	3.5	2.5	2.5
Numbers	6	2	3.5	6	5.0	5.0	5.0
			5.0	12		7.5	10
				36			15

For each of the sensitivity values HOMER simulates all the systems in their respective search space. An hourly time series simulation for every possible system type and configuration is done for a one-year period. A feasible system is defined as a solution or hybrid system configuration that is capable of meeting the load. HOMER eliminates all infeasible combinations and ranks the feasible systems according to

increasing net present cost. It also allows a number of parameters to be displayed against the sensitivity variables for identifying an optimal system type.

A total of 144 sensitivity cases (product of wind speed (4), solar radiation (3), diesel price (3) and fuel cell cost multipliers (4)) were tested with each of the 43200 system configurations resulting in nearly 6.22 million alternatives being examined. The total simulation time was 27 hours 12 minutes on a 2.67 GHz Intel personal computer. Warnings were generated indicating insufficiency in search space for wind turbine, converter, electrolyzer and hydrogen tank. An increase in the number of components would have required even longer time without significantly affecting the outcome. Therefore, no further attempts were made to modify the search space.

The optimization results in graphical form are shown in figures 2.14 to 2.19. Here, various Optimal System Types (OST) are displayed as functions of different sensitivity parameters. In Figures 2.14 to 2.17, these plots are given in terms of wind speed and solar irradiation data. This allows identification of system configurations for various locations around Newfoundland.

Considering present fuel cell cost and diesel price (\$0.35/L), a wind/diesel/battery based hybrid system is suitable for stand-alone loads around St. John's (Figure 2.14). The total Net Present Cost (NPC), Capital Cost and Cost of Energy (COE) for such a system is \$48,454, \$28,450 and \$0.497/kWh, respectively. For a region with very low wind penetration, a diesel generator/battery system might be suitable. Although the capital cost and NPC are lower for such a system, the COE is much higher (\$0.776/kWh).

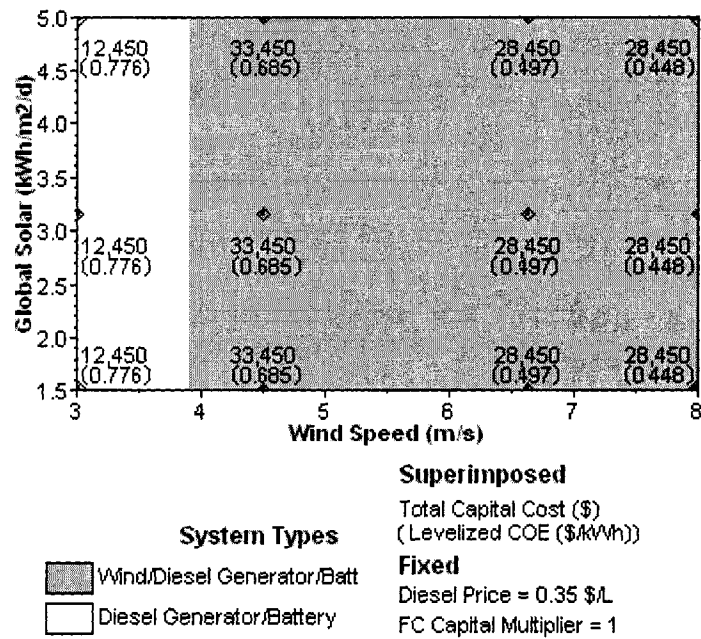


Figure 2.14: OST with diesel price = \$0.35/L and FC cost = 100%

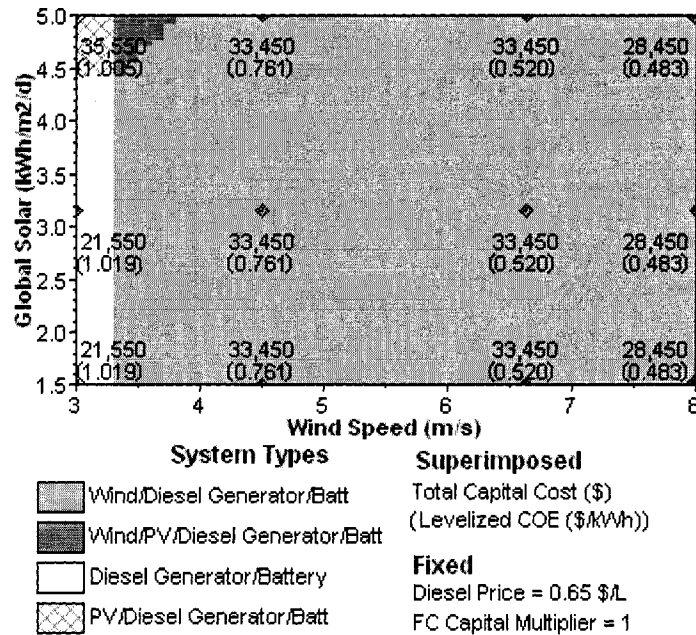


Figure 2.15: OST with diesel price = \$0.65/L and FC cost = 100%

Figure 2.15 represents a scenario where diesel cost is elevated to \$0.65/L, due to remoteness of a site or an unforeseen price hike. As a result, the associated costs of hybrid systems are also increased. One important observation is that, a photovoltaic based system comes into the picture only when wind resource is very limited, solar energy density is very high and cost of diesel is elevated. For Newfoundland, such a constrained situation is not generally expected. Therefore, utilization of solar energy is not feasible for most remote installations. This observation is reinstated in other OST plots as well (Figures 2.14-2.19). Another conclusion from these figures (Figures 2.14, and 2.15) is that integration of fuel cells into a hybrid system is not feasible at the current market price of fuel cell systems.

With an expectation that fuel cell costs might reduce in near future [25,45], the observations in figures 2.16 and 2.17 are done with lower cost levels. A wind/fuel cell/diesel generator/battery system would be preferable for St. John's, if the fuel cell cost reduces to 65 % of its current cost. The capital cost, NPC, and COE for such systems might be around \$36,738, \$47,910 and \$0.492/kWh, respectively.

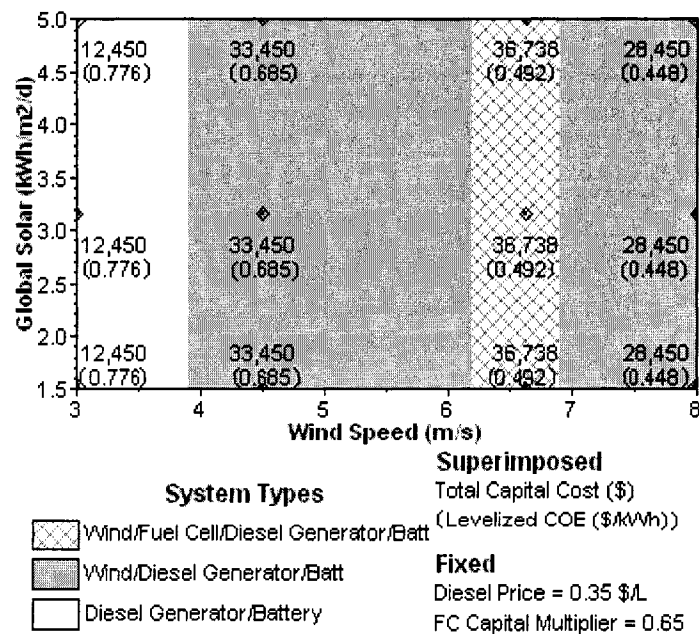


Figure 2.16: OST with diesel price = \$0.35/L and FC cost = 65%

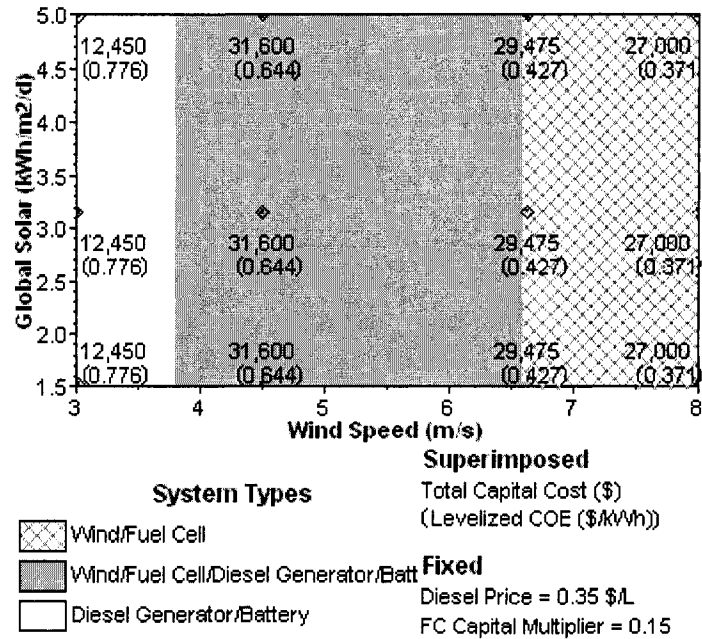


Figure 2.17: OST with diesel price = \$0.35/L and FC cost = 15%

If the fuel cell cost drops around 15 % of its present market price, only a wind/fuel cell system would be sufficient for the remote application being considered here (Figure 2.17). For such a system, the expected capital cost, NPC and COE would be around (\$29,475, \$41,425, and \$0.427/kWh, respectively) depending on the magnitude of average wind speed.

Selection of an OST is investigated from a different perspective in Figure 2.18, where a fixed renewable resource is considered (for St. John's only). Diesel price and fuel cell cost multiplier are taken as the sensitivity parameters. Irrespective of the diesel price, a wind/fuel cell system would be feasible if the fuel cell cost reduces towards 15 % (Figure 2.18). This figure stresses the fact that at the present fuel cell cost (65 % or above), a wind/diesel generator/battery system is probably the only feasible solution.

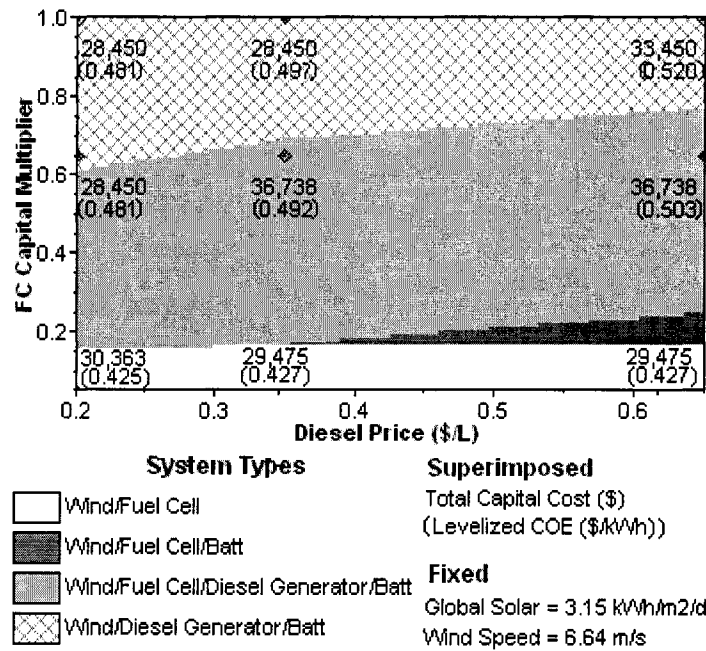


Figure 2.18: OST with solar irradiation = 3.15 kWh/m²/d and wind speed = 6.64 m/s

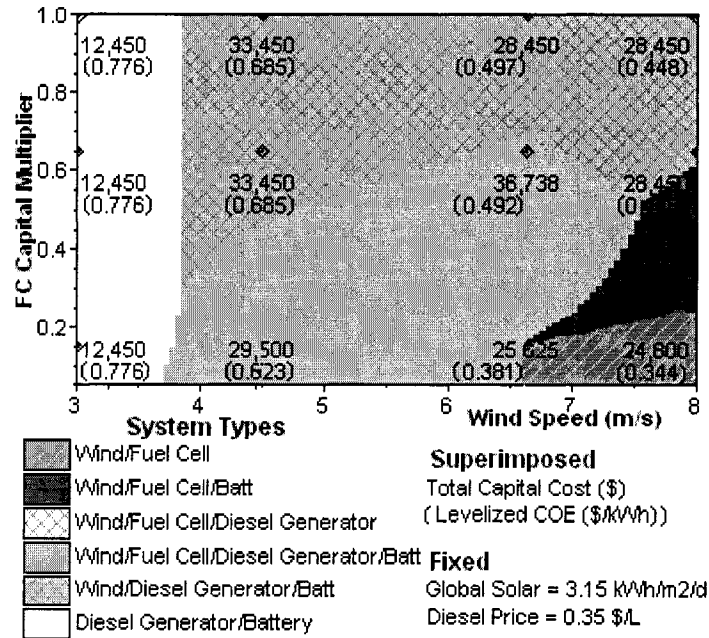


Figure 2.19: OST with solar irradiation = 3.15 kWh/m²/d and diesel price = \$0.35/L

In Figure 2.19, the optimal system types are shown as functions of wind speed and fuel cell cost. This allows identification of suitable hybrid systems based on various wind regimes. At lower wind speeds, the use of a diesel generator/battery system is the only option. At intermediate wind speeds, a wind turbine or fuel cell could be added (depending on fuel cell cost) and reduction in COE could be achieved. On the other hand, at higher wind speeds, a wind/fuel cell or wind/fuel cell/battery system might also prove to be feasible if the fuel cell cost drops significantly.

2.3 Optimization results

In HOMER the optimization results could be categorized for a particular set of sensitivity parameters. Considering the diesel price fixed at \$0.35/L, the fuel cell cost can be varied to identify an optimal system type (OST) for St. John's (wind speed = 6.64 m/s and solar irradiation = 3.15 kWh/m²/d). This, in other words, implies an optimistic case where the fuel cell cost is expected to reduce.

At present, a wind/diesel generator/battery system is the most suitable solution as the fuel cell cost is very high (Figure 2.20). For a remote home (25 kWh/d, 4.73 kW peak load), this system might consist of one BWC Excel-R wind turbine, one 5 kW diesel generator, two batteries and a 3.5 kW power converter.

FC Capital Multiplier							PV (kW)	XLR	FC (kW)	DG (kW)	Batt. (kW)	Conv. (kW)	Elec. (kW)	H2 (kg)	Total Capital	Total NPC	COE (\$/kWh)	Ren. Frac.	Diesel (L)	FC (hrs)	DG (hrs)
1									1	5	2	3.5			\$ 28,450	\$ 48,454	0.497	0.93	998		1,041
0.65									1	1.5	5	2	3.5	2.5	\$ 36,738	\$ 47,910	0.492	0.93	270	1,401	283
0.15									1	3.5			3.5	7.5	\$ 29,475	\$ 41,424	0.427	0.90		4,286	
0.05									1	3.5			3.5	7.5	\$ 25,625	\$ 36,980	0.381	0.90		4,286	

Figure 2.20: Optimization results for wind speed = 6.64 m/s, solar irradiation = 3.15 kWh/m²/d, and diesel price = \$0.35/L

With a reduction in fuel cell cost (cost multiplier = 0.65), a wind/fuel cell/diesel generator/battery system appears as a feasible solution. Considerable reduction in carbon emission, and dependency on fossil fuel could be achieved by replacing the diesel

generator with a fuel cell system. System integration issues could also be simplified by eliminating the need for batteries in a wind/fuel cell system. However, such a solution is cost-competitive only when the fuel cell price reduces by 85 % or more.

The major obstacle in using hydrogen as a storage medium is the high cost associated with it. However, indications are, cost of the fuel cell may reduce significantly in near future (around year 2010) and reach a level of \$300/kW [25,45]. This implies a capital cost multiplier of 0.1 (present cost \$3000/kW to future cost \$300/kW) is not impractical. Considering a more futuristic scenario, the following discussion focuses on discerning the applicability of a wind-fuel cell hybrid system in Newfoundland.

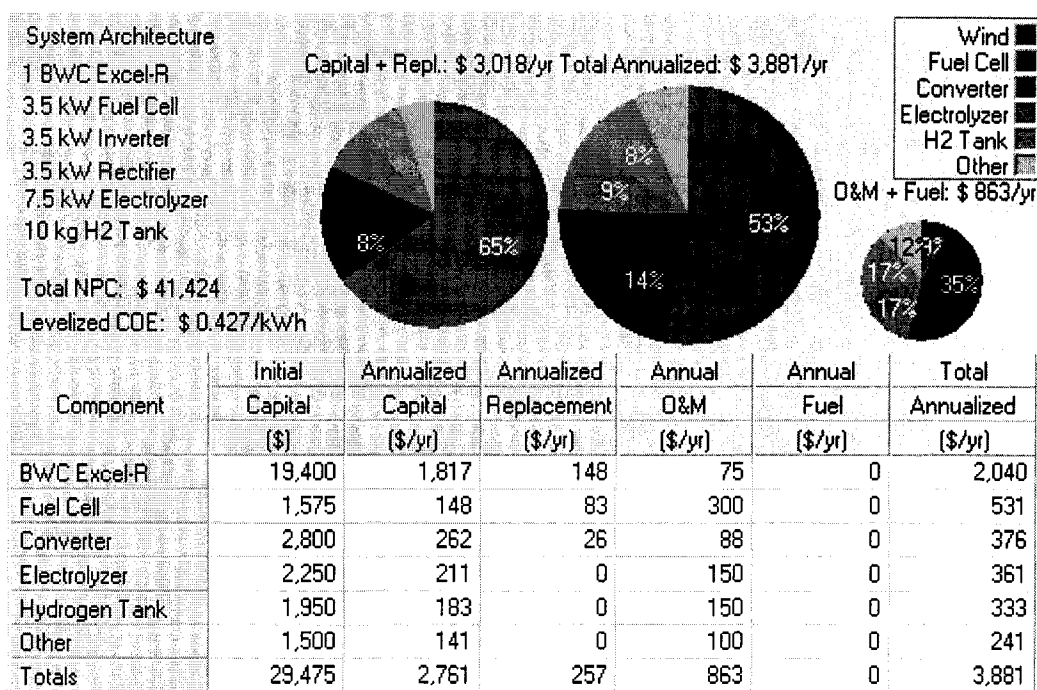


Figure 2.21: Wind-fuel cell system cost analysis (HOMER Screenshot)

A wind fuel cell system for remote homes having an energy rating of 25 kWh/d (4.73 kW peak) should include one 3.5 kW fuel cell, one 3.5 kW converter (inverter & rectifier), one 7.5 kW electrolyzer and a hydrogen tanks with 10 kg capacity. Details of various cost indices are shown in Figure 2.21.

Annual extracted wind energy is 25,384 kWh and fuel cell power delivery is 2,762 kWh. Therefore, the wind turbine meets 90 % demand and the remaining 10 % is contributed by the fuel cell. Excess electricity, unmet load and capacity shortage are 9,328 kWh, 32 kWh, and 55 kWh, respectively. The fuel cell operates 4,268 hours in a year and hydrogen usage is 165.7 kg/yr (efficiency 50 %).

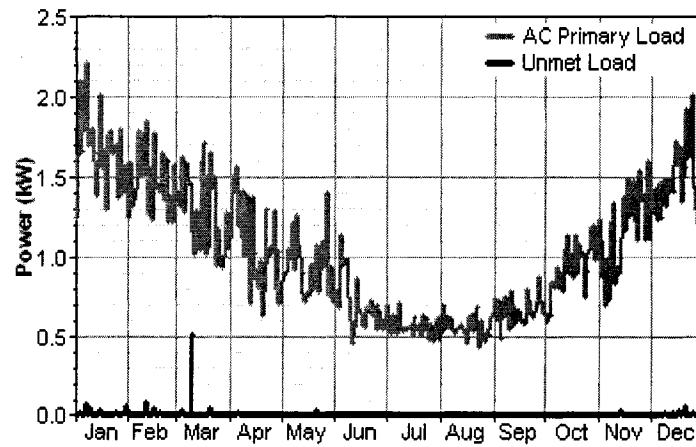


Figure 2.22: Primary load and unmet load

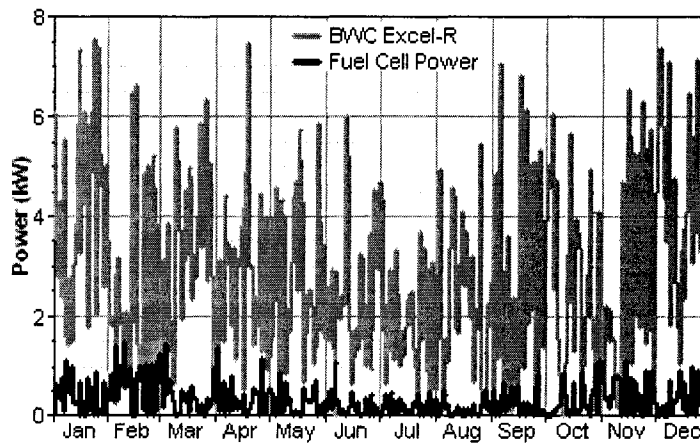


Figure 2.23: Wind power and fuel cell power

The primary load is served with 9,093 kWh and the electrolyzer consumes 8,716 kWh in a year. Peak unmet load is 0.5 kW (Figure 2.22) and excess electricity production is 7,650 kWh. With reduced wind speed during the summer months (Figure 2.5), wind power production reduces in a proportionate manner (Figure 2.23). The fuel cell average power delivery (0.644 kW) is much lower than the rated value of 3.5 kW (Figure 2.23). However, it supplies occasional peak load and serves as a secondary power source. The excess electricity, whenever available might be used in water pumping or space heating, which would elevate the overall efficiency.

2.4 Summary

At present, renewable energy based low-emission hybrid energy systems with hydrogen storage are not cost competitive against conventional fossil fuel based stand-alone or grid interfaced power sources. However, the need for cleaner power and improvements in alternative energy technologies bear good potential for widespread use of such systems. Various energy sources (wind, solar, and diesel generator) and storage systems (battery, and electrolyzer-tank) were considered in this analysis. NREL's optimization tool HOMER was used to identify probable hybrid configurations and their applicability. The focus of this preliminary analysis has been on hydrogen-based systems as an emerging technology for use in stand-alone applications in St. John's, Newfoundland. The following conclusions are drawn based on this analysis:

- Wind resources in Newfoundland provide excellent potential compared to solar energy and utilization of solar resources might not be cost effective in most cases.
- At present, a wind-diesel-battery system is the most suitable solution for stand-alone applications. The cost of energy for such a small system in St. John's (delivering 25 kWh/d, peak 4.73 kW), is around \$0.497/kWh.
- With a reduction of fuel cell cost to 65 %, a wind-diesel-fuel cell-battery system would be feasible.

- A wind-fuel cell system would be a more attractive choice if the fuel cell cost reduces to 15 % of its present market price. In such a case, Capital Cost, Net Present Cost and Cost of Energy would be around \$29,475, \$41,425, and \$0.427/kWh, respectively.
- Instead of using single stand-alone units, larger hybrid systems would be cost-competitive for remote communities and the economies of scale might bring down the cost of energy towards the present utility electricity price (\$0.07/kWh).
- Significant advancement in small wind turbine technology and fuel cell research is needed before a wind-fuel cell system could be commercially feasible.

Chapter 3

Modeling of Wind-Fuel Cell Hybrid Energy System

To investigate the performance of a renewable energy based hybrid energy system a thorough review of available resources, operational cost, load demand etc. need to be carried out. Based on this analysis, proper combination of technologies and their sizes could be determined.

In Chapter 2, a pre-feasibility study was carried out to understand the applicability of a wind-fuel cell hybrid energy system to be used in a stand-alone house in St. John's, Newfoundland. It was found that for a 25 kWh/d load having 4.73 kW peak demand, a hybrid system consisting of a wind turbine, PEM fuel cell, hydrogen storage tank and power converters would be suitable in near future. The functions, sizes and numbers of these components are given in Table 3.1.

Table 3.1: Hybrid energy system component sizes and models

<i>Function</i>	<i>Technology</i>	<i>No.</i>	<i>Size</i>	<i>Model Type</i>
Renewable Energy Source (Primary)	Wind Turbine	1	7.5 kW	Bergey Excel-R [42]
Non-Renewable Energy Source (Secondary)	Fuel Cell (PEM)	1	3.5 kW	Ballard MK5-E type [43]
Energy Storage	Electrolyzer	1	7.5 kW	PHOEUBS type [88]
	Hydrogen Tank	1	10 kg	-
Power Converter	Inverter	1	3.5 kW	-

In order to undertake a more realistic modeling approach, a thorough survey was conducted to identify commercially available systems. A wind turbine having similar performance ratings for our requirement was readily available. To date, the fuel cell and electrolyzer industry has not evolved to its fullest potential and very limited models matched the specified ratings. Therefore, variants of experimental prototypes of fuel cell and electrolyzer are considered. Available information from published articles, manufacturer's website and technology reports are consulted in modeling these devices. The model types are given in Table 3.1 and detailed theoretical approach for modeling these components is described in the following sections.

3.1 Wind Energy Conversion Systems (WECS)

A modern day wind turbine captures the kinetic energy available in the wind through an electro-mechanical coupling for generating electricity. In addition to the rotor-generator assembly, a complete wind energy conversion system (WECS) consists of several other mechanisms such as, yaw regulator, speed controller, protection devices, and power converter [48-51].

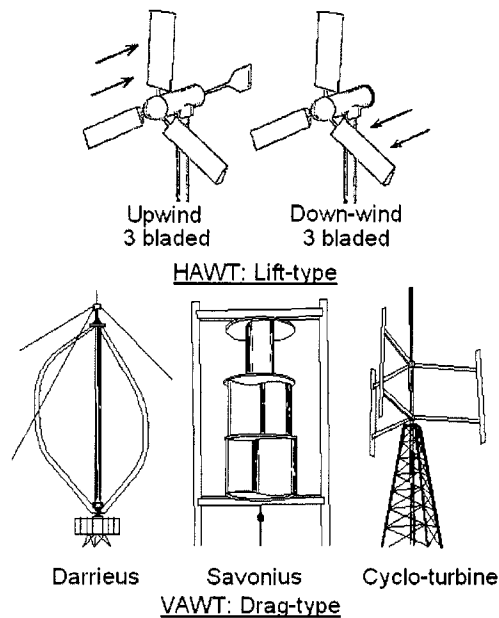


Figure 3.1: Diversity of wind turbine design concepts [50,51]

The history of windmill and wind-pump dates back to 1000 BC and this field of engineering is still evolving very rapidly. Research in wind energy has an elaborate past and requires good understanding of aerodynamics, structural analysis, and electro-mechanics. A wide variety of wind machines having diverse blade configurations, rotor orientations, and designs have been tested. These wind turbines could be classified from many different perspectives. Based on rotor axis orientation, two distinct classes of wind turbines could be found in the literature (Figure 3.1), which are, horizontal axis wind turbines (HAWT) and vertical axis wind turbine (VAWT). To date, the Danish concept of three bladed horizontal-upwind type designs has gained the widest acceptance [48-51].

For efficient operation of a WECS, concepts of stall regulation, pitch control, yaw motion and variable speed operation have emerged. Different safety measures (furling, braking etc.) could also be incorporated in a machine to govern the over-speed characteristics. In a modern day WECS, direct current (DC), synchronous, permanent magnet or induction generators could be used for electro-mechanical energy conversion. Based on turbine size (power or rotor area), two major classes of wind turbines are available in the industry. Typical design and operational characteristics of these two categories are given in Table 3.2.

Table 3.2: Typical aspects of small and large WECS

<i>Criteria</i>	<i>Small WECS</i>	<i>Large WECS</i>
Power	50 W ~ 10 KW	500 KW ~ 4 MW
Diameter	1 ~ 7 m	10 ~ 100 m
Hub-height	~ 30 m	~ 130 m
Control/Regulation	Stall, Yaw, Pitch, Variable speed etc.	Pitch, Constant/Variable speed etc.
Over-speed Protection	Horizontal/Vertical furling	Controlled braking
Generator	DC, Permanent Magnet Alternator	Induction/Synchronous Generator
Application	Stand-alone, Grid connections	Grid connections, Off-shore/Inland

Although a great volume of publications regarding large WECS is available, a systematic approach for modeling, analysis and design of small wind turbines is not abundant. Design of small WECS requires a delicate balance of simplicity of operation, ruggedness in aerodynamic design, and long-term reliability. There exists a great need for sound research, development, and testing toward the success of this technology [6].

In the following section, the dynamic model of a 7.5 kW Bergey Excel-R type wind turbine is formulated. A fuzzy logic controller (FLC) is designed to operate the WECS in varying wind conditions. A dynamic wind field model is considered for emulating realistic wind patterns. The dynamics of the rotor-blade assembly are also taken into account in simplified forms.

3.1.1 Small WECS Systems

Small wind turbines have long been used throughout the world for water pumping and milling. Electricity generation with small turbines came into light around 1980's. In present times, these machines are mostly used in stand-alone mode for battery charging, telecommunication installations, and remote homes. With policy liberalization on net metering, small WECS are also being used for grid supply in many places.

Available power from the wind is proportional to the cube of wind speed, V_{wind} (m.s^{-1}). It also depends on blade swept area and air density.

$$P_{wind} = \frac{1}{2} \rho A_{wt} V_{wind}^3 \quad (3.1.1)$$

where ρ denotes air density ($\sim 1.223 \text{ kg.m}^{-3}$) and A_{wt} is the blade swept area of the wind turbine (m^2).

The maximum useful power that could be extracted by the turbine is limited by a theoretical derivation known as Betz limit. This power coefficient has a constant magnitude, $C_{pb} = 16/27 = 0.5925$. In practice, this factor is much lower and an optimum value of $C_p = 0.45$ could be achieved by well-designed machines. The wind flow in the

atmosphere (V_{wind}) and the effective wind (V_{eff}) that causes the turbine to generate power is slightly different. Therefore, equation (3.1.1) could be modified further, and the extractable aerodynamic power, P_a is written as:

$$P_a = C_p \frac{1}{2} \rho A_{wt} V_{eff}^3 \quad (3.1.2)$$

Small WECS are generally equipped with a down-wind tailfin that pulls the rotor axis into the wind. These turbines also have mechanisms to withstand high winds without causing excessive damage to the mechanical parts. This could be achieved by furling actions. In a furling-type wind turbine, the rotor axis is slightly offset from the tower center. Under normal winds, the rotor is kept into the wind by the tail vane, which is hinged by springs. But, as the wind speed increases the tail starts to fold and wind pushes the rotor around. This furling process starts at rated output and causes the blades to face away from the wind at very high speeds (Figure 3.2).

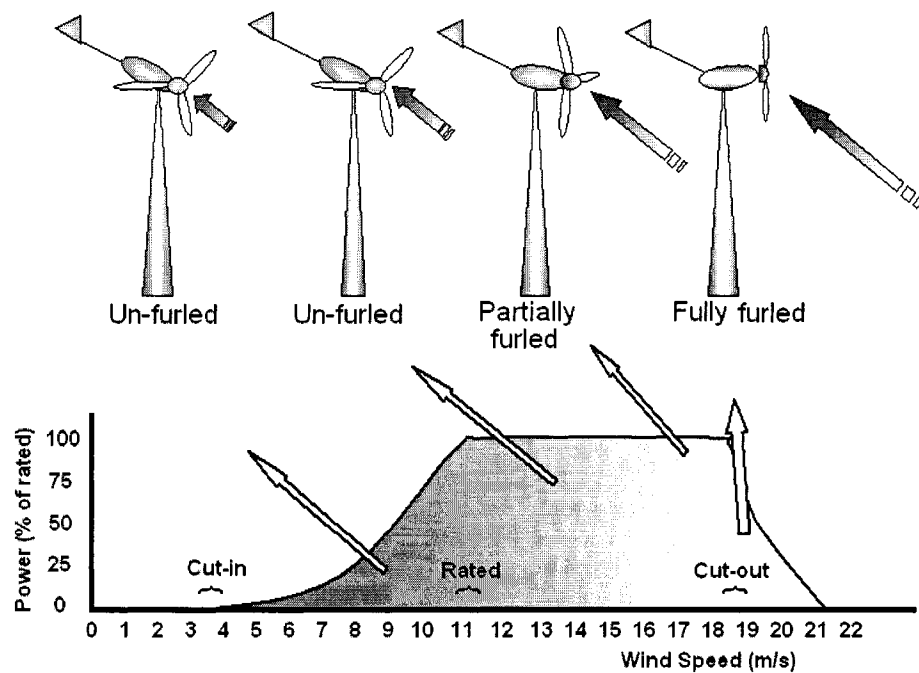


Figure 3.2: Power curve and furling mechanism

The combined action of yawing, furling and variable speed operation allows the turbine to capture useful energy from wind. The power curve of a wind turbine indicates captured power with variations in wind speed (Figure 3.2).

There are four key regions of operation: below cut-in, below rated, rated, and shutdown. At cut-in wind speed the generator starts to generate power and below this speed the turbine's output is barely usable. Rated power is available at near-rated wind speeds. At cut-out wind, the turbine is heavily furling and attempts to face away from the wind for safety reasons [42,48-53]. Survival wind speed is a term generally used to indicate the maximum allowable wind speed beyond which there could be significant damage to the turbine structure.

A search was conducted to identify a commercially available wind turbine, which meets the sizing requirement of the hybrid energy system being investigated. Bergey Wind Power Company's BWC-Excel-R model appeared to be the best match [42]. This is a three-bladed, horizontal upwind model with a permanent magnet alternator. The BWC-Excel wind turbine series is normally rated at 10 kW. For battery charging applications in remote homes, Excel-R model is modified for optimum performance and is rated at 7.5 kW. It has a yaw and passive furling mechanism as found in most other small wind turbines [42,52,53].

Table 3.3: Small wind turbine design parameters (BWC Excel-R type)

<i>Symbol</i>	<i>Parameter</i>	<i>Value</i>	<i>Unit</i>
P_{r_wt}	Wind turbine Rated power	7500	W
P_{max_wt}	Maximum power	8500	W
R_{wt}	Rotor radius	3.2	m
ω_{ro}	Rated rotor speed	32.5	rad.s ⁻¹
V_{cutin}	Cut-in wind speed	3.5	m.s ⁻¹
V_{rated}	Rated wind speed	13.5	m.s ⁻¹
V_{cutout}	Cut-out wind speed	15.5	m.s ⁻¹
V_{surv}	Survival wind speed	55	m.s ⁻¹
λ_o	Optimum TSR	7.5	-
C_{po}	Opt. Power coefficient	0.44	-
V_{to_wt}	Rated terminal voltage	240	V

The wind turbine has a built-in rectifier that could be adjusted for 24 V, 48 V, 120 V or 240 V DC output. Cut-in, rated and cut-out wind speed of this machine are around 3.5, 13.5 and 15.5 m.s⁻¹, respectively.

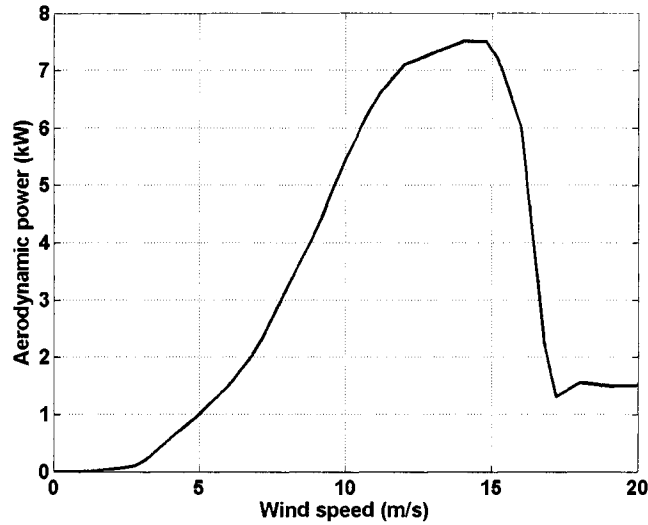


Figure 3.3: Power curve of BWC Excel-R type wind turbine

The essential design parameters, power ratings and operating conditions attributed to a BWC-Excel type wind turbine are given in Table 3.3. The plot of the power curve of such a machine is shown in Figure 3.3. This curve is available from the manufacturer's specifications, which is obtained by averaging experimental data.

3.1.2 Small WECS Model Formulation

In stand-alone applications, a small wind turbine is generally connected in hybrid configuration for parallel operation with other energy source or storage. A controller could adjust the dump load for regulating the rotor speed and maintaining optimum operation. For a DC generator based WECS, a DC-DC power converter is used for interfacing the variable output of the turbine into a common DC bus (Figure 3.4).

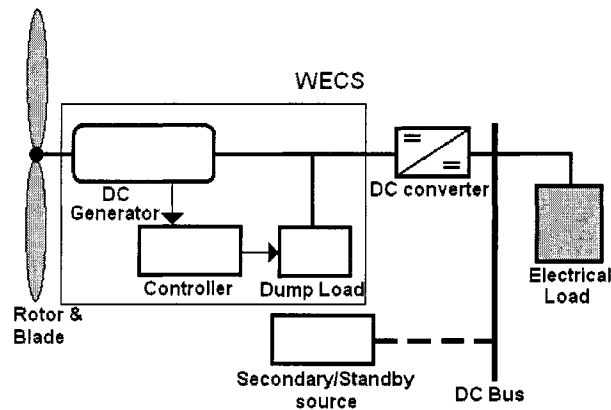


Figure 3.4: Small WECS in a hybrid application

In order to simplify the model formulation of the WECS, several assumptions are made. These considerations are common in various similar analyses [55,56,58-60].

- Perfect yaw regulation and furling mechanism are assumed. This allows the captured power pattern to follow the power curve.
- The turbine is directly driven and no gear coupling is necessary.
- Wind shear effects are not considered.
- No interaction between the drive train and tower dynamics is considered.
- No periodic disturbance due to gravitational force acting on the blades is considered.
- The blade-rotor assembly is considered as a lumped-single mass.
- Instead of a permanent magnet alternator (PMA), a permanent magnet DC (PMDC) generator is considered.
- The rotor torque is estimable by a torque sensor or numerical estimator.

In order to generate realistic patterns of wind variation, a wind field model is considered in this investigation. This wind is further altered to incorporate the wind-rotor interactions. Any rotation of the shaft is converted into electrical output by the permanent magnet DC generator.

3.1.2.1 Wind Field

The variations of wind speed with time are predominantly random. This pattern depends on various factors such as time of day, season, land surface and near by obstacle. Understanding of a wind turbine's performance and design of controller require a realistic set of wind data having random components of wind variation. Such a wind data set generally contains a rapidly varying turbulence component superimposed on a slowly varying mean wind speed [50,51,54].

$$V_{wind} = V_{turb} + V_{avg} \quad (3.1.3)$$

A first order wind model that generates the turbulent component, V_{turb} by filtering random white noise, $m_{wind}(t)$ is given below [55]:

$$\begin{aligned} \frac{dV_{turb}}{dt} &= -\frac{1}{T_v} V_{turb} + m_{wind}(t) \\ T_v &= \frac{10.5z}{V_o} \end{aligned} \quad (3.1.4)$$

The terms z and V_o stand for turbine hub height and median wind speed, respectively. A typical set of data is given in Table 3.4, from which the time constant T_v could be determined.

The addition of average wind, V_{avg} to V_{turb} yields the wind speed having a more realistic time varying pattern. Equation (3.1.3) in conjunction with equation (3.1.4) is used in order to determine the wind speed, V_{wind} .

Table 3.4: Small wind turbine model parameters

<i>Symbol</i>	<i>Parameter</i>	<i>Value</i>	<i>Unit</i>
ρ	Air density	1.223	Kg.m ⁻³
C_{pb}	Betz coefficient	0.5925	-
z	Turbine hub height	30	m
V_o	Median wind speed	7	m.s ⁻¹
a	Spatial filter empirical parameter	0.55	s ⁻¹
V_{wf}	Wind field average wind speed	9.5	m.s ⁻¹
ϕ_d	Decay factor over blade surface	1.3	-
a_i	Induction lag empirical parameter	1.17	-
τ_l	Induction lag time constant	9	s
k	Generator constant	23.31	-
ϕ	Magnetic flux	0.264	V.rad ⁻¹ .s ⁻¹
B	Damping constant	0.025	N.m.rad.s ⁻¹
J	Moment of inertia	2.25	Kg.m ²
L_a	Armature inductance	13.5	mH
R_a	Armature resistance	0.275	Ω
T_r	Rated rotor torque	230.77	N.m
T_{max}	Maximum rotor torque	261.54	N.m
k_T	Controller parameter	0.682	-
k_w	Controller parameter	2.15	-

3.1.2.2 Rotor Aerodynamics

The rotor of the wind turbine experiences a wind variation slightly different from wind measured at the hub height. This may happen due to several filtering effects such as spatial filtering or induction lag filtering.

3.1.2.2.1 Spatial Filtering

Inspected wind at a point on the surface of the blade swept area is different from the actual cumulative effect on the whole rotor plane. A point wind data is essentially averaged over the swept area, which acts as a low-pass filter. A second order model could be used in associating this spatial filtering effect as given in [55]:

$$\frac{V_{filt}}{V_{wind}} = \frac{\sqrt{2} + \beta s}{(\sqrt{2} + \sqrt{a} \beta s) \left(1 + \frac{\beta}{\sqrt{a}} s\right)} \quad (3.1.5)$$

where, β and a are empirical parameters. The constant, β could be determined by the following expression:

$$\beta = \frac{\phi_d R_{wt}}{V_{wf}} \quad (3.1.6)$$

where, V_{wf} is wind field average wind speed for the period of observation, R_{wt} is rotor radius and ϕ_d is a decay factor over the blade surface (Table 3.1.3).

For the wind turbine model under consideration, equation (3.1.5) could be modified for a rotor radius of $R_{wt} = 3.2$ m, and is given in equation (3.1.7):

$$\frac{V_{filt}}{V_{wind}} = \frac{0.43795s + 1.4142}{0.1918s^2 + 1.1598s + 1.4142} \quad (3.1.7)$$

While large turbines have wider blade surface area, small units generally show lower effects of spatial filtering. The parameter values for this model are given in Table 3.4.

3.1.2.2.2 Induction Lag

The phenomenon of induction lag is dominant when the blades react to a sudden change in wind speed. During such a change, the turbines yaw mechanism exhibits over/undershoots. As a result, the rotor experiences a wind speed, V_{eff} , which deviates further from the incident wind and is represented by a transfer function of lag filter [55,63]:

$$\frac{V_{eff}}{V_{flt}} = \frac{a_i s + \frac{1}{\tau_i}}{s + \frac{1}{\tau_i}} \quad (3.1.8)$$

where, a_i is an empirical parameter and τ_i is associated time constant (Table 3.4).

The generated power is dependent on the effective wind speed, V_{eff} , and could be estimated by the power curve (Figure 3.3). Determination of the actual power is computationally demanding and requires an understanding of the interaction between the rotor's aerodynamics, drive train design, wind conditions etc. Although the power curve data is not practically realizable in all operating conditions, this method simplifies the modeling scheme without affecting the observations significantly.

3.1.2.3 Permanent Magnet DC Generator

In a permanent magnet DC generator, the field flux is constant and is provided by the magnet. The speed-voltage term is related through the machine constant and magnetic flux. Based on load current and aerodynamic torque, rotor speed is determined. Equations representing a DC generator are given below [56]:

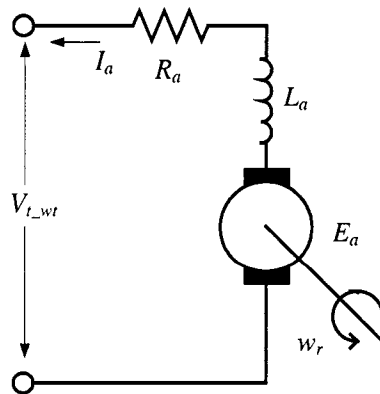


Figure 3.5: Equivalent circuit of a permanent magnet DC generator

$$\begin{aligned}
T_l &= k\phi I_a \\
T_a &= T_l + J \frac{d\omega_r}{dt} + B\omega_r \\
E_a &= k\omega_r \phi \\
V_{t_wt} &= E_a - L_a \frac{dI_a}{dt} - R_a I_a
\end{aligned} \tag{3.1.9}$$

where T_l is load torque (N.m), k is machine constant, I_a is load current, ϕ is field flux ($\text{V}\cdot\text{rad}^{-1}\cdot\text{s}^{-1}$), T_a is aerodynamic torque input to the generator, J is generator moment of inertia ($\text{kg}\cdot\text{m}^2$), ω_r is rotor speed ($\text{rad}\cdot\text{s}^{-1}$), B is damping co-efficient, E_a is generated emf (V), L_a is armature inductance (mH), R_a is armature resistance (Ω), and V_{t_wt} is terminal voltage (V). Associated parameters are given in Table 3.4.

3.1.3 Controller Design

The control problem of the wind energy converter could be defined as follows: at below rated wind speed, (V_{rated}) the control goal is to extract maximum available power. When the wind exceeds cut-out limit (V_{cutout}), decrease of rotor's speed is necessary in order to prevent excessive stress on the machine parts. At intermediate wind speeds ($V_{rated} \leq V_{wind} \leq V_{cutout}$), the controller should maintain constant rated power, P_{r_wt} at the output.

A PD-type fuzzy logic controller (FLC) is employed in this scheme to extract optimum power at various wind speed levels. The key assumption for the controller's operation is that, the rotor torque at any instant could be determined by means of a torque sensor or torque estimator. The rotor torque is employed in generating desired reference rotor speed that would enable optimum power extraction. This reference rotor speed is compared with the actual rotor speed and the controller adjusts a dump load (R_{dump}) using the error signal. Changes in the dump load vary the armature current, I_a as well as the armature torque T_l (Figure 3.5), which sets the rotor speed towards the desired level. The effective power output of the wind turbine, P_{wt} is therefore, the difference of aerodynamic

power input, P_a and dump load dissipation, P_{dump} .

$$P_{wt} = P_a - P_{dump} \quad (3.1.10)$$

The controller design procedure is divided into two steps: determination of reference rotor speed and design of fuzzy logic controller. These procedures are described below.

3.1.3.1 Determination of Reference Rotor Speed

The algorithm for determining reference rotor speed from an estimated/measured rotor torque could be established from the basic principles of wind energy engineering [55,57-63]. The fundamental expression of extractable wind power given in equation (3.1.2) is modified for consideration of the rotor radius.

$$P_a = C_p \frac{1}{2} \rho (\pi R_{wt}^2) V_{eff}^3 \quad (3.1.11)$$

The tip speed ratio (TSR), λ is a measure of the rotor's rotational speed at any given wind speed compared to the wind velocity. This is given by equation (3.1.12).

$$\lambda = \frac{\omega_r R_{wt}}{V_{eff}} \quad (3.1.12)$$

The power coefficient C_p , could be related to another term, namely, torque coefficient C_t by equation (3.1.13).

$$C_p = C_t \lambda \quad (3.1.13)$$

For a given power and rotational speed, the aerodynamic torque input to the system can be found by the equation below:

$$T_a = \frac{P_a}{\omega_r} \quad (3.1.14)$$

Modifying equation (3.1.11) by using equations (3.1.12 to 3.1.14), the following expressions of rotor torque is found [55,57]:

$$T_a = C_t \frac{1}{2} \rho (\pi R_{wt}^3) V_{eff}^2 \quad (3.1.15)$$

$$T_a = C_p \frac{1}{2} \rho (\pi R_{wt}^5) \frac{1}{\lambda^3} \omega_r^2 \quad (3.1.16)$$

Rated rotor torque, T_r and maximum rotor torque, T_{max} could be found by dividing rated power, P_{r_wt} and maximum power, P_{max_wt} (Table 3.4) with rated rotor speed, ω_{ro} , respectively. Assuming the estimated torque, T_a' to be the same as actual rotor torque, T_a three regions of operation are identified as:

$$T_a' < T_r; T_r \leq T_a' < T_{max}; \text{ and } T_a' \geq T_{max}.$$

Various techniques for torque determination, including the use of neural network and Kalman filters in conjunction with observers and estimators are available in the literature [55]. Design of such estimator is beyond the scope of this work and left for later development.

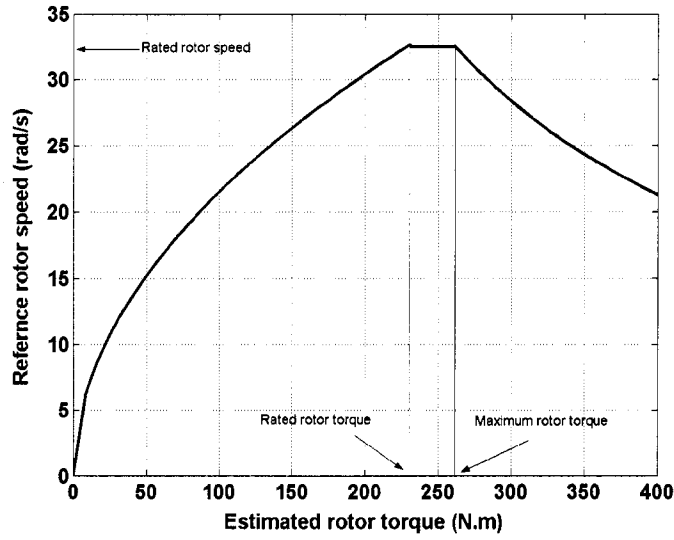


Figure 3.6: Rotor torque and reference rotor speed

At below rated winds ($T_a' < T_r$), the control goal is to extract maximum available power. This is possible when the power co-efficient and tip speed ratio (TRS) both have optimum values, C_{po} and λ_o , respectively. Therefore, equation (3.1.16) yields:

$$T_a' = C_{po} \frac{1}{2} \rho (\pi R_{wt}^5) \frac{1}{\lambda_o^3} \omega_{ref}^2 = k_T \omega_{ref}^2 \quad (3.1.17)$$

Modifying this equation, the below rated reference rotor speed is found as:

$$\omega_{ref} = \sqrt{\frac{T_a'}{k_T}} = k_w \sqrt{T_a'} \quad (3.1.18)$$

where the control parameter k_T (depends on C_{po} and λ_o) and k_w (depends k_T) are given by:

$$k_T = C_{po} \frac{1}{2} \rho (\pi R_{wt}^5) \frac{1}{\lambda_o^3}; k_w = \frac{1}{\sqrt{k_T}} \quad (3.1.19)$$

Using the turbine design parameters from Table 3.3, these controller coefficients could be calculated (Table 3.4).

At intermediate conditions ($T_r \leq T_a' < T_{max}$), the desired rotor speed is considered to be the rated speed. Since the turbine operates in near-rated region and the interval is quite narrow (Figure 3.6), such simplification would induce little error.

$$\omega_{ref} = \omega_{ro} \quad (3.1.20)$$

When the wind speed increases beyond the cut-out ratings and the rotor torque reaches the maximum allowable torque, ($T_a' \geq T_{max}$), the extracted power should be limited to the maximum design limit. In such conditions, the rotor speed and torque should be such that only maximum power, P_{max} could be captured. The reference rotor speed is therefore dependent on rated maximum power and rotor torque, as given in equation (3.1.21)

$$\omega_{ref} = \frac{P_{max_wt}}{T_a'} \quad (3.1.21)$$

Equations (3.1.18), (3.1.20) and (3.1.21) are therefore sufficient to determine the reference rotor speed in all operating regions for use in the controller.

3.1.3.2 Design of Fuzzy Logic Controller

A fuzzy logic controller (FLC) provides a systematic and efficient mean for associating qualitative fuzzy linguistic information for controlling a process by using rules of thumb. Fuzzy controllers are model free and could be employed successfully where system information is insufficient and operational conditions are uncertain [64, 65].

Since the aerodynamics involved with a wind turbine's operation is fairly uncertain and its performance is highly site dependent, a fuzzy controller appears suitable

in such application. Furthermore, variable speed operation as attributed to the turbine under consideration, requires separate sets of control objective. Use of PID type controller would require more than one controller and gain scheduling scheme. However, a PD type FLC used here could operate individually for all ranges and without precise scheduling [58,59,60,62].

Fuzzy set theory originated in an attempt to encounter many uncertain engineering processes [64]. This theory defines an approach for associating logical information available from subjective description or linguistic statements, into numerical values. Design of a fuzzy controller (FLC) involves several steps, such as [62,58,65]:

- *Variable Identification*: Determination of input and output variables.
- *Fuzzification*: Describing system states in terms of fuzzy membership functions
- *Rules of inference*: Establishing relationships between input(s) and output(s)
- *Defuzzification*: Conversion of fuzzy output into crisp values

In order to design a controller for the small wind turbine under investigation, the error, e (difference between reference and actual rotor speed) and rate of change in error de/dt are taken as the inputs to the controller. The value of dump load, R_{dump} , which needs to be added or removed at the turbine's terminal, is the controller output.

$$e(t) = \omega_{ref} - \omega_r$$

$$\frac{de(t)}{dt} = Lt_{\Delta t \rightarrow 0} \frac{e(t) - e(t-1)}{\Delta t} \quad (3.1.22)$$

Fuzzification is done using five Gaussian membership functions for each of the parameters. The inputs are named as NB (negative big), NM (negative medium), ZR (zero), PM (positive medium) and PB (positive big), depending on the magnitude of deviation from zero. Similarly, the output variable is named with following linguistic functions: VL (very low), LO (low), MD (medium), HI (high) and VH (very high).

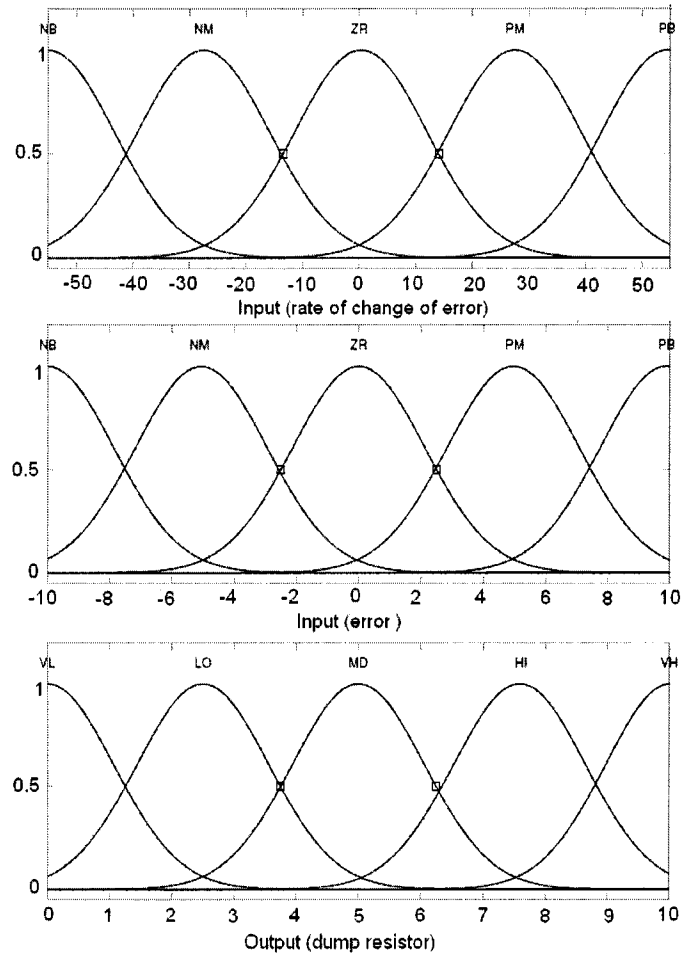


Figure 3.7: Fuzzy variables and membership functions

Fuzzy rules that map the inputs to the output, often called fuzzy associative memory (FAM), are given in Table 3.5. This table introduces the rules of inference and corresponding control surface is shown in Figure 3.8.

Table 3.5: Fuzzy associative memory (FAM)

$e\Delta e$	NB	NM	ZR	PM	PB
NB	VL	VL	LO	LO	MD
NM	VL	LO	LO	MD	HI
ZR	LO	LO	MD	HI	HI
PM	LO	MD	HI	HI	VH
PB	MD	HI	HI	VH	VH

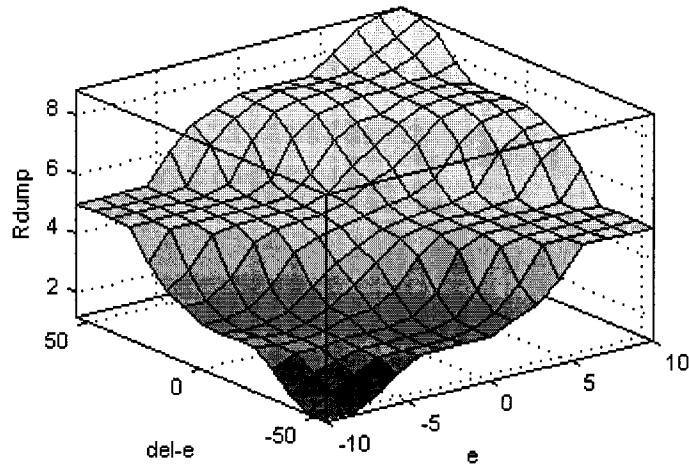


Figure 3.8: Fuzzy rule surface view

Comparing the fuzzified inputs and determining their degree of fulfillment (DOF) for each of the given rules in the FAM, the minimum (AND operation) of an output could be found. This output needs to be defuzzified for having a crisp value. In other words, the defuzzification process converts the results of fuzzy inference into numerical values. The centroid method (Mamdani method) of defuzzification is employed in this analysis [65].

3.1.4 Summary

In this section, a brief overview of various small wind energy conversion technologies is provided. The discussion was extended for dynamic modeling of a commercially available system (BWC Excel-R). Several relevant aspects, such as wind field, rotor aerodynamics, design of controller are also presented. Use of the proposed control algorithm alleviates the need for conventional method of wind speed sensing with anemometers for use in controllers. In other words, it allows a mechanical sensorless control, provided a suitable torque estimation technique is available. A single fuzzy logic controller can be used to control the turbine over a wide range of wind speeds. Such a fuzzy logic controller would be able to maintain rotor speed and output power within

design limits. Further work might include, modeling of PM alternator and design of torque estimator. The wind energy converter model outlined in this section will be integrated into a stand-alone hybrid energy system.

3.2 Fuel Cell System

Fuel cells are electrochemical devices that convert energy contained in a fuel (typically hydrogen) directly into electrical and thermal energy. Higher energy efficiency in cogeneration mode, low emission, good transient response, high scalability, and superior durability are some of the favorable factors towards potential success of this technology. Therefore, in addition to renewable sources (such as, wind, solar and micro-hydro), fuel cell technology has received heightened research focus in recent times. Although, the automobile industry has played a major role in advancing this technology, it is expected that various stationary applications such as remote houses, telecommunication installations, and distributed generators would also benefit from fuel cell research [66,67].

Various types of fuel cells in different stages of development could be found. Proton exchange membrane (interchangeably called polymer electrolyte membrane, PEM) fuel cell uses a solid polymer based ion exchange membrane as the electrolyte. Rapid start-up capability, low operating temperature (50 ~ 90°C), modularity in construction, and higher specific energy have made PEM fuel cells the most promising solution for many mobile and stationary applications [66,67].

Successful implementation of this technology greatly depends on its performance evaluation, design and optimization. Computer based modeling and simulation is an essential first step in that regard. However, a complete mathematical model requires detailed understanding of many physical, electrochemical, thermal and fluid-dynamic issues. Such analyses are generally computationally complex, require a wide range of parameter values and engage high simulation time. For integration of fuel cells with renewable energy sources or vehicle propulsion systems, development of a model that is

sufficiently accurate, mathematically simple, and readily useable, is of great importance. From electrical engineering point of view, a simplified model that could be accessed as a black box for investigating various control and power electronic issues would also prove useful [68,69].

A number of mathematical models of PEM fuel cells are available in the literature. Many of them investigate the fundamental physical interactions outlaying fuel cell behavior [68,71-74]. Attempts in performance analysis with empirical equations in steady state domain have also produced some useful models [69,70,75]. However, optimization of system performance and avoidance of stack degradation require the model to be capable of addressing various dynamic effects including variations of load, reactant flow, cell electrochemistry, and energy balance. For a given load profile, evaluation of need for hydrogen storage devices and interaction with an electrical network also require investigation of fuel cell dynamics. Although a great volume of publications on dynamic modeling of PEM fuel cell could be found [72-74,76,77,80-85,90,91], this issue requires further investigation. For simplicity and reduction of simulation time, empirical models are generally preferable over relatively complicated physical models as found in [72,73,74]. Experimental verification is reported in a limited number of cases [72,76], whereas only experimental results [77-79] or theoretical propositions could be found widely [73,74,80-85,90-91].

An overview of the related literature to date shows that there could be three major issues, which give rise to dynamic phenomena within a fuel cell. These are, dynamics of fuel cell electrochemistry [72,73,74,83,85], thermodynamics [76,82] and reactant flow dynamics [80,81,84,90,91]. An attempt towards unifying these three aspects within one empirical model along with experimental verification is almost non-existent.

A PEM fuel cell empirical model is proposed in this thesis that reflects dynamic features of cell electrochemistry, energy balance and reactant flow. A general steady state model is extended for dynamic electrochemical analysis. Thermal modeling and reactant flow analysis are done for a scaled down model of the well-researched fuel cell stack, Ballard MK5-E [78,79].

3.2.1 PEM Fuel Cell Systems

A PEM fuel cell consists of a membrane-electrode assembly (MEA) where a solid polymeric membrane acting as an electrolyte is pressed between two electrodes (anode and cathode). Each electrode contains platinum or platinum-bearing catalyst layer and a gas diffusion layer (GDL). The MEA is compacted with conductive plates on both sides and there are reactant flow channels within the plates (Figure 3.9). Several cells could be connected in series and a fuel cell stack can be formed to deliver sufficient power.

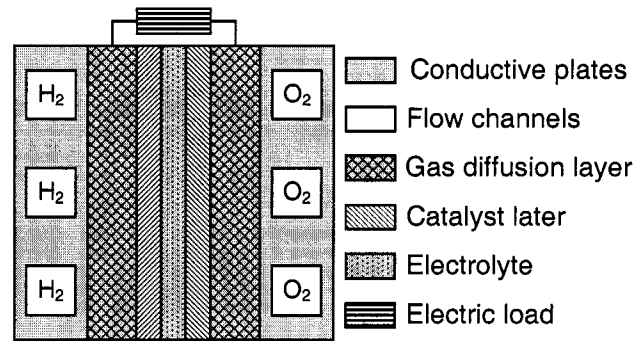


Figure 3.9: Single PEM fuel cell cross sections

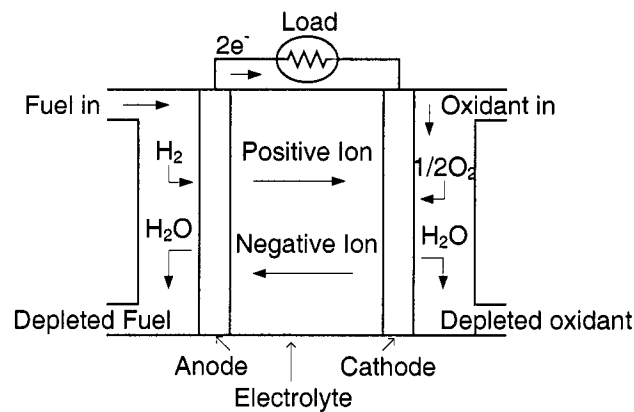
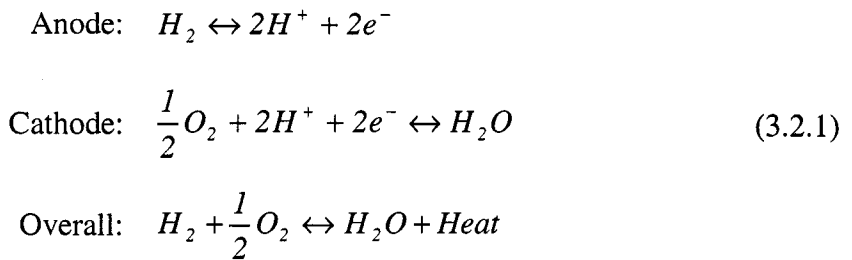


Figure 3.10: Reactions in anode and cathode [66]

Pressurized hydrogen fuel is supplied continuously to the anode and oxygen (or air) is fed to the cathode. The electrochemical reactions take place at the three-phase

interfaces formed between the reactants, electrolyte and catalysts. At the anode, hydrogen flows in the channels and diffuses through the porous electrode into the three-phase interface. Here, hydrogen ions (protons) are generated and carried by the electrolyte membrane towards the cathode interface. Liberated electrons are carried through the load towards the cathode electrode. On the other hand, oxygen at the cathode interface combines with protons (carried through the membrane) and electrons (through the load) to produce water molecules (Figure 3.10). This electrochemical reaction results in DC electricity, water and heat as shown in the equations below [66,67]:



A complete fuel cell system consists of a number of auxiliary devices in addition to the main stack. A fuel processor unit may contain gas reformer, filter, storage tank, humidifier, pressure regulator etc. Similarly, an air supply system may require compressor, expander, filter, flow controller, and humidifier to allow sufficient airflow. Additional mechanisms for coolant flow, thermal management, and water removal are also required [65,66,86].

Fuel cell stacks are very modular in construction and could be reconfigured by addition or removal of single-cell blocks. Since, a 3.5 kW system is required for the analysis in this thesis and to date, most of the research has been focused on the Ballard MK5-E system (5 kW, 35 cells in series), a scaled down model (3.5 kW, 24 cells) is considered here. Associated parameters are tabulated in Table 3.6.

Table 3.6: Fuel cell stack design parameters (Ballard MK5-E type)

<i>Symbol</i>	<i>Parameter</i>	<i>Value</i>	<i>Unit</i>
P_{r_fc}	Rated power	3.5	kW
N_{fc}	Number of cells	24	-
A_{fc}	Cell area	232	cm ²
l_{mem}	Membrane thickness	178	μm

In a Ballard system, dry hydrogen from a pressurized tank is fed to the anode through a pressure regulator that keeps the anode pressure at 3 atm. A mass flow meter records the hydrogen flow rate at the anode and excess gas is re-circulated. Purified air from a compressor is supplied to the anode and a back pressure regulator (BPR) maintains the cathode pressure at 3 atm (Figure 3.11).

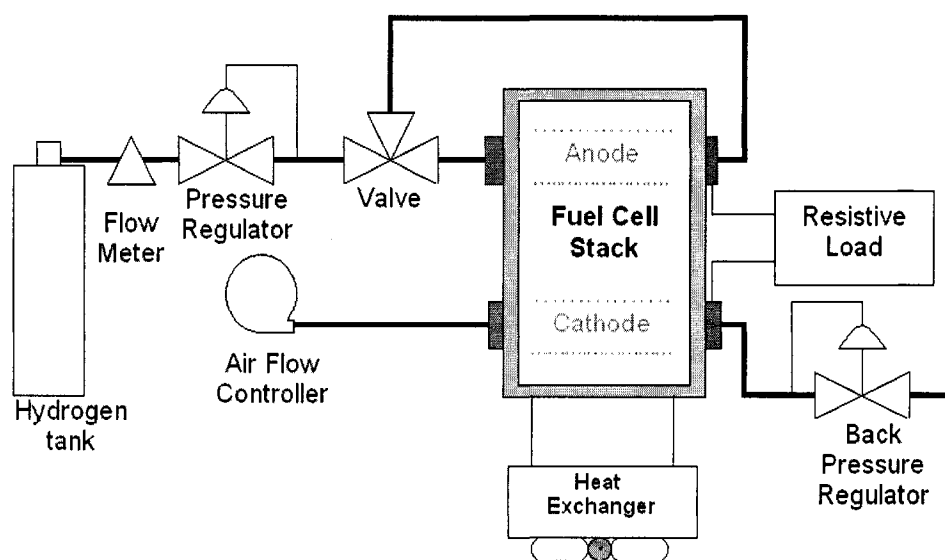


Figure 3.11: Schematic of PEM fuel cell system (Ballard MK5-E type)

The MK5-E system is internally humidified where a circulating water stream keeps the reactants humidified. It also serves the purpose of stack temperature management. The operational stack temperature is around 75°C, minimum stack voltage is around 13 V (0.53 V per cell) and the maximum current is 300 A (1300 mA.cm⁻²) [75,76,78,79,93].

3.2.2 PEM Fuel Cell Model Formulation

The behavior of a PEM fuel cell is highly non-linear and is dependant on a range of factors such as, temperature, reactant pressure, membrane hydration, reactant concentrations, and electrical load. To simplify this analysis, a set of assumptions commonly undertaken in similar studies is also considered here [72,75].

- Reactants are considered as ideal gases
- The reactants are saturated with vapor.
- The membrane is fully saturated with water.
- The reactant partial pressures in the flow channels are dependant on inlet flow rates, consumptions, etc.
- The model is lumped and one-dimensional.
- The system is isothermal and the temperature is uniform throughout the stack.
- The total pressure inside the stack is uniform, whereas variations in reactant partial pressures affect the system.
- Total energy input to the system is dissipated in the load, stack, surface and cooling systems only.

3.2.2.1 Electrochemical Model

Several important steady-state empirical models were developed and reported by Amphlett *et al.* [68,69] and Kim *et al.* [70]. A more recent work by Mann *et al.* [75] has outlined a model that could adequately describe several different types fuel cells. Here, this generalized model is considered and incorporated with dynamic features for developing a basic fuel cell model.

The characteristics of a PEM fuel cell are generally described with polarization curves. The thermodynamic equilibrium potential of hydrogen/oxygen reaction is reduced by various overvoltage terms that depend on different mass transport, kinetic and ohmic

phenomena within the cell. In other words, the output voltage of a single cell is attributed to different current, temperature and pressure dependent factors.

The output voltage of a single fuel cell could be defined by the sum of three voltage terms: thermodynamic potential, E_{Nemst} , activation overvoltage η_{act} , and ohmic overvoltage η_{ohmic} [68,69].

$$V_{cell} = E_{Nemst} + \eta_{act} + \eta_{ohmic} \quad (3.2.2)$$

These two overvoltage terms are both negative and represent non-ideal conditions of fuel cell reaction. A third term (concentration overvoltage) has been used in other studies to consider the effects of mass transport [66,67,70,79]. However, it has been shown that, appropriate parametric modeling with equation (3.2.2) would allow sufficient scope for exhibiting such phenomenon [68,69,71,75].

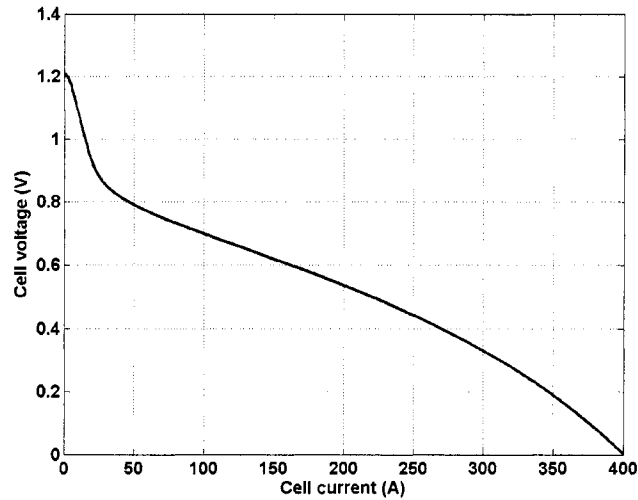


Figure 3.12: Polarization curve of a PEM fuel cell

For N_{fc} number of cells connected in series to form a stack, the total voltage, V_{stack} is given by:

$$V_{stack} = N_{fc} V_{cell} \quad (3.2.3)$$

The total electrical power output of the stack is given as:

$$P_{fc} = V_{stack} I_{fc} \quad (3.2.4)$$

The polarization curve for a fuel cell is shown in Figure 3.12. The sharp voltage drop at low currents is defined as activation overvoltage. The linear drop at intermediate currents is due to ohmic overvoltage and rapid voltage reduction at higher currents is attributed to concentration overvoltage.

3.2.2.1.1 Thermodynamic Potential

The thermodynamic potential or the reversible cell voltage is obtained in the open circuit condition at thermodynamic balance. A modified Nernst equation is used to express this voltage, which is generally termed as Nernst potential. According to the Nernst equation, at standard state (298.15 K, 1 atm), the overall reaction between hydrogen and oxygen within a single cell gives rise to a thermodynamic potential, E_{Nernst} given by equation (3.2.5) [67,68]:

$$E_{Nernst} = E^{\circ} + \frac{RT_{fc}}{nF} \ln \left[p'_{H_2} (p'_{O_2})^{0.5} \right] \quad (3.2.5)$$

where E° represents reference potential at unity activity (1.229 V at standard state), p'_{H_2} , and p'_{O_2} are hydrogen, and oxygen partial pressures (atm), respectively. Here, T_{fc} denotes cell temperature (K), R is the universal gas constant (8.314 J.mol⁻¹.K⁻¹) and F represents the Faraday constant 96485 (C.mole⁻¹).

Deviations from standard conditions could be incorporated within a temperature dependent expression for E° as given in equation (3.2.6) [67,68]:

$$E_{Nernst} = 1.229 - 8.5 \times 10^{-3} (T_{fc} - 298.15) + \frac{RT_{fc}}{2F} \ln \left[p_{H_2}' (p_{O_2}')^{0.5} \right] \quad (3.2.6)$$

In the presence of an electrical path, current flow between the anode and the cathode gives rise to activation and ohmic drops. Therefore, the open circuit voltage reduces by a great extent depending on cell current and operating conditions.

3.2.2.1.2 Activation Overvoltage

The activation overvoltage is predominant at low currents and mostly attributed to cathode reaction. An empirical model reported by in the literature by Amphlett *et al.* is widely used to express this term [68,69,75,76-79].

$$\eta_{act} = \xi_1 + \xi_2 T_{fc} + \xi_3 T_{fc} (\ln(c'_{O_2})) + \xi_4 T_{fc} (\ln(I_{fc})) \quad (3.2.7)$$

where c'_{O_2} is the oxygen concentration at the cathode/membrane interface ($\text{mol}\cdot\text{cm}^{-3}$), I_{fc} is the cell current (A), and $\xi_1 \dots \xi_4$ are parametric coefficients. Although different schemes in determining values of these coefficients have been published, a more generalized steady state model given in [75] is adopted.

$$\begin{aligned} \xi_1 &= -0.948 \\ \xi_2 &= 0.00286 + 0.0002 \ln(A_{fc}) + 4.3 \times 10^{-5} \ln(c'_{H_2}) \\ \xi_3 &= 7.6 \times 10^{-5} \\ \xi_4 &= -1.93 \times 10^{-4} \end{aligned} \quad (3.2.8)$$

where A_{fc} is cell active area (cm^2), and c'_{H_2} is hydrogen concentration at the anode/membrane interface ($\text{mol}\cdot\text{cm}^{-3}$). The reactant concentrations at the

electrode/membrane interfaces could be determined by Henry's law equations (3.2.9, 3.2.10) [69].

$$c'_{o_2} = p'_{o_2} \times 1.97 \times 10^{-7} \exp\left(\frac{498}{T_{fc}}\right) \quad (3.2.9)$$

$$c'_{H_2} = p'_{H_2} \times 9.174 \times 10^{-7} \exp\left(\frac{-77}{T_{fc}}\right) \quad (3.2.10)$$

A dynamic model outlined in [67,73,83] incorporates the effects of charge double layer capacitance with the activation overvoltage term. This results in a first order model where a sudden change in cell current is associated with slower variations in output voltage [67,73,87]. The development of the charge double layer capacitance could be explained with the electric field created at the electrode-electrolyte interfaces due to the flow of protons in one direction. The mobile charges in the electrolyte distribute themselves over this field and the charge density of the electrode is limited within the surface. A circuit model given in Figure 3.13 could realize this capacitive effect.

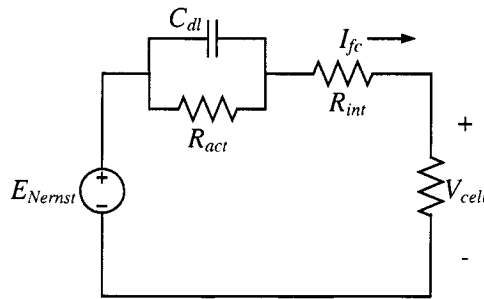


Figure 3.13: Circuit model of a single cell

For a given cell current, the activation voltage drop could be considered across an activation resistance, R_{act} . The activation voltage term, η_{act} introduced in equation (3.2.2) has a negative value. By negating this term, a positive activation voltage, V_{act} is found,

which is used for obtaining the activation resistance, R_{act} . Equations (3.2.11-3.2.13) could describe the first order dynamics of the activation overvoltage term in reference to the equivalent circuit model shown in Figure 3.13.

$$V_{act} = -\eta_{act} \quad (3.2.11)$$

$$R_{act} = \frac{V_{act}}{I_{fc}} \quad (3.2.12)$$

$$\frac{dV_{act}}{dt} = \frac{I_{fc}}{C_{dl}} - \frac{V_{act}}{R_{act}C_{dl}} \quad (3.2.13)$$

The term C_{dl} denotes the double layer capacitance of a single cell (F). Quantitative analysis in determining its value for a PEM fuel cell is rare. A wide range of values (0.013 F.cm⁻² to 0.042 F.cm⁻²) could be found in literature [72,80]. Therefore, an intermediate value is chosen and given in Table 3.7.

3.2.2.1.3 Ohmic Overvoltage

The ohmic voltage drop in a PEM fuel cell might arise due to various reasons, such as, contact potential, and electrode and membrane resistances. However, accurate measurement of these parameters is generally difficult and an empirical approach is preferred. The membrane's resistance to proton conduction is considered to be the most dominant ohmic component [71,72,75,90]. The ohmic overvoltage term in equation (3.2.2) is given by:

$$\eta_{ohmic} = -I_{fc}R_{int} \quad (3.2.14)$$

where R_{int} is the internal resistance (Ω) attributed to the electrolyte membrane. Taking r_M as the membrane resistivity (Ω .cm), the internal resistance is expressed as [75]:

$$R_{int} = \frac{r_M l_{mem}}{A_{fc}} \quad (3.2.15)$$

where l_{mem} is the membrane thickness (cm) and A_{fc} is the effective cell area (cm²). An empirical expression for determining the membrane resistivity for Nafion™ membranes is opted for this analysis [75].

$$r_M = \frac{181.6 \left[1 + 0.03 \left(\frac{I_{fc}}{A_{fc}} \right) + 0.062 \left(\frac{T_{fc}}{303} \right)^2 \left(\frac{I_{fc}}{A_{fc}} \right)^{2.5} \right]}{\left[\lambda_{mem} - 0.634 - 3 \left(\frac{I_{fc}}{A_{fc}} \right) \right] \exp \left[4.18 \left(\frac{T_{fc} - 303}{T_{fc}} \right) \right]} \quad (3.2.16)$$

The term λ_{mem} is considered as a function of membrane humidity, stoichiometric ratio of anode inlet gas, time in service and other factors. It could take values ranging from 10 to 23. However, to simplify the analysis a mean value is chosen here (Table 3.7), as done in similar other studies [75,83].

Equations (3.2.6) to (3.2.16) could be solved to determine different voltage terms for use in equation (3.2.2). The stack voltage can then be determined by a straight multiplication of cell voltage with the total number of cells as shown in equation (3.2.3).

Table 3.7: Fuel cell model parameters

Symbol	Parameter	Value	Unit
E^o	Reference potential at unity activity	1.229	V
R	Universal gas constant	8.314	J.mole ⁻¹ .K ⁻¹
F	Faraday constant	96485	C.mole ⁻¹
C_{dl}	Double layer capacitance	0.035×232	F
λ_{mem}	Membrane resistivity parameter	12.5	-

The dynamic model for a PEM fuel cell electrochemistry described in this section is based on a generalized empirical set of equations. It is expected that, this model would be useful in analyzing different types of PEM fuel cells. Therefore, by identifying appropriate parameters (such as, cell numbers, cell area, membrane thickness, etc.) fuel cells with varying sizes, structures, and materials can also be modeled and relevant dynamics could be studied.

3.2.2.2 Thermal Model

The performance of a fuel cell is greatly dependent on stack temperature. Higher temperature levels generally shift the polarization curve (Figure 3.12) upwards. On the other hand, too high temperature may cause membrane dehydration and stack degradation. Therefore, maintaining a reasonable temperature is vital for achieving optimum performance. In externally cooled fuel cell systems, this is done by controlled coolant flow with external means. In other units, the thermal management could be done internally, where a controller sets the cooling water flow at certain specified conditions (such as, Ballard MK5-E with PGS-105B control and monitoring system). In a PEM fuel cell system, stack temperature is generally kept below 80°C. Changes in electrical load greatly affect the operating temperature. An increase in load current is associated with higher power dissipation within the stack and subsequent temperature elevation.

Several thermal modeling schemes with varying levels of difficulty have been reported [76,79,82]. A mathematical analysis and its experimental verifications could be found in [76]. Although this model shows good correlations with actual data, it requires a wide range of parameter values (flow rates of reactants and water, inlet-outlet temperature, anode-cathode operating condition parameters). Other simpler models are not adequately compared with experimental results [79,82] leaving scope for further analysis. In this thesis, a simpler model is given. Unlike electrochemical modeling of a single fuel cell, thermal modeling is generally done for a lumped system.

The total energy delivered by the inlet hydrogen into a fuel cell stack could be used up in four different methods. These are, consumption by electrical load, heat removal by coolant, heat loss at the surface, and absorption by the stack (Figure 3.14).

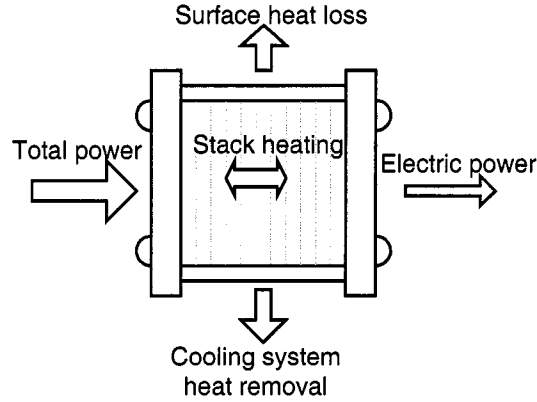


Figure 3.14: Energy balance model for a PEM fuel cell stack

The electrical power delivered to the load is the effective output (unless exhaust heat is used by additional mechanisms), whereas heat absorbed by the system causes rise in stack temperature. Considering a lumped model, the system temperature could be related to the heat absorbed by the stack with a first order differential equation [88,93].

$$C_{t_fc} \frac{dT_{fc}}{dt} = \dot{Q}_{stack_fc} \quad (3.2.17)$$

where C_{t_fc} is the thermal capacitance ($\text{kJ} \cdot \text{°C}^{-1}$), T_{fc} is the stack temperature in °C and \dot{Q}_{stack_fc} is heat absorption rate ($\text{J} \cdot \text{s}^{-1}$) by the stack. Considering the energy balance between different methods of dissipation outlined above, this equation is modified further.

$$C_{t_fc} \frac{dT_{fc}}{dt} = P_{tot_fc} - P_{fc} - \dot{Q}_{cool_fc} - \dot{Q}_{loss_fc} \quad (3.2.18)$$

In equation (3.2.16), P_{tot_fc} is the total power delivery into the stack (W), P_{fc} is the power consumption by electrical load (W), \dot{Q}_{cool_fc} is the heat flow rate for cooling methods ($J.s^{-1}$), and \dot{Q}_{loss_fc} is the heat flow rate through the stack surface ($J.s^{-1}$).

The total power input to the stack is directly related to the amount of hydrogen consumed. Since, hydrogen consumption is dependent on the stack current and number of cells, the following expression is used to determine total power input:

$$P_{tot_fc} = \dot{m}_{H_2\ used} \Delta H = \frac{N_{fc} I_{fc}}{2F} \Delta H \quad (3.2.19)$$

where, ΔH is the hydrogen enthalpy of combustion ($285.5 \text{ kJ.mol}^{-1}$), $\dot{m}_{H_2\ used}$ is the rate of hydrogen consumption (mol.s^{-1}).

The rate of heat removal by the cooling water could be related to the surface area of the heat exchanger and log mean temperature difference (LMTD) between the stack and inlet/outlet cooling water [87].

$$\dot{Q}_{cool_fc} = UA_{HX_fc} LMTD_{fc} = UA_{HX_fc} \frac{(T_{fc}' - T_{cw,in}) - (T_{fc}' - T_{cw,out})}{\ln\left(\frac{T_{fc}' - T_{cw,in}}{T_{fc}' - T_{cw,out}}\right)} \quad (3.2.20)$$

The parameter UA_{HX_fc} is a measure of the exchanger size ($W.^{\circ}C^{-1}$), whereas $T_{cw,in}$ and $T_{cw,out}$ are the inlet and outlet water temperatures ($^{\circ}C$), respectively. An empirical formula used in [87] is opted to determine the value of UA_{HX_fc} .

$$UA_{HX_fc} = h_{cond_fc} + h_{conv_fc} I_{fc} \quad (3.2.21)$$

where h_{cond_fc} and h_{conv_fc} are parameters to characterize conduction and convection properties of the heat exchangers having units of $W.^{\circ}C^{-1}$ and $W.^{\circ}C^{-1}.A^{-1}$, respectively. The stray heat loss by the surface of the stack is proportional to the stack temperature and the ambient temperature.

$$\dot{Q}_{loss_fc} = \frac{T_{fc}' - T_{amb}}{R_{t_fc}} \quad (3.2.22)$$

Table 3.8: Parameters for the thermal model of Ballard MK5-E type system

<i>Symb.</i>	<i>Parameter</i>	<i>Value</i>	<i>Unit</i>
ΔH	Hydrogen enthalpy of combustion	285.5	$kJ.mol^{-1}$
$T_{cw,in}$	Inlet cooling water temperature	25	$^{\circ}C$
$T_{cw,out}$	Outlet cooling water temperature	30	$^{\circ}C$
T_{amb}	Ambient temperature	25	$^{\circ}C$
h_{cond_fc}	Heat exchanger conduction index	35.55	$W.^{\circ}C^{-1}$
h_{conv_fc}	Heat exchanger convection index	0.025	$W.^{\circ}C^{-1}.A^{-1}$
MC	Product of stack mass and average specific heat	35	$kJ.K^{-1}$
hA	Stack heat transfer coefficient	17	$W.K^{-1}$
R_{t_fc}	Thermal resistance	0.115	$^{\circ}C.W^{-1}$
C_{t_fc}	Thermal capacitance	17.9	$kJ.^{\circ}C^{-1}$
τ_{fc}	Time constant	2059	s

In equation (3.2.20), R_{t_fc} is the thermal resistance of the stack ($^{\circ}C.W^{-1}$), and T_{amb} is the ambient temperature ($^{\circ}C$). The product of thermal resistance and thermal capacitance determine the time constant associated with equation (3.2.18). This is given by,

$$\tau_{fc} = R_{t_fc} C_{t_fc} = \frac{MC}{hA} \quad (3.2.23)$$

where, MC is the product of stack mass and average specific heat (kJ.K^{-1}) and hA is the stack heat transfer coefficient (W.K^{-1}). A quantitative estimation of these parameters for the Ballard MK5-E system is outlined in [76] and is given in Table 3.8. Choosing $R_{t_fc} = 0.115$, C_{t_fc} is determined from equation (3.2.23).

Equations (3.2.19-3.2.23) are solved and various heat flow rate/power terms are determined for use in equation (3.2.18), which expresses the dynamic variation of stack temperature.

3.2.2.3 Reactant Flow Model

Reactant flow rates at the anode and cathode along with the magnitude of stack current determine the effective partial pressure of hydrogen and oxygen. From an analytical point of view, an increase in fuel cell current would be associated with elevated level of hydrogen and oxygen consumption. This in turns implies a reduction in reactant pressure. Fuel cell systems come with different flow regulation and control mechanisms. The operation of the Ballard MK5-E system is discussed in section 3.2.1 and is considered here for further modeling.

Based on the ideal gas law ($PV = nRT$), and the principle of mole conservation, the partial pressure of each gas is obtained using the methods outlined in [80,81,84,89-93]. Reactant pressure at any instance is proportional to the amount of gas inside the stack, which is equal to the gas inlet flow rate minus gas outlet flow rate and gas usage. For the anode this is expressed by equation (3.2.24):

$$\frac{V_a}{RT_{fc}} \frac{d p'_{H_2}}{dt} = \dot{m}_{H_2,in} - \dot{m}_{H_2,out} - \dot{m}_{H_2,used} \quad (3.2.24)$$

where V_a is anode volume (m^3), $\dot{m}_{\text{H}_2,\text{in}}$, and $\dot{m}_{\text{H}_2,\text{out}}$ are hydrogen inlet and outlet flow-rates (mol.s^{-1}), respectively. Since, total hydrogen usage is related to the number of cells and stack current, this equation is modified further:

$$\frac{V_a}{RT_{fc}} \frac{d p'_{\text{H}_2}}{dt} = \dot{m}_{\text{H}_2,\text{in}} - \dot{m}_{\text{H}_2,\text{out}} - \frac{N_{fc} I_{fc}}{2F} \quad (3.2.25)$$

The anode of the Ballard system is supplied with pure hydrogen (99.99%) from a storage tank. A pressure regulator regulates hydrogen pressure and excess hydrogen is re-circulated to the anode. The difference between hydrogen partial pressure and downstream pressure (regulated pressure) is related to the molar outlet flow rate as shown in [80,81,84]:

$$\dot{m}_{\text{H}_2,\text{out}} = k_a (p'_{\text{H}_2} - p_{\text{tank}}) \quad (3.2.26)$$

where k_a is a flow constant for the anode ($\text{mol.s}^{-1}.\text{atm}^{-1}$). The inlet flow rate $\dot{m}_{\text{H}_2,\text{in}}$ is determined by a model of a regulator or controller that takes hydrogen partial pressure as the feedback parameter and tank pressure as the reference. Using equations (3.2.24-3.2.25), the hydrogen partial pressure for a given load and temperature is found.

Similar modeling method is undertaken for the cathode. Cathode mole conservation equation is given as:

$$\frac{V_c}{RT_{fc}} \frac{d p'_{\text{O}_2}}{dt} = \dot{m}_{\text{O}_2,\text{in}} - \dot{m}_{\text{O}_2,\text{out}} - \dot{m}_{\text{O}_2,\text{used}} \quad (3.2.27)$$

where V_c is cathode volume (m^3), $\dot{m}_{\text{O}_2,\text{in}}$, and $\dot{m}_{\text{O}_2,\text{out}}$ are oxygen inlet and outlet flow-rates (mol.s^{-1}), respectively.

Relating total oxygen consumption to the number of cells and stack current, this equation is modified further:

$$\frac{V_c}{RT_{fc}} \frac{d p'_{o_2}}{dt} = \dot{m}_{o_2, in} - \dot{m}_{o_2, out} - \frac{N_{fc} I_{fc}}{4 F} \quad (3.2.28)$$

The cathode of the system under consideration has a back pressure regulator that keeps oxygen pressure at the outlet at a pre-defined level. The difference between oxygen partial pressure inside the stack and downstream pressure (regulated pressure) could be related to the molar outlet oxygen flow rate as shown in the following equation:

$$\dot{m}_{o_2, out} = k_c (p'_{o_2} - p_{BPR}) \quad (3.2.29)$$

where k_c is the flow constant for the cathode ($\text{mol.s}^{-1}.\text{atm}^{-1}$). The inlet oxygen flow rate, $\dot{m}_{o_2, in}$ could be determined by multiplying the air inlet flow rate with the mole fraction of oxygen in air (21%).

Table 3.9: Parameters for the reactant flow models

<i>Symb.</i>	<i>Parameter</i>	<i>Value</i>	<i>Unit</i>
V_a	Anode volume	0.005	m^3
k_a	Anode flow constant	0.065	$\text{mol.s}^{-1}.\text{atm}^{-1}$
V_c	Cathode volume	0.01	m^3
k_c	Cathode flow constant	0.065	$\text{mol.s}^{-1}.\text{atm}^{-1}$
$p_{in,k}$	Hydrogen pressure at the inlet	3	atm
p_{BPR}	Oxygen pressure at the outlet	3	atm
p_{refO_2}	Reference oxygen pressure	3	atm
K_{pfc}	Air flow controller proportional gain	750	-
K_{dfc}	Air flow controller differential gain	0	-
K_{ifc}	Air flow controller integral gain	250	-

Solving equations (3.2.27-3.2.29), the oxygen partial pressure at any instance is calculated for a given air inlet flow rate, temperature and stack current. A thorough search for suitable parameters for the Ballard system's reactant flow model did not yield much success. Therefore, some values were chosen from other similar articles [81,90,91] and a few were assumed. These parameters are listed in Table 3.9.

3.2.2.4 Air Flow Controller

In order to ensure proper and safe operation of a PEM fuel cell system, both hydrogen fuel and air need to be pressurized at an optimum level. Higher operating pressure generally increases the overall efficiency and elevated output voltage level. On the other hand, construction of the stack limits high reactant pressures and power consumption of an air compressor impacts negatively on the system efficiency [89-91].

With variations in fuel cell current, the reactant pressures may change significantly. In the Ballard MK5-E type system, hydrogen pressure is regulated at the input by a pressure regulator. The air flow at the cathode is controlled by a mass flow controller. Since the hydrogen is supplied from a pressurized tank, no provision for hydrogen flow control is given. However, to ensure proper stoichiometry of oxygen at the cathode, a PID type controller in the air flow system is considered in this analysis [94]. In addition to a back pressure regulator at the cathode output, this controller attempts to regulate sudden changes in oxygen pressure by adjusting the air flow rate.

$$\frac{\dot{m}_{o_2, in}(s)}{e_{p_{o_2}}(s)} = \frac{K_{pfc}s + K_{dfc}s^2 + K_{ifc}}{s} \quad (3.2.30)$$

$$e_{p_{o_2}}(t) = p_{ref_{o_2}} - p'_{o_2}(t)$$

where $e_{p_{o_2}}$ is the error in oxygen pressure (difference of reference and actual oxygen pressure) and K_{pfc} , K_{dfc} , K_{ifc} are controller gains (Table 3.9).

3.2.3 Summary

In this section, the modeling of a polymer electrolyte membrane (PEM) fuel cell system with relevant dynamics is discussed. The analysis is based on empirical equations and fundamental physical relationships. It reflects various features arising from transients in cell electrochemistry, energy balance and reactant flow. A scaled-down model similar to the Ballard MK5-E fuel cell is considered for emulating the operation of a practical system. Published experimental results have shown a good match with the proposed model. The verifications of the model with test results are expected to appear in [95]. This model is studied for system design, integration and performance evaluation of the wind-fuel cell hybrid energy system. Further simplification, generalization, system-independent modeling would be useful in analyzing the operation of different types of fuel cell systems with varying size, structure, and component.

3.3 Electrolyzer

In a hybrid energy system, the excess energy from the renewable source is used in hydrogen production for later use by the fuel cell stack. With electrical energy and pure water as input, an electrochemical device named electrolyzer could decompose water into hydrogen and oxygen. The characteristic of an electrolyzer is broadly conceived as opposite to that of a fuel cell system. However, from constructional and operational point of view, these two technologies have several distinct attributes.

An electrolyzer is a vital part in the concept of hydrogen fueling stations for electric vehicles. Commercial production of hydrogen may find application in many other areas such as synthetic fuel manufacturing, and heating or power plant operations. The issue of small-scale hydrogen production in remote applications has not received enough attention mainly due to high investment cost. However, research in large-scale electrolyzer technology has gained substantial momentum and is expected to evolve further into low-cost small-sized units [96-99].

Electrolysis of water is done in many different methods such as, alkaline, PEM, acidic, high temperature, thermochemical, photochemical, photoelectrochemical or biochemical electrolysis. Although the PEM technique is being considered for an alternative solution (reversible fuel cell) [96], most of the available systems are of alkaline type. Therefore, in this analysis, further discussion is done with alkaline electrolyzers.

In this section, the dynamics of an alkaline electrolyzer are discussed. Steady state electrochemical features are expressed through empirical equations and these are coupled with a dynamic thermal model. This model is a scaled-down version of the PHOEBUS electrolyzer reported in [88] and relevant modifications are discussed in the following sections.

3.3.1 Alkaline Electrolyzer Systems

The electrolyte used in an alkaline electrolyzer is typically aqueous potassium hydroxide (KOH). A stack consists of several cells and needs a DC power source. At the anode, hydroxide ions are converted into gaseous oxygen and liquid water. Liberated electrons at the anode are carried through the DC source into the cathode. Liquid water at the cathode combines with these electrons and forms hydrogen gas. The newly formed hydroxide ions at the cathode reaction are carried towards the anode through the electrolyte (Figure 3.15).

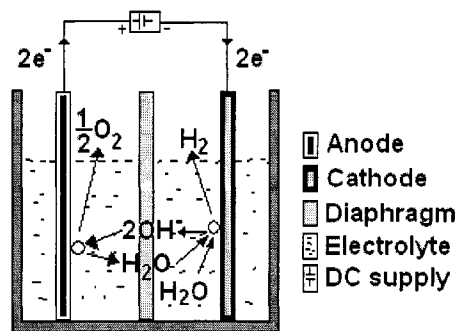
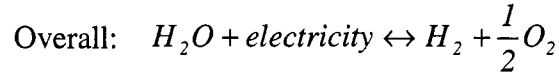
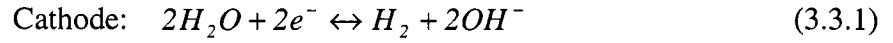
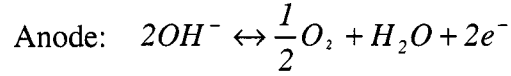


Figure 3.15: Single cell reaction in an alkaline electrolyzer

The electrochemical reactions for an alkaline electrolyzer are given as:



A complete electrolyzer stack consists of several auxiliary devices such as heat exchanger, flow separator, compressor and storage tank (Figure 3.16). However, modeling of all of these components is not carried out and only the electrolyzer stack is considered in this thesis.

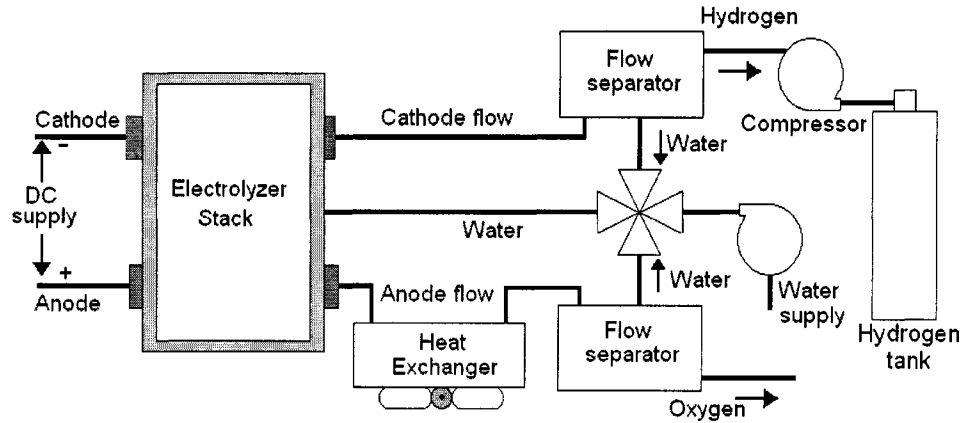


Figure 3.16: Schematic of an electrolyzer system

Since electrolyzers are constructed in a modular manner, the size of a stack can be modified by addition or removal of single cells. For the hybrid energy system being modeled, a 7.5 kW unit is necessary and literature regarding such a system is unavailable. Here a modified model of the PHOEBUS electrolyzer (26 kW, 26 cells) investigated in [88] is considered. This prototype is an advanced type of alkaline electrolyzer having low voltage-high current relationship.

Table 3.10: Alkaline electrolyzer design parameters (PHOEBUS type).

<i>Symbol</i>	<i>Parameter</i>	<i>Value</i>	<i>Unit</i>
P_{r_elz}	Electrolyzer rated power	7.5	kW
N_{elz}	Number of cells in electrolyzer stack	6	-
A_{elz}	Electrode area	0.25	m ²

The electrolyte (KOH) concentration inside the cell is about 30% wt. and operating pressure and temperature is 7 atm and 80°C, respectively. Several design specifications of this system are given in Table 3.10.

3.3.2 Alkaline Electrolyzer System Model Formulation

The electrolyzer model is composed of an electrochemical analysis followed by a dynamic energy balance formulation. To maintain an overall simplicity without affecting the results significantly, several assumptions are made.

- Hydrogen and oxygen gasses are assumed to be ideal.
- Water is incompressible.
- Gas/liquid phases are separable.
- The stack is a lumped unit having isothermal characteristics.
- Total energy input to the system is dissipated in the stack, surface and cooling systems only.

3.3.2.1 Electrochemical Model

The basic current-voltage relationship of a cell can be derived from the fundamentals of thermodynamic analysis. The plot of I-V curve is given in Figure 3.17 and the cell voltage, U_{cell} can be expressed as a function of current and other variables as found in [19,88,98]:

$$U_{cell} = U_{rev} + \frac{r_1 + r_2 T_{elz}}{A_{elz}} I_{elz} + s \log \left(\frac{t_1 + t_2 / T_{elz} + t_3 / T_{elz}^2}{A_{elz}} I_{elz} + I \right) \quad (3.3.2)$$

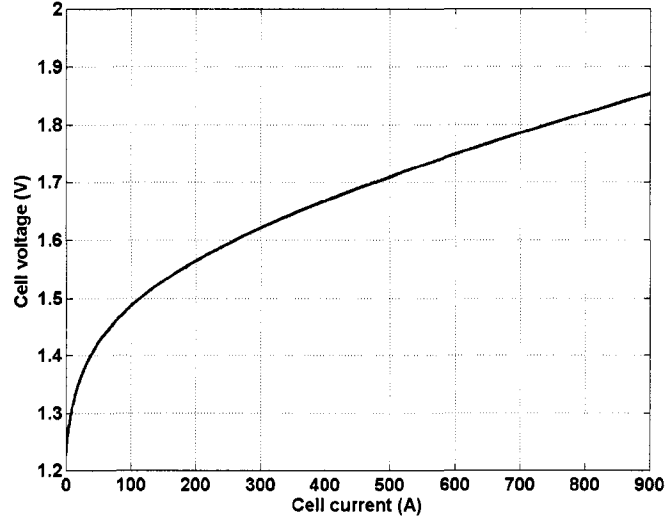


Figure 3.17: Current-voltage characteristics of an electrolyzer cell

where U_{rev} is the reversible cell potential, A_{elz} is the electrode surface area, T_{elz} electrolyzer temperature and I_{elz} is electrolyzer current. Here, $r_1, r_2, s, t_1, t_2,$ and t_3 are empirical parameters and their values are listed in Table 3.11.

The ratio of actual to theoretical hydrogen production by an electrolyzer is termed as Faraday efficiency. The loss in hydrogen production is related to parasitic current flow and an empirical formula is considered in that regard.

$$\eta_F = \frac{(I_{elz} / A_{elz})^2}{f_1 + (I_{elz} / A_{elz})^2} f_2 \quad (3.3.3)$$

In equation (3.3.3), η_F is the Faraday efficiency, and f_1, f_2 are empirical parameters related to Faraday efficiency term. These parameters are approximated as linear functions of stack temperature and are found from [88]:

$$\begin{aligned} f_1 &= 2.5T_{elz} + 50 \\ f_1 &= -0.00075T_{elz} + 1 \end{aligned} \quad (3.3.4)$$

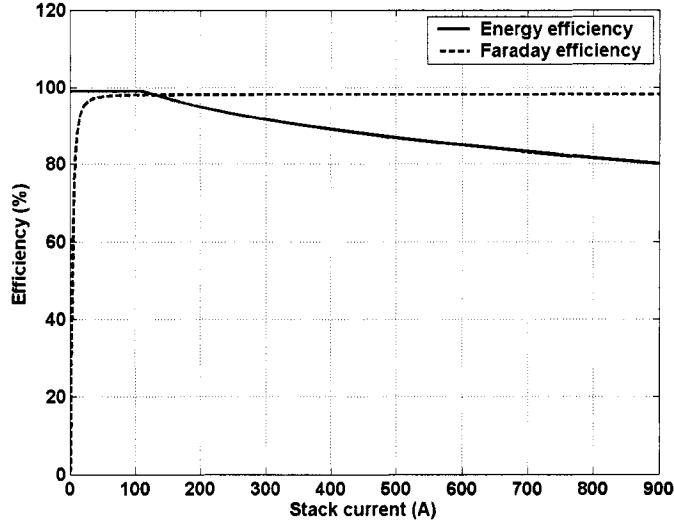


Figure 3.18: Efficiency parameters of an electrolyzer stack

Following Faraday's law of electrolysis, the hydrogen production rate is directly related to the magnitude of current flow and number of cells in the stack. Since, there is a loss associated with this current flow, the Faraday efficiency term is also associated in determining the rate of hydrogen production. The hydrogen flow rate is found by equation (3.3.5):

$$\dot{n}_{H_2} = \eta_F \frac{N_{elz}}{zF} I_{elz} \quad (3.3.5)$$

Another term indicating overall efficiency of the system is named as energy efficiency (Figure 3.18) and is given by the following equation:

$$\eta_e = \frac{U_m}{U_{cell}} \quad (3.3.6)$$

Here, U_m is the thermoneutral cell potential and U_{cell} is the cell voltage at any instance. The total power consumed by the electrolyzer is given as:

$$P_{elz} = N_{elz} U_{cell} I_{elz} \quad (3.3.7)$$

Table 3.11: Electrolyzer electrochemical model parameters

<i>Symb.</i>	<i>Parameter</i>	<i>Value</i>	<i>Unit</i>
U_{rev}	Reversible cell voltage	1.229	V
U_m	Thermo-neutral cell voltage	1.482	V
r_1	Parameter related to ohmic resistance	8.05×10^{-5}	$\Omega \cdot m^2$
r_2	Parameter related to ohmic resistance	-2.5×10^{-7}	$\Omega \cdot m^2 \cdot ^\circ C^{-1}$
s	Coefficient of overvoltage on electrode	0.185	V
t_1	Overyoltage coefficient	-0.1002	$A^{-1} \cdot m^2$
t_2	Overyoltage coefficient	8.424	$A^{-1} \cdot m^2 \cdot ^\circ C$
t_3	Overyoltage coefficient	247.3	$A^{-1} \cdot m^2 \cdot ^\circ C^2$
z	Number of electrons transferred per reaction	2	-
F	Faraday constant	96485	$C \cdot mole^{-1}$

The set of steady-state equations (3.3.2-3.3.7) described in this section allows one to determine the stack voltage, hydrogen production rate, and efficiency for a given operating condition.

3.3.2.2 Thermal Model

The thermal model described here follows similar thermodynamic analysis given in the fuel cell model (section 3.2.2.2). The generated heat within the stack is dissipated in three different ways. A portion of the heat is removed by the cooling system and surface losses. The remaining energy is used for stack heating. This distribution could be expressed by the following energy balance equation:

$$\dot{Q}_{gen_elz} = \dot{Q}_{stack_elz} + \dot{Q}_{cool_elz} + \dot{Q}_{loss_elz} \quad (3.3.8)$$

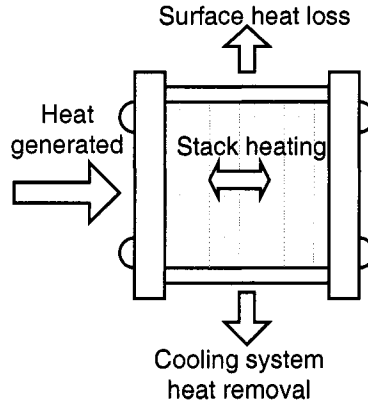


Figure 3.19: Electrolyzer energy balance

Assuming the system to be a lumped isothermal model, the heat capacity of the stack is used in the first order differential equation to relate electrolyzer temperature with the rate of heating [19,88,93]:

$$C_{t_elz} \frac{dT_{elz}}{dt} = \dot{Q}_{stack_elz} \quad (3.3.9)$$

where C_{t_elz} is the electrolyzer thermal capacitance ($\text{kJ} \cdot \text{C}^{-1}$), \dot{Q}_{stack_elz} is the heat absorption rate ($\text{J} \cdot \text{s}^{-1}$) of the stack. Using the energy balance principle in equation (3.3.8), this could be further modified as:

$$C_{t_elz} \frac{dT_{elz}}{dt} = \dot{Q}_{gen_elz} - \dot{Q}_{cool_elz} - \dot{Q}_{loss_elz} \quad (3.3.10)$$

In equation (3.3.10), \dot{Q}_{cool_elz} is the heat flow rate by cooling unit ($\text{J} \cdot \text{s}^{-1}$), and \dot{Q}_{loss_elz} is the heat flow rate through the stack surface ($\text{J} \cdot \text{s}^{-1}$). Since the overall electrical energy input to the system and operating efficiency is directly related to the losses and

subsequent temperature rise, these parameters are related through the following expression

$$\dot{Q}_{gen_elz} = N_{elz} U_{cell} I_{elz} (1 - \eta_e) \quad (3.3.11)$$

The rate of heat removal by the cooling water is expressed as a function of the surface area of the heat exchanger and log mean temperature difference (LMTD) between the stack and inlet/outlet cooling water [19,88].

$$\dot{Q}_{cool_elz} = UA_{HX_elz} LMTD_{elz} = UA_{HX_elz} \frac{(T_{elz} - T_{cw,in}) - (T_{elz} - T_{cw,out})}{\ln\left(\frac{(T_{elz} - T_{cw,in})}{(T_{elz} - T_{cw,out})}\right)} \quad (3.3.12)$$

The parameter UA_{HX_elz} is a measure of the electrolyzer heat exchanger size ($W \cdot ^\circ C^{-1}$), whereas $T_{cw,in}$ and $T_{cw,out}$ are the inlet and outlet water temperatures ($^\circ C$), respectively. An empirical formula used in [19, 88] is used in determining the value of UA_{HX_elz} .

$$UA_{HX_elz} = h_{cond_elz} + h_{conv_elz} I_{elz} \quad (3.3.13)$$

where h_{cond_elz} and h_{conv_elz} are parameters which characterize conduction and convection properties of the electrolyzer heat exchanger having units of $W \cdot ^\circ C^{-1}$ and $W \cdot ^\circ C^{-1} \cdot A^{-1}$, respectively. The stray heat loss by the surface of the stack is proportional to the stack temperature and the ambient temperature.

$$\dot{Q}_{loss_elz} = \frac{T_{elz} - T_{amb}}{R_{t_elz}} \quad (3.3.14)$$

In equation (3.3.13), R_{t_elz} is the thermal resistance of the stack ($^{\circ}\text{C}\cdot\text{W}^{-1}$), and T_{amb} is the ambient temperature ($^{\circ}\text{C}$). The product of thermal resistance and thermal capacitance determine the time constant associated with equation (3.3.8). This is given by,

$$\tau_{elz} = R_{t_elz} C_{t_elz} \quad (3.3.15)$$

Assuming $\tau_{elz} = 20925$ s, and $C_{t_elz} = 1.35 \times 10^5$ $\text{kJ}\cdot^{\circ}\text{C}^{-1}$ (Table 3.12), the thermal resistance could be found. The parameters needed for thermal modeling of the electrolyzer stack are given in Table 3.12. Using equations (3.3.11) to (3.3.15), the magnitude of the temperature at any instance is found by equation (3.3.10).

Table 3.12: Parameters for the thermal model of electrolyzer stack

<i>Symb.</i>	<i>Parameter</i>	<i>Value</i>	<i>Unit</i>
$T_{cw,in}$	Inlet cooling water temperature	25	$^{\circ}\text{C}$
$T_{cw,out}$	Outlet cooling water temperature	30	$^{\circ}\text{C}$
T_{amb}	Ambient temperature	25	$^{\circ}\text{C}$
h_{cond_elz}	Heat exchanger conduction index	3.5	$\text{W}\cdot^{\circ}\text{C}^{-1}$
h_{conv_elz}	Heat exchanger convection index	0.005	$\text{W}\cdot^{\circ}\text{C}^{-1}\cdot\text{A}^{-1}$
R_{t_elz}	Thermal resistance	0.155	$^{\circ}\text{C}\cdot\text{W}^{-1}$
C_{t_elz}	Thermal capacitance	1.35×10^5	$\text{kJ}\cdot^{\circ}\text{C}^{-1}$
τ_{elz}	Time constant	20925	s

3.3.3 Summary

In this section the dynamic model of an alkaline electrolyzer is described. This analysis is based on a downscaled prototype of a larger electrolyzer system (PHOEBUS [19,88]). Several steady state electrochemical expressions are related to the temperature dynamics, which are explained through an energy balance model. Further investigation is needed in order to establish a generalized model with more accurate performance evaluation.

3.4 Power Converter

Interconnection of various energy sources and loads in a hybrid energy system needs proper power electronic interfacing. The output of a wind energy conversion system greatly depends on wind variations. The performance of a fuel cell is inherently non-linear and depends on a great many operational conditions. On the other hand, loads connected to such systems typically have specific ratings for proper operation. Such mismatch in various voltage and frequency levels could be overcome by suitable power electronic modules.

In a power electronic system, the flow of electrical energy is processed and controlled in order to maintain specific supply to the load [100,101]. The use of power converters for optimum performance, reliability and efficiency itself is a broad issue and requires detailed investigation. However, in this thesis, in-depth analysis of the power conversion methods is not carried out. The software tool used in modeling the hybrid system elements (MATLAB-Simulink[®]) is not particularly suitable for such analysis and a different method could be considered as part of a future work.

A high voltage DC bus is generally considered as a common interface between various components of a hybrid energy system [102,103]. DC-DC interconnection could be done with buck, boost or buck-boost converters depending on the type of application. Almost all of the household loads are of AC type and supply to such loads requires nameplate voltage and frequency specifications to be met. Therefore, a DC-AC interface or inverter is also required to allow continuous power flow to the load.

3.4.1 Power Converter Model Formulation

In this thesis, power converters are considered for steady state modeling with simplified fundamental relationships. Various components of the hybrid energy system are connected through a common high voltage DC bus having a rating of 200 V. The outputs of the wind turbine and the fuel cell systems are variable DC, and DC-DC converters are

used for integrating these into the DC bus. The electrical load is supplied with a single-phase inverter (Figure 3.20). The load voltage and frequency are considered to be 120 V and 60 Hz, respectively.

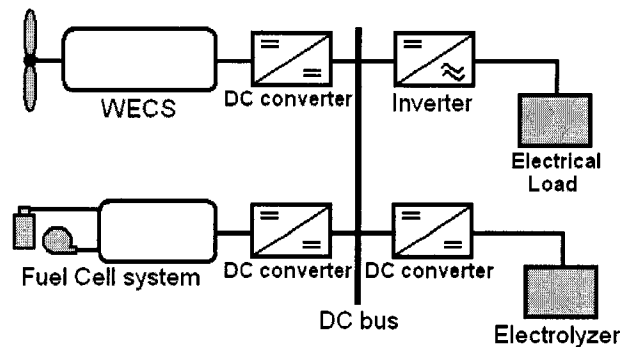


Figure 3.20: Power converters in wind-fuel cell hybrid energy system

Instead of implementing circuit models in the simulation environment, the mathematical principles of power conversion for various converters are taken into account. Several assumptions are made for simplifying the models and reducing the simulations time. These are:

- The output of a DC-DC converter is considered to be perfect DC and ripple free.
- All the solid-state switches in the power converters are assumed to have ideal on-off characteristics.
- Due to the power losses in switching, the efficiency of the converters is considered to be 90%.

3.4.1.1 WECS Buck-Boost Converter

The wind energy converter described in section 3.1.1, has a voltage rating of 240 V DC. Variations in wind might cause the voltage to vary significantly beyond this voltage. In order to allow power extraction both at low and high levels of voltages, a buck-boost type

converter is used. The terminal voltage of the WECS, V_{t_wt} is regulated at the DC bus voltage, V_{bus} . In steady state, this conversion is given by [101]:

$$\frac{V_{bus}}{V_{t_wt}} = \frac{D_{wt}}{1 - D_{wt}} \quad (3.4.1)$$

where D_{wt} is the duty ratio of the wind turbine buck-boost converter. With variations in V_{t_wt} , a near-constant bus voltage, V_{bus} is achieved by controlling the duty ratio. A PID controller discussed in section 3.2.2.4 is considered in that regard.

$$\begin{aligned} \frac{D_{wt}(s)}{e_{vwt}(s)} &= \frac{K_{pwt}s + K_{dwt}s^2 + K_{iwt}}{s} \\ e_{vwt}(t) &= V_{bus_ref} - v_{bus}(t) \end{aligned} \quad (3.4.2)$$

where e_{vwt} is the error in converter output (difference of reference bus voltage and actual output) and K_{pwt} , K_{dwt} , K_{iwt} are controller gains.

3.4.1.2 Fuel Cell Boost Converter

The DC output of a fuel cell depends primarily on the cell current (Figure 3.12). It also varies depending on stack temperature, reactant pressure etc. The voltage output of the fuel cell stack being considered is below 30 V. Therefore, for this simplistic analysis, a boost converter is required to meet the interfacing requirements.

$$\frac{V_{bus}}{V_{stack}} = \frac{1}{1 - D_{fc}} \quad (3.4.3)$$

where V_{stack} is the fuel cell stack's output voltage and D_{fc} is the duty ratio of the boost converter. A PID controller is also considered in regulating the bus voltage around 200 V.

$$\frac{D_{fc}(s)}{e_{vfc}(s)} = \frac{K_{pfc}s + K_{dfc}s^2 + K_{ifc}}{s} \quad (3.4.4)$$

$$e_{vfc}(t) = V_{bus_ref} - v_{bus}(t)$$

where e_{vfc} is the error in converter output and K_{pfc} , K_{dfc} , K_{ifc} are controller gains.

3.4.1.3 Electrolyzer Converter

An electrolyzer can operate both in current controlled or voltage controlled mode [19,97]. Use of current controlled mode of operation simplifies the mathematical implementation of the electrolyzer model developed in section 3.3.2. However, in such a case a DC-DC voltage to current source converter is required, which complicates the formulation to some extent. Therefore, a hypothetical power converter is conceived here. This converter senses the difference between available power and consumed power by the electrolyzer. This error is then used in a PID controller to adjust the electrolyzer current accordingly.

$$\frac{I_{elz}(s)}{e_{pelz}(s)} = \frac{K_{pelz}s + K_{delz}s^2 + K_{ielz}}{s} \quad (3.4.5)$$

$$e_{pelz}(t) = P_{ava_elz}(t) - P_{elz}(t)$$

In equation (3.4.5), e_{pelz} is electrolyzer power consumption error signal, P_{ava_elz} is the available power for use in the electrolyzer, and P_{elz} denotes actual consumption. The symbols K_{pelz} , K_{delz} , K_{ielz} stand for controller gains and are given in Table 3.13. It should be stressed that, a better power electronic analysis is essential in order to associate the unique operational characteristics of an electrolyzer.

3.4.1.4 Load Inverter

A full-bridge sinusoidal pulse width modulated (PWM) inverter is considered here for delivering power to an AC load. The inverter is connected to the bus (Figures 3.20, 3.21) and an LC filter is used to eliminate higher order harmonics at the inverter output. The load consists of a resistive and an inductive element.

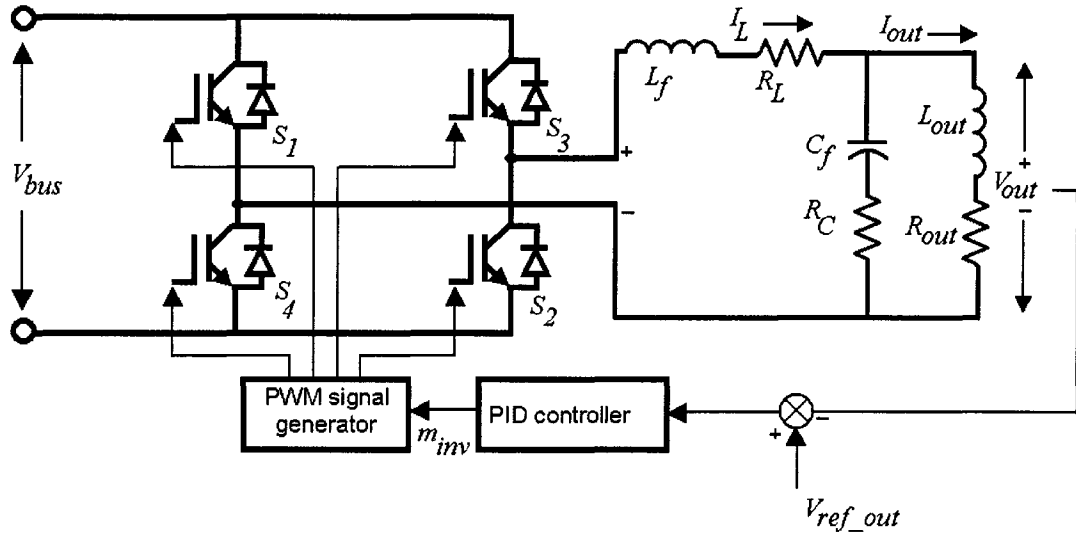


Figure 3.21: Inverter load arrangement

For each complementary switching state of the full bridge inverter (S_1 - S_2 or S_3 - S_4), the inverter output, V_{inv} becomes positive or negative of the DC bus voltage ($+V_{bus}$ or $-V_{bus}$) in an ideal inverter (Figure 3.21). The filter inductor, L_f smooths the current through it depending on the difference of inverter voltage, V_{inv} and output voltage V_{out} , as given by the following transfer function:

$$\frac{I_L(s)}{V_{inv_out}(s)} = \frac{1}{sL_f + R_L} \quad (3.4.6)$$

$$v_{inv_out}(t) = v_{inv}(t) - v_{out}(t)$$

On the other hand, the filter capacitor smoothes the voltage at the load, depending on the difference of inductor current, I_L and load current, I_{out} .

$$\frac{V_{out}(s)}{I_{L_out}(s)} = \frac{sC_f R_C + 1}{sC_f} \quad (3.4.7)$$

$$i_{L_out}(t) = i_L(t) - i_{out}(t)$$

The filter parameters are chosen such that, the output voltage becomes near sinusoidal and these are listed in Table 3.13. The inverter switches are operated through four sinusoidal pulse width modulated signals generated by a PWM signal generator. A PID controller is employed in order to maintain a fixed AC (120 V, 60 Hz) output at the load. The load consists of a fixed inductive load, L_{out} and a variable resistive element R_{out} . The voltage-current relationship for the R-L load branch can be shown with the following fundamental expression:

$$v_{out} = L_{out} \frac{di_{out}}{dt} + R_{out} i_{out} \quad (3.4.8)$$

Indicating the power factor angle by θ , the real power output at the load is given as:

$$P_{out} = V_{out} I_{out} \cos \theta \quad (3.4.9)$$

The controller senses the difference between the actual output and reference voltage. This error signal is then used in generating proper modulations index for use in the PWM signal generator.

$$\frac{m_{inv}(s)}{e_{vout}(s)} = \frac{K_{pinv}s + K_{dinv}s^2 + K_{iinv}}{s} \quad (3.4.10)$$

$$e_{vout}(t) = V_{ref_out} - v_{out}(t)$$

In equation (3.4.10), e_{vout} is the error signal and m_{inv} is the modulation index. The controller gains are given by K_{pinv} , K_{dinv} , and K_{iinv} (Table 3.13).

Table 3.13: Power converter parameters

<i>Symb.</i>	<i>Parameter</i>	<i>Value</i>	<i>Unit</i>
V_{bus_ref}	DC bus reference voltage	200	V
K_{pwt}	Buck-boost controller proportional gain	3.5	-
K_{dwt}	Buck-boost controller differential gain	0	-
K_{iwt}	Buck-boost controller integral gain	0.15	-
K_{pfc}	Boost controller proportional gain	5	-
K_{dfc}	Boost controller differential gain	0	-
K_{ifc}	Boost controller integral gain	2	-
K_{pelz}	Electrolyzer controller proportional gain	5	-
K_{delz}	Electrolyzer controller differential gain	0	-
K_{ielz}	Electrolyzer controller integral gain	1.5	-
L_f	Filter inductance	10	mH
R_L	Resistance in filter inductor	0.025	Ω
C_f	Filter capacitance	1	mF
R_C	Resistance in filter capacitance	0.25	Ω
V_{ref_out}	Reference output voltage	120	V
K_{pinv}	Inverter controller proportional gain	6.5	-
K_{dinv}	Inverter controller differential gain	0	-
K_{iinv}	Inverter controller integral gain	0.15	-
V_{ref_out}	Reference output	120	V
L_{out}	Inductive load	10	mH
R_{out}	Resistive Load	4.5-15.5	Ω

3.4.2 Summary

Various power conversion issues are discussed in this section with emphasis on simplified models. A buck-boost converter is used in the wind turbine and a boost

converter is considered for the fuel cell system. The electrolyzer power conversion is modeled with a hypothetical converter, which operates in unique conditions and requires further investigation. The inverter used in interfacing the AC load is coupled with an LC filter. An R-L element is considered as the ultimate load for this hybrid energy system.

3.5 System Integration

The hybrid energy system and its components need to be integrated such that various energy elements perform in a synchronous manner. The models formulated in the previous sections are combined in the integrated structure shown in Figure 3.22. Theoretically, the only three resources being consumed by the system are: the energy from the wind, pure water as electrolyzer feed, and ambient air as fuel cell oxidant.

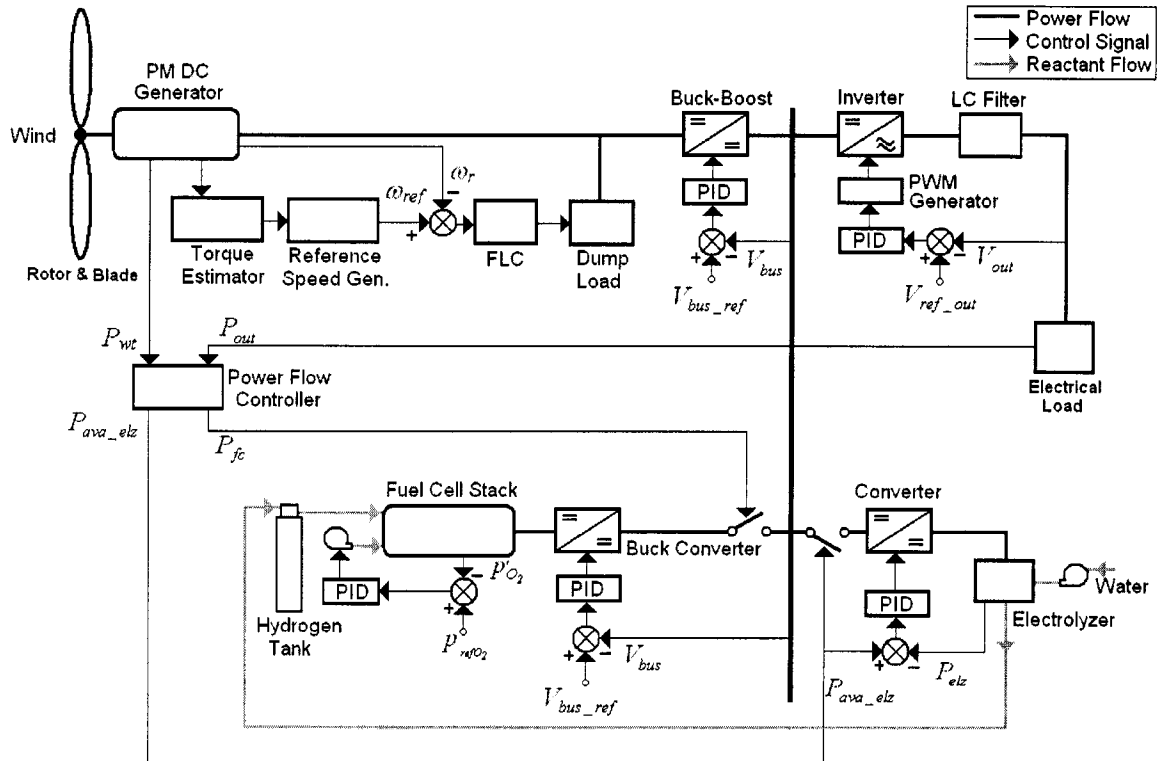


Figure 3.22: Hybrid energy system interconnections

The wind turbine controller regulates the speed of the WECS for optimum operation. The buck-boost converter connected with the wind turbine converts the variable DC into a standard DC-bus voltage of around 200 V. The fuel cell system consumes stored hydrogen generated by the electrolyzer. It also needs a controlled air flow mechanism. A boost converter interfaces the fuel cell system with the bus. The load is connected through an inverter-filter arrangement (Figure 3.22).

A power flow controller allows proper interconnection of the wind turbine, fuel cell, electrolyzer and load. The principle of operation of the wind-fuel cell system is to deliver necessary electricity to the load from the wind turbine and/or fuel cell system. Any excess energy from the wind energy converter needs to be diverted for hydrogen production for later use in the fuel cell system. The control sequence of the system could be shown by the flow-chart below:

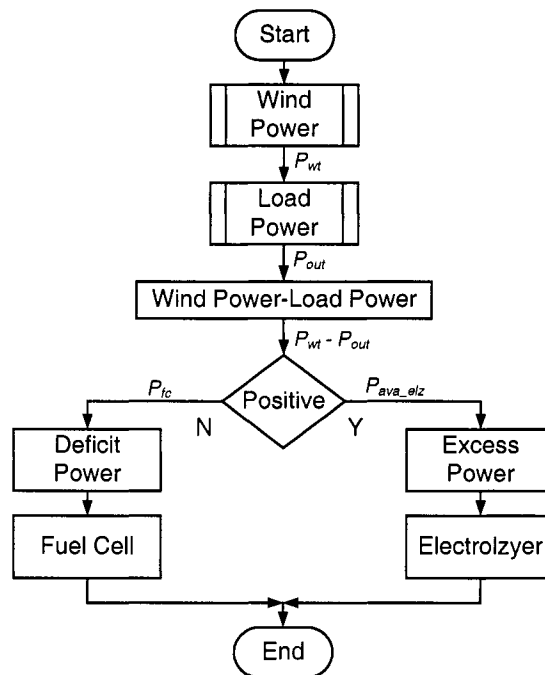


Figure 3.23: Flow chart of power flow controller

The control algorithm senses available power in the wind as well as the demand by the load. If there is a surplus in wind energy, this causes the electrolyzer to operate

and produce hydrogen. On the other hand, the fuel cell stack meets any deficit in the wind turbine's output (Figure 3.23).

In the pre-feasibility analysis given in Chapter 2, appropriate sizes of various components were determined for a given load. Therefore, it is assumed that there would be very rare instances when a load requirement could exceed total available energy from the wind turbine and fuel cell combined. The interconnection scheme and control strategy described above are based on this assumption, and a computer-aided simulation of the complete process is described in the chapters to follow.

Chapter 4

System Integration and Simulation

The wind-fuel cell hybrid energy system, and its various components were discussed and the mathematical models were formulated in the previous chapter. Computer aided simulation is a useful tool in understanding the interactions within the system. It also gives valuable insights in design and performance evaluation.

In this thesis, MATLAB-Simulink[®] is used for simulating the mathematical models. MATLAB Version: 6.5.1.199709 (R13) and Simulink Version 5.1: (R13SP1) were employed. In Simulink various graphical blocks from the built-in library are connected together to implement an equation. Several equations can be grouped in a subsystem. These subsystems when linked together, form a full system.

In MATLAB, variables are computed as matrices and solution of a given problem is calculated by iterative methods. As the number of equations and variables increase, the problem becomes complicated. Occasionally the iterative method fails to converge properly. In order to facilitate the convergence process and avoid unrealistic numerical values, additional blocks need to be used. In this chapter, the development and organization of the simulation program is discussed.

In Figure 4.1, a Simulink implementation of the complete wind-fuel cell system is shown. Block diagrams of the associated subsystems (SS) are given in Appendix A. The blocks are self-explanatory and all the significant variables along with their units (in braces) are given. In this model, three parameters are considered for introducing step

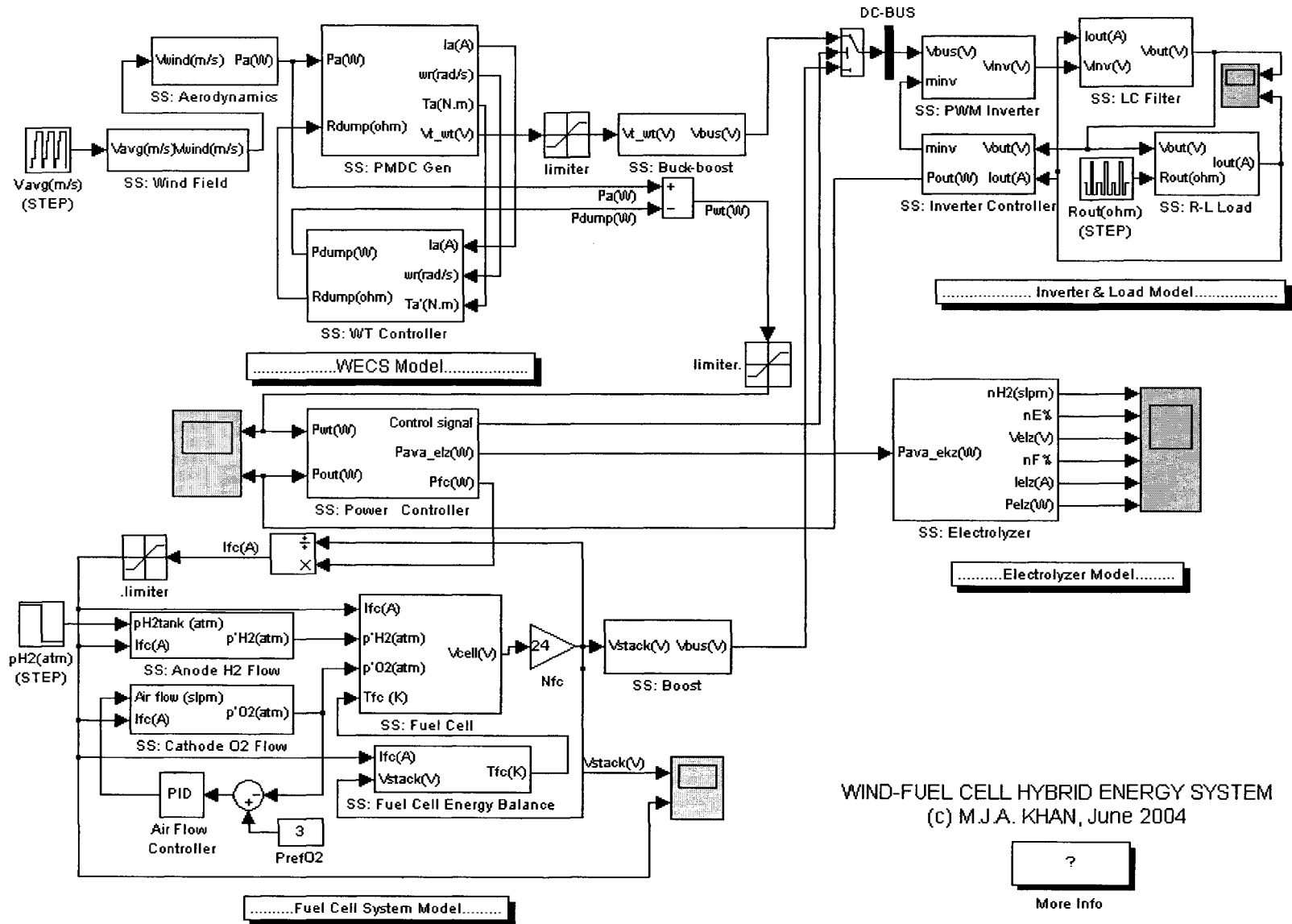


Figure 4.1: MATLAB-Simulink® Implementation of Wind-Fuel cell hybrid energy systems

changes into the system. These are: wind speed, hydrogen pressure, and resistive load indicated by '*Vavg(m/s)*', '*pH2(atm)*', and '*Rout(ohm)*' blocks, respectively. The first two variables represent changes in the system input and the latter parameter alters the conditions at the system output. In order to eliminate unrealistic over/under-shoots arising from convergence problems, several limiters are placed at appropriate nodes in the system. The lower and upper limits of these blocks are chosen such that no clipping occurs in the realistic range of solutions.

4.1 WECS Model

The wind energy conversion system is represented by four subsystems. These are: '*SS: Wind Field*', '*SS: Aerodynamics*', '*SS: PMDC Gen*', and '*SS: WT Controller*'. The wind field given by equations (3.1.3) and (3.1.4) is implemented in the '*SS: Wind Field*' block (Figure A.1). The effects of spatial filtering and induction lag as shown in equations (3.1.5 to 3.1.8) are considered in the '*SS: Aerodynamics*' subsystem (Figure A.2). Model of the permanent magnet DC generator (equation 3.1.9), is realized through '*SS: PMDC Gen*' block (Figure A.3). The subsystem '*SS: WT Controller*' incorporates the FLC controller along with the reference signal generator scheme (Figure A.4).

4.2 PEM Fuel Cell System Model

The mathematical expressions for the PEM fuel cell are coupled with the energy balance and reactant flow models through the subsystems of Figures A.5 to A.8. The '*SS: Fuel Cell*' subsystem is the key element that implements equations (3.2.2) to (3.2.16) for realizing a single PEM fuel cell. A gain block ($N_{fc} = 24$) at the terminal of this subsystem, multiplies the voltage output with the number of cells to obtain the stack voltage (Figure 4.1).

The thermal model is labeled as '*SS: Fuel Cell Energy Balance*' subsystem and it implements equations (3.2.17) to (3.2.22). The temperature of a stack remains virtually

constant for a short period of observation (5 – 50 seconds). Investigation of thermal dynamics takes very long simulation time and could not be carried out with the available computing resources. Therefore, a provision for bypassing the thermal model and considering only a fixed temperature (72°C) is given (Figure A.6).

Pressurized hydrogen from a storage tank and compressed air through an air flow controller (Figure 4.1) are the essential inputs to this system. In the ‘SS: Anode H2 Flow’ subsystem given in Figure A.7, a conversion factor ($1 \text{ slpm} \approx 7.034 \times 10^{-4} \text{ mole.s}^{-1}$) is used in converting the hydrogen inlet flow rate from slpm (standard liter per minute) to mole.s^{-1} . Mole fraction of hydrogen is considered to be 99%. The function of the pressure regulator (*PR*) at the anode is realized using a simple PID block, which takes hydrogen pressure inside the stack as a feedback parameter and the tank pressure as the set point. Similar to the anode, ‘SS: Cathode O2 Flow’ subsystem shown in Figure A.8, models the air circulation system. The oxygen content of air is assumed to be 21% and its conversion factor is 7.036×10^{-4} ($1 \text{ slpm} \approx 7.036 \times 10^{-4} \text{ mole.s}^{-1}$). The effect of the back pressure regulator (*Pbpr*) is modeled with a constant block showing a fixed downstream pressure. A PID controller block implements equation (3.2.30) using the parameters in Table 3.8.

4.3 Electrolyzer Model

Simulink blocks for the electrolyzer (Figure 4.1) are given in Figure A.9 (‘SS: Electrolyzer’). It also contains the energy balance model of the electrolyzer indicated as ‘SS: Electrolyzer Energy Balance’. Similar to the fuel cell model, the dynamics for temperature variation are not considered and a fixed stack temperature of 80°C is assumed (Figure A.10). Hydrogen production rate is converted into standard liter per minute (slpm) from mol.s^{-1} by a conversion factor of 1421.67. A PID block corresponding to the current controller given in equation (3.4.5) is also implemented.

4.4 Power Converter Model

The power electronic modules of the wind turbine, fuel cell and output load are realized through 'SS: *Buck-boost*', 'SS: *Boost*', and 'SS: *PWM Inverter*' subsystems, respectively (Figure 4.1). Corresponding connection diagrams are shown in figures A.11, A.12, and A.13. The harmonic elimination filter given by equations (3.4.6) and (3.4.7) is considered in 'SS: *LC Filter*' subsystem (Figure A.14). The PID controller for adjusting the inverter modulation index is given in 'SS: *Inverter Controller*' block (Figure A.15). An R-L load at the output corresponding to equation (3.4.8) is employed in 'SS: *R-L Load*' subsystem (Figure A.16).

4.5 System Integration

To coordinate an effective power flow mechanism, a control algorithm was proposed in section 3.5.1. This is realized in 'SS: *Power Controller*' subsystem (Figure A.17). It takes the power output from the wind turbine and power demand by the load as inputs. The difference of these two power levels is calculated and the excess energy is directed to the electrolyzer. The bus voltage is determined by the availability of power from the two sources and is controlled by a signal from the power controller. In case of insufficient wind power, the fuel cell stack supplies the deficit. Based on this power and stack output voltage, the current demand of the fuel cell is calculated (Figure 4.1).

Simulation of the integrated model appeared particularly difficult and slow. Therefore, a combination of fixed step and variable step simulation was considered. The WECS model is simulated in 'Fixed Step/ODE-5(Dormand-Prince)' method [30]. The electrolyzer model posed problems with algebraic loops and invalid initial conditions. This model is solved with 'Fixed Step/ODE-4(Runge-Kutta)' method. The rest of the system is simulated with a more comprehensive method: 'Variable Step/ODE-23(Bogacki-Shampine)'. The relative and absolute tolerance was taken as 1×10^{-5} and 1×10^{-3} , respectively. The complete simulation time for 15 seconds is around 13 minutes.

Chapter 5

Results and Discussion

The performance of a wind-fuel cell hybrid energy system depends on various internal and external operating conditions. Changes in wind speed, and load power are the two most significant external factors. On the other hand, wind turbine controller action, fuel cell reactant pressure and power electronic conversion are a few of the internal issues.

The stand-alone energy system described in Chapter 3 is simulated in MATLAB-Simulink[®]. A wide range of parameters is studied for analyzing various operating states. In this chapter, the performance of the overall system, as well as individual elements is investigated with several specific sets of inputs. These inputs are coordinated and synchronized such that a number of possible scenarios can be emulated.

The simulation was carried out for 15 seconds. Step inputs for average wind speed, load resistance and hydrogen pressure are introduced. These events are listed in Table 5.1. It should be stated that, all the results of this discussion are related to these inputs either directly or indirectly. In a real situation, wind consists of a turbulent component superimposed on the average velocity. Initially a simulation is conducted with random components in the wind, along with the events listed in Table 5.1. However, standard method of transient analysis is to analyze the step responses. Therefore, a concluding simulation considers only the step inputs (Table 5.1) and their responses.

Table 5.1: Simulation event chart

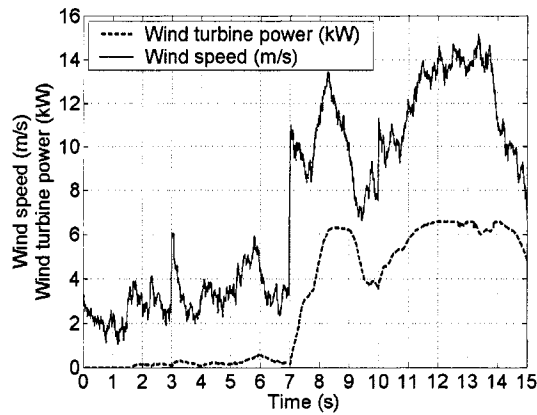
<i>No.</i>	<i>Time</i>	<i>Event</i>	<i>Magnitude</i>
1	t = 0 s	Wind speed step change (start up)	0 - 3 m.s ⁻¹
2	t = 0 s	Load step change (start up)	0 - 8.75 Ω
3	t = 0 s	Hydrogen pressure rise (start up)	0 - 3 atm
4	t = 1.5 s	Load step change	8.75 - 4.5 Ω
5	t = 3 s	Wind speed step change	3 - 6.5 m.s ⁻¹
6	t = 6 s	Load step change	4.5 - 15.5 Ω
7	t = 7 s	Wind speed step change	6.5 - 13.5 m.s ⁻¹
8	t = 9 s	Load step change	15.5 - 4.5 Ω
9	t = 10 s	Wind speed step change	13.5 - 17 m.s ⁻¹
10	t = 12 s	Hydrogen pressure drop	3 - 1.5 atm
11	t = 13.5 s	Load step change	4.5 - 8.75 Ω

5.1 Simulation with Randomly Varying Wind Component

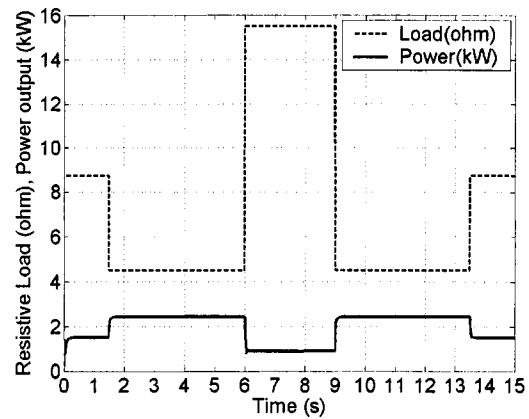
The wind field model as described in section 3.1.2.1 is implemented through the Simulink blocks in Figure A.1. It imposes randomness on the average wind given in Table 5.1 and is shown in Figure 5.1(a). The rotor-blade assembly and the associated aerodynamics act as a low pass filter on this wind. Therefore, the captured power excludes higher frequency changes.

In Figure 5.1, power flow within various sources and loads are shown. The effective power from the wind turbine is consumed by the load (Figure 5.1(b)) and also by the electrolyzer (Figure 5.1(d)). As the wind penetration is low for $t < 7$ s, the fuel cell contributes most of the power (Figure 5.1(c)) in this interval.

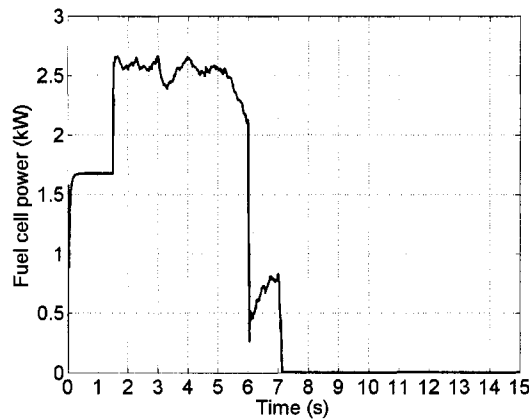
The WECS generates around 6.5 kW when the wind speed goes beyond 12 m.s⁻¹. With variations in load from 4.5 Ω to 15.5 Ω, the power dissipation at the load varies within 900 W to 2455 W. At low winds, the fuel cell delivers this power plus the losses in the power converters (boost and PWM inverter). Excess energy at high winds is directed into the electrolyzer. Its consumption varies from 1 kW to 5.5 kW depending on availability of redundant energy from the wind turbine (Figure 5.1).



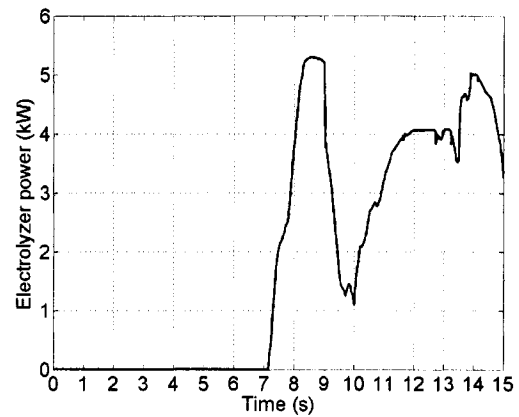
(a) Wind speed and turbine power



(b) Load resistance and load demand



(c) Fuel cell power output

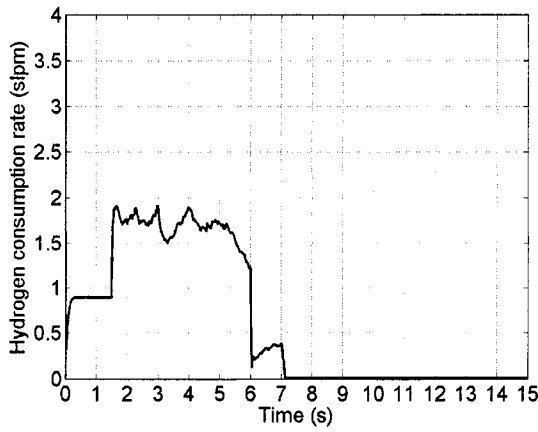


(d) Electrolyzer power consumption

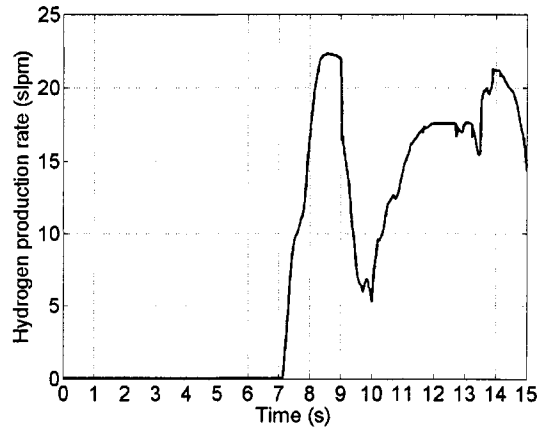
Figure 5.1: Power balance under randomly varying wind

One of the most important requirements of a stand-alone system is that, the system needs to be autonomous. This implies that the depleted hydrogen from the storage tank should be replenished from the electrolyzer.

In Figure 5.2, the rates of hydrogen consumption and production for the period of observation are shown. During the sizing analysis (Chapter 2), the electrolyzer and storage tank sizes were found to be larger than the fuel cell ratings. This allows a faster rate of hydrogen fill up during a short period of high winds as shown in these figures.



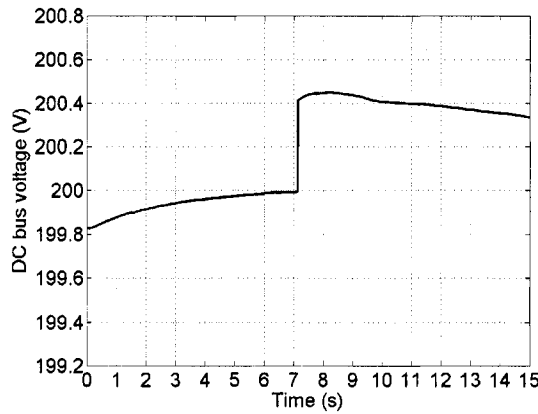
(a) Fuel cell hydrogen consumption



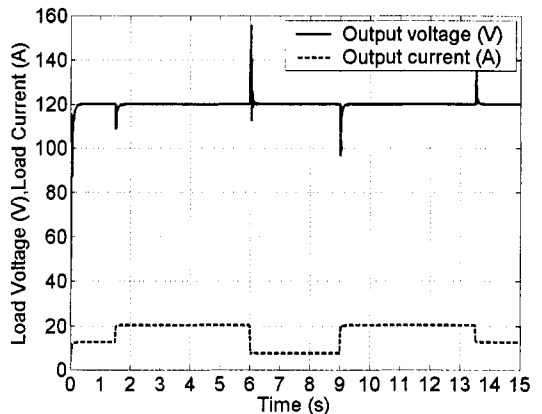
(b) Electrolyzer hydrogen production

Figure 5.2: Hydrogen consumption and production

Various power converters facilitate smooth flow of energy within the system. The DC bus and the load terminals are regulated at 200 V DC and 120 V-60 Hz AC, respectively.



(a) DC bus voltage



(b) Output voltage and current

Figure 5.3: Power conversion at the load

In Figure 5.3, several key results of using power converters are shown. The bus voltage has negligible variations (0.5 %). However, the inverter output shows some significant overshoots and undershoots ($t = 6$ s, overshoot 25%; $t = 9$ s, undershoot 21%).

The durations of these transients are less than 0.15 seconds (9 cycles). During this period the load current varies from 7.5 A to 20.5 A.

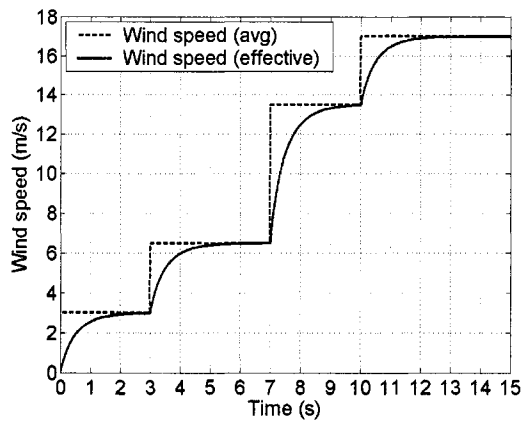
The causes of these over/undershoots could be attributed to three aspects of system design and simulation. These are: PID controller parameters, LC filter parameters and simulation method. For a practical system the voltage transients need to be reduced for safe and reliable operation. Further tuning of the inverter controller and LC filter parameters would significantly reduce these transient effects. The simulation method applied in this analysis could also be adjusted to generate more accurate response.

5.2 Simulation with Step Inputs

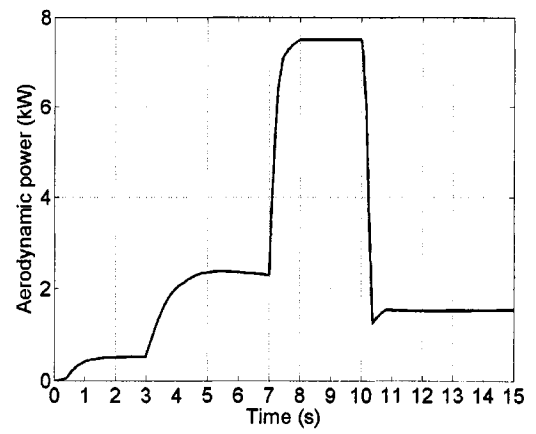
Analysis with step inputs (wind speed, load power, hydrogen pressure etc.) provides a better insight into the transient conditions. In the following sections, simulation results with emphasis on transient analysis are presented .

The wind regimes (cut-in, rated and shut-down) described in section 3.1.1 are incorporated in Figure 5.4(a). At $t = 7$ s, the wind turbine starts to operate in rated condition where the power output approaches the peak (Figure 5.4(b)). Beyond this range, the turbine safety mechanism acts for over-speed regulation and the power generation drops significantly. For below rated ($t < 7$ s) and below cut-in ($t < 3$ s) regions, the turbine's output is minimal.

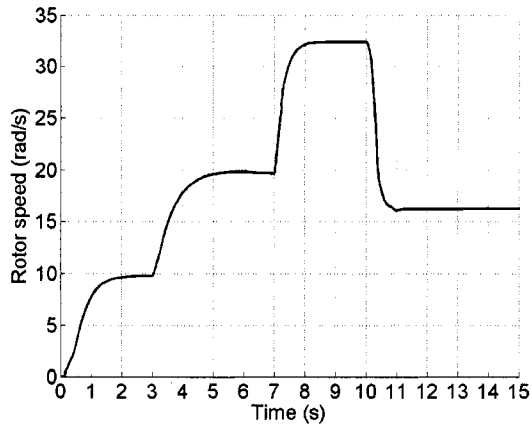
The fuzzy logic controller designed in section 3.1.2.1 regulates the rotor speed by the addition and removal of dump load (Figure 5.4 (c, e)). At high winds the value of the dump resistor is low such that higher current flows and subsequent higher dissipation takes place. This slows down the turbine around the rated speed of 32.5 rad.s^{-1} . The rotor torque shown in Figure 5.4(d) is assumed to be estimable by a suitable sensor or estimator. The effective power output from the wind turbine is the difference between the aerodynamic captured power (Figure 5.4(b)) and dump load dissipation (Figure 5.4(f)). The power balance amongst various elements is shown in Figure 5.5.



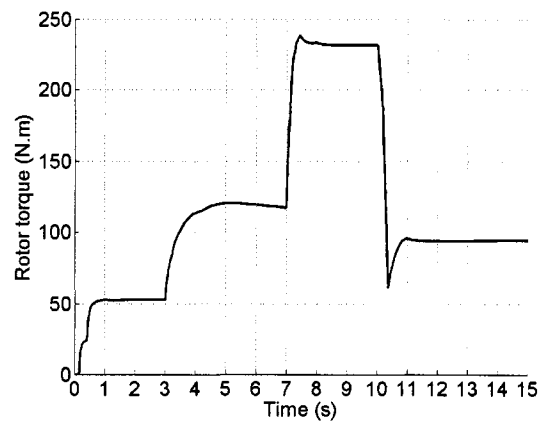
(a) Average and effective wind speed



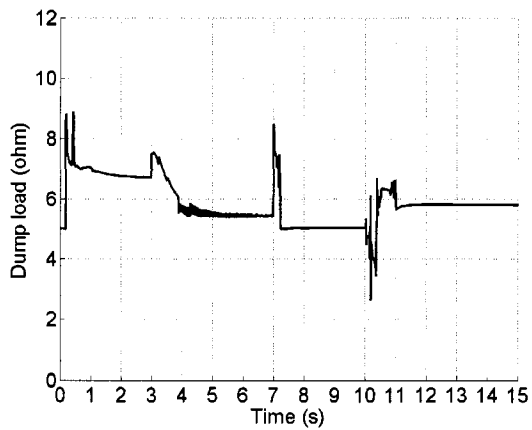
(b) Captured aerodynamic power



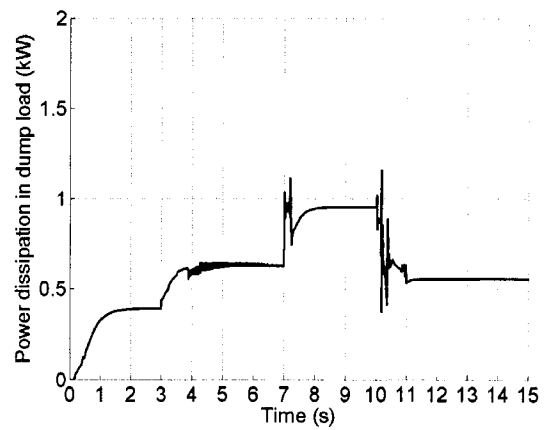
(c) Rotor speed with FLC controller



(d) Rotor torque



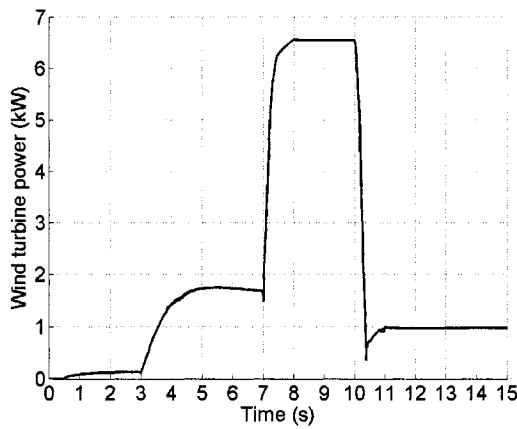
(e) Dump resistance with FLC controller



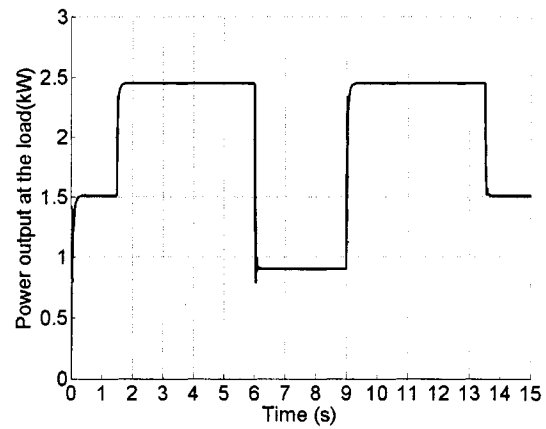
(f) Power dissipation in dump load

Figure 5.4: Wind energy converter performance

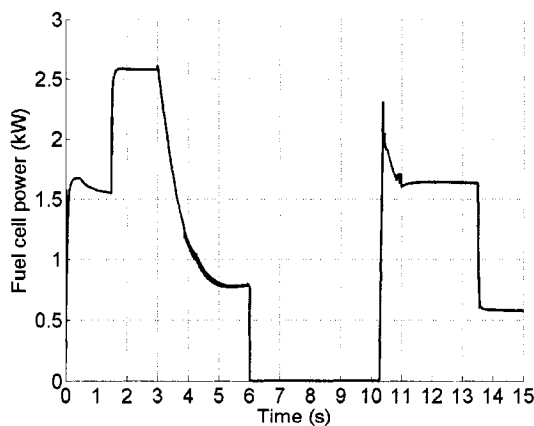
Similar to the discussion of Figure 5.1, a coordinated power flow structure is shown Figure 5.5. For $t < 3.5$ s, most of the power is contributed by the fuel cell. It also accommodates changes in load power (at $t = 1.5$ s). With increasing wind availability ($t = 3.5$ s to 6 s), the wind turbine's output increases. For $6 < t < 10$ s, only the wind turbine delivers energy to the load and electrolyzer. During this period the fuel cell system goes to stand-by mode. When the wind turbine is shut down due to very high winds ($t > 10.5$ s), the fuel cell starts again and meets the load demand. In this case, the power consumption and hydrogen production by the electrolyzer turns off.



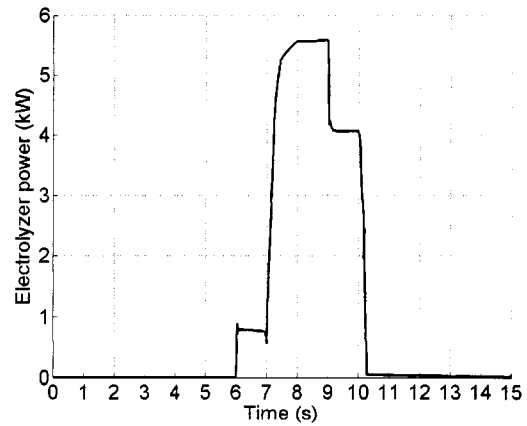
(a) Effective wind turbine power



(b) Load power demand



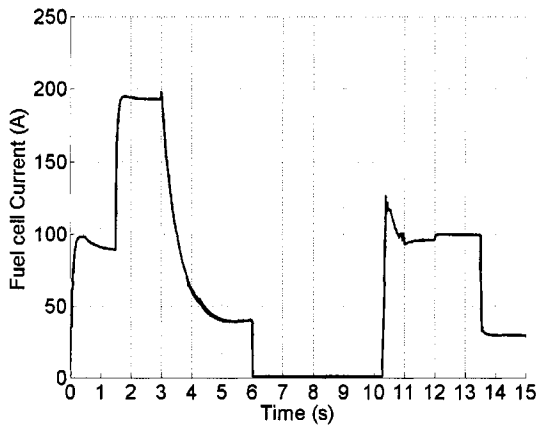
(c) Fuel cell power output



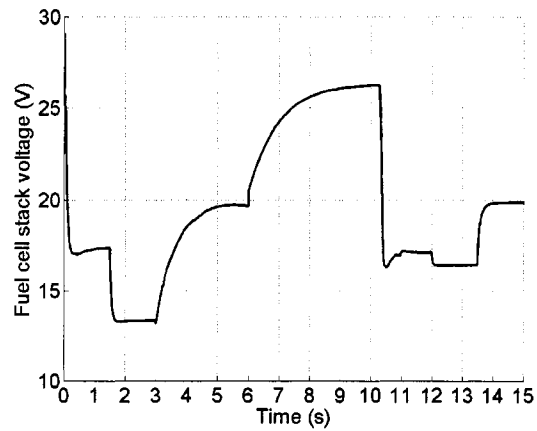
(d) Electrolyzer power consumption

Figure 5.5: Power balance with step changes in inputs

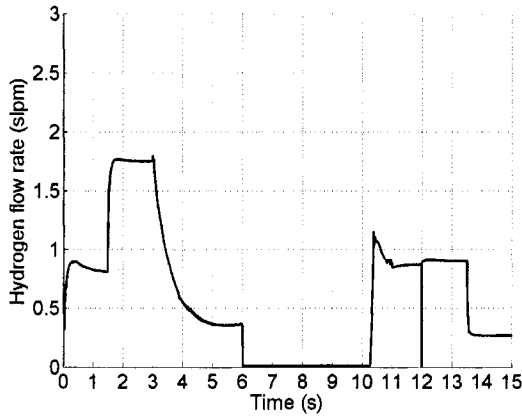
The dynamic mathematical model of the PEM fuel cell system is investigated with the observations in Figure 5.6.



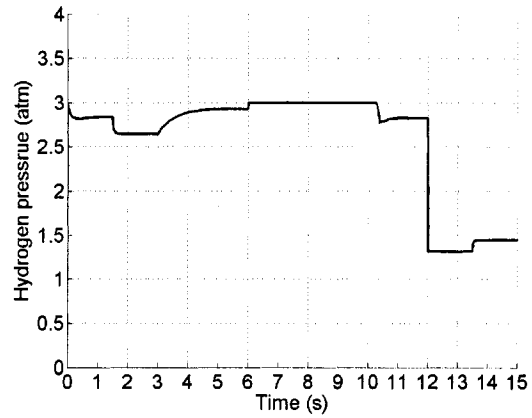
(a) Fuel cell current



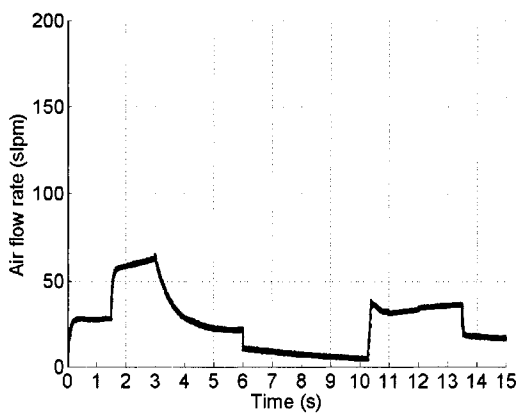
(b) Fuel cell stack voltage



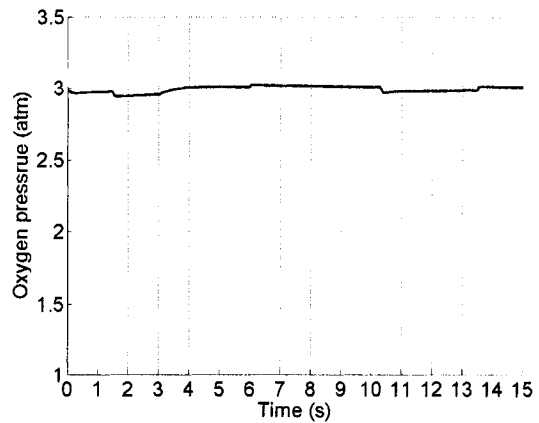
(c) Hydrogen consumption in fuel cell



(d) Hydrogen pressure inside the stack



(e) Air consumption in fuel cell



(f) Oxygen pressure inside the stack

Figure 5.6: Fuel cell system performance

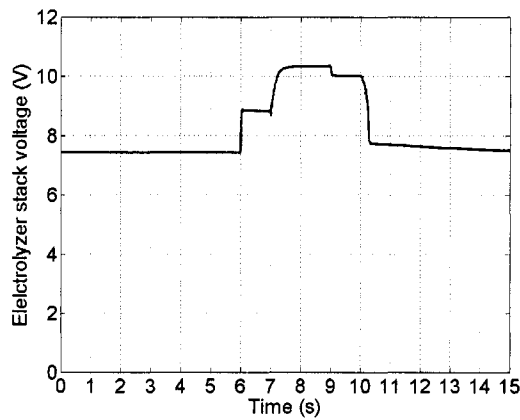
The stack current (Figure 5.6(a)) follows the similar pattern as the fuel cell power (Figure 5.5 (c)). However, fuel cell voltage maintains an inverse relationship as shown by the polarization curve in Figure 3.12. This could also be seen in Figure 5.6 (b), where the stack voltage reaches about 26 V ($t = 9$ to 10 s) when the cell current is zero.

At $t = 12$ s, the hydrogen tank pressure drops from 3 atm to 1.5 atm. This causes the hydrogen partial pressure inside the stack to drop further. As seen in Figure 5.6(c), this pressure is around 1.25 atm and causes the voltage to drop from 17 to 16 V. The consumption of hydrogen increases with higher power delivery (Figure 5.6(c)) to meet increased level of electrochemical reaction.

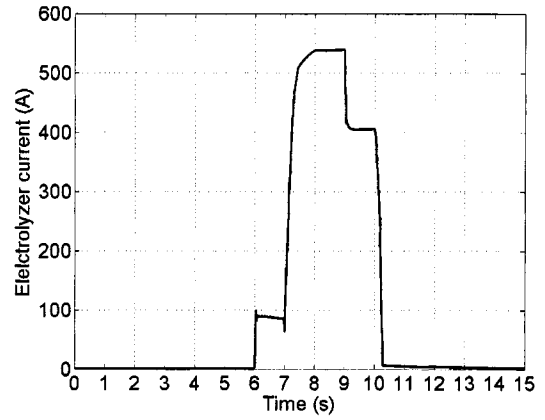
The mass flow controller designed in section 3.2.2.4 regulates the air flow rate (Figure 5.6 (e)) within 0 to 62.5 slpm, maintaining the oxygen pressure around the reference of 3 atm (Figure 5.6 (f)).

The performance of the electrolyzer stack is shown in Figure 5.7. Since the model is characterized by high-current/low-voltage design, its terminal voltage is quite low (maximum 11 V) throughout the whole range of operation. With a current of 540 A, the electrolyzer produces hydrogen at a rate of 23 standard liter per minute (slpm). The efficiency of this device varies from 86 % to 99 % during this interval (Figure 5.7 (d)).

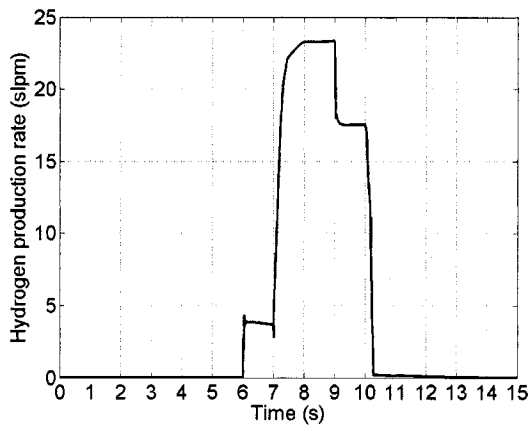
Step changes in electrolyzer operation at $t = 7$ s and $t = 9$ s are due to changes in wind speed and load consumption, respectively. Since, the thermal dynamics of the electrolyzer is not simulated, the model essentially works as a steady-state system.



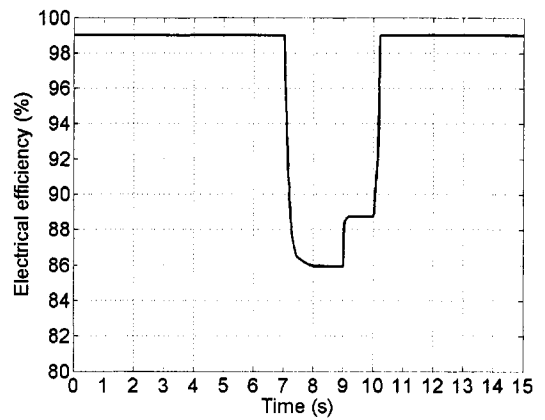
(a) Electrolyzer terminal voltage



(b) Electrolyzer current



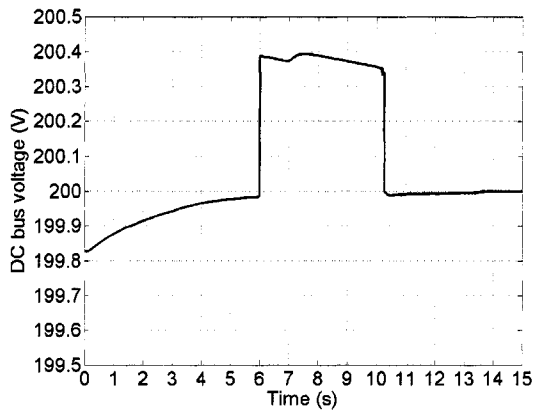
(c) Hydrogen production rate



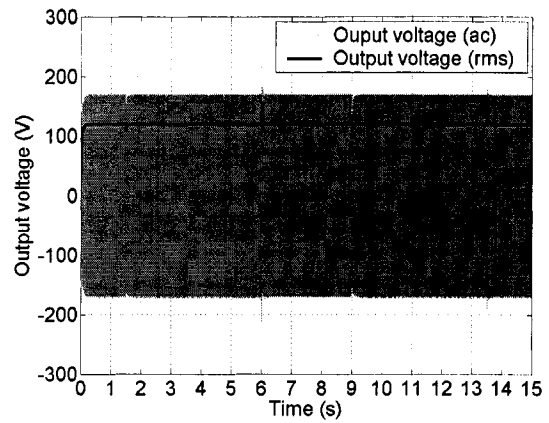
(d) Electrical efficiency

Figure 5.7: Electrolyzer performance

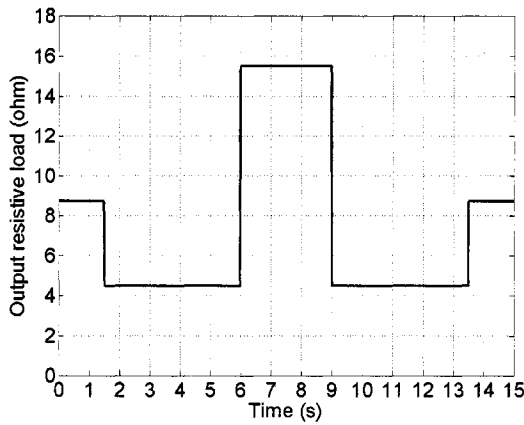
The performance of the power electronic interface between the high voltage DC bus and the AC load is highlighted through the plots in Figure 5.8. The bus voltage is fairly constant at 200 V (Figure 5.8 (a)) and the deviation around this reference is less than 0.5 %. With the PWM Inverter-LC filter combination, the terminal voltage is regulated at 120 V AC (Figure 5.8 (b)). However, the magnitudes of overshoots and undershoots are of questionable level (25 % and 21%, respectively). This stresses further improvements in the inverter/filter design.



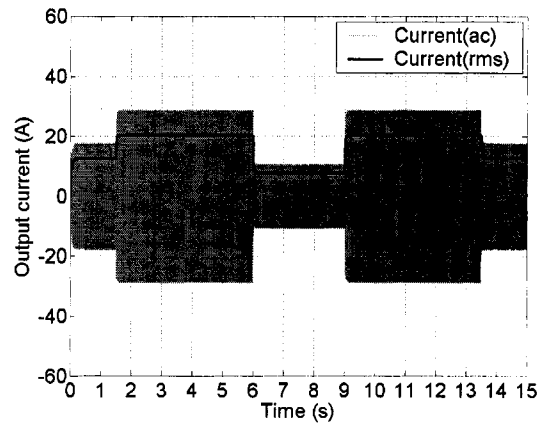
(a) DC bus voltage



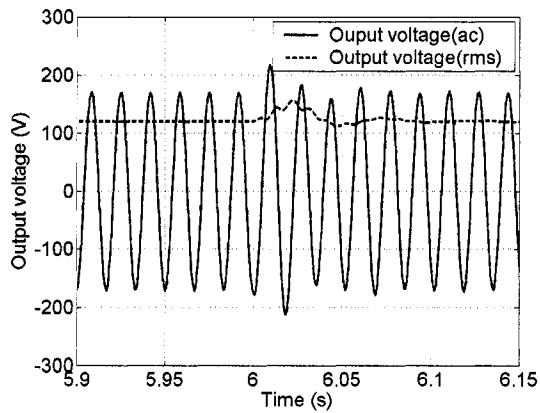
(b) Voltage at the system output



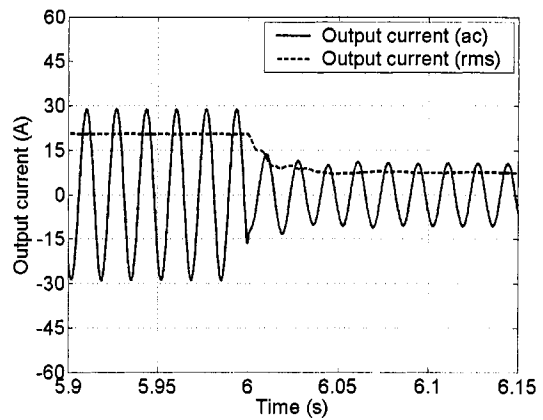
(c) Step change in load resistance



(d) Current in the R-L load



(e) Load Voltage (around $t = 6.025$ s)



(f) Load Current (around $t = 6.025$ s)

Figure 5.8: Power converter performance

A variation of load resistance (Figure 5.8(c)) causes the current at the system output to vary (Figure 5.8(d)). In figures 5.8 (e, and f) the effects of using an LC filter are shown. The square wave output of the PWM inverter is filtered and a near sinusoidal wave (120 V, 60 Hz) is generated. The load current is further smoothed, as an inductor ($L = 10 \text{ mH}$) appears in the load branch. A decrease in load current from 20.5 A to 7.5 A at $t = 6 \text{ s}$, causes a short instability, which lasts for about 0.15 seconds.

5.3 Summary

Various simulation results of the proposed wind-fuel cell hybrid energy system were presented in this chapter. The transient durations in the wind energy conversion system were found to be less than 2.2 seconds. Fuel cell transients prevailed for about 0.5 seconds, in general. It was found that the control and coordination algorithm developed in the previous chapters provided effective means for allowing various components to be integrated within one system. The basic goal of delivering available wind power to the load and excess energy to the electrolyzer was achieved in the simulation environment. The performance of the fuel cell system also appeared to be within the acceptable limits.

Chapter 6

Conclusion

6.1 General Summary

Utilization of renewable energy bears significant long term potential against fossil fuel based systems in terms of economic and environmental benefits. Particularly, in remote locations where grid interface is inaccessible and conventional methods of off-grid power generation are difficult, energy from the environment could be exploited effectively by suitable means. However, availability of energy from a renewable source depends greatly on the environmental conditions that surround it. Generally, an energy storage device such as battery is used for storing the excess energy, whenever available, for later use by a secondary converter. With the advent of various hydrogen energy technologies, the concept of using hydrogen as an energy carrier is gaining favorable attention. Various cost, design and performance aspects of a wind-hydrogen autonomous power system have been discussed in this thesis.

A pre-feasibility analysis was carried out towards identifying the cost, size and applicability of a wind-fuel cell hybrid energy system for use in stand-alone applications in St. John's, Newfoundland. Based on this analysis, dynamic models of various components were developed. These models were then integrated through a control and power electronic mechanism such that utilization of available energy within the system is maximized. Simulation results were presented and discussed. Several specific

conclusions, contributions and limitations of the proposed scheme are highlighted in the following discussion.

6.2 Contributions

- A pre-feasibility study of using renewable energy based hybrid power systems for application in St. John's, Newfoundland has been presented. A number of alternative technologies such as wind, solar, diesel generator, battery, and fuel cell were considered. A comparative overview of various technology options, cost projection and performance indices were also presented.
- A dynamic model of a small wind energy conversion system has been presented. This also includes, a mechanical sensorless control algorithm that employs fuzzy logic theory. A single controller has been shown to be sufficient for controlling the wind turbine in various wind conditions.
- A mathematical model incorporating electrochemical, thermal and reactant flow dynamics for a polymer electrolyte membrane (PEM) fuel cell system has been presented. Various empirical and physical relationships were considered for this simplified model.
- A coordinated power flow mechanism has been developed to integrate the models of various components (wind turbine, fuel cell, electrolyzer etc.) using PID controllers and power electronic interfaces. The complete model of the hybrid energy system has been simulated using MATLAB-Simulink®. A number of possible scenarios with varying wind speed, load power and hydrogen pressure have been investigated. Overall performance and transient responses were also discussed.

- A good number of articles have been generated during the course of this work. The list and citation of these works are given in Appendix B. These publications would give a broader overview of the issues presented in this thesis. In paper 1, significant findings of the pre-feasibility study are given. The dynamic model of the fuel cell system described in this thesis is formulated and validated with test results in Paper 2. Paper 3,6, and 7 present a method of wind resource assessment for a given geographical location. In Paper 4, a simplified model of a wind-fuel cell system is discussed. A concept of fuel cell based grid connected power generation system is presented in Paper 5. Various simulation results of the wind energy converter model along with its fuzzy control system are presented in Paper 8. In Paper 9 (workshop presentation), several contemporary issues of stand-alone power generation for remote telecommunication sites are overviewed.

6.3 Conclusions

An off-grid residential house designed with energy saving measures might typically consume around 25 kWh/d with a peak demand of 4.73 kW. In St. John's, Newfoundland, wind resource is more promising compared to other renewable alternatives. At present, a wind-diesel-battery system is the most cost-effective solution for stand-alone power generation in Newfoundland. With an expected decrease in fuel cell cost (about 15 % of the present market price), a wind-fuel cell system might prove to be a superior solution. The essential components of a wind-hydrogen hybrid energy system delivering the aforementioned remote home are: one 7.5 kW wind turbine, one 3.5 kW fuel cell, 3.5 kW power converters, one 7.5 kW electrolyzer and one 10 kg Hydrogen tank. The cost of energy from such a system would be around \$0.427/kWh and the total capital cost would be \$29,475.

A set of mathematical models for these components has been formulated using fundamental empirical and physical relationships. In order to emulate a more practical system, emphasis has been given on considering off-the-shelf technologies and

experimental prototypes. A mechanical sensorless fuzzy logic controller for the wind turbine has been proposed. However, it requires an estimator to determine the rotor torque at any instance. Dynamic models of fuel cell and electrolyzer were also developed. Simplified steady-state models of power converters such as buck-boost, boost and PWM inverters were used in interfacing the variable DC output of the power sources with a fixed R-L type AC load.

Separate PID type controllers were used for the fuel cell air flow system, electrolyzer current regulator, wind turbine buck-boost converter, fuel cell boost converter and load PWM inverter. A power flow controller was used that initiates the operation of the fuel cell or electrolyzer. Simulation with MATLAB-Simulink® indicated that the wind turbine works within the rated limits for a wide range of wind variations. At around rated wind speed (13.5 m.s^{-1}), most of the power is delivered to the load from the wind energy converter. Any surplus energy is diverted to the electrolyzer and is used for hydrogen production. With very low or extreme high winds, most of the power is provided by the fuel cell system. Transient durations in the wind energy system, fuel cell and power electronic converters were found to be less than 2.2 s, 0.5 s and 0.15 s, respectively. The AC voltage at the output terminal indicated a maximum overshoot of 25 %, providing scope for further improvement in inverter/filter modeling.

In general, the performance of the wind-fuel cell hybrid energy system appeared to be satisfactory and within allowable limits. Further advancements in small wind turbine and hydrogen energy technology would allow a more flexible, durable and efficient design.

6.4 Further Work

Thermal dynamics play an important role in fuel cell and electrolyzer performance. Models of these devices have been developed with considerations for such analysis. However, a computer-aided simulation for 30 to 350 minutes is required for generating a complete response that would show significant variations in temperature.

The software tool used in this work appeared unsuitable for handling such long simulation times and consequently failed to converge. Therefore, only constant temperature simulations have been carried out and attempts for hourly/yearly simulation are left for a possible future work.

Power electronic converters were modeled with steady-state equations and a complete formulation of the electrolyzer DC-DC converter were not presented. Various auxiliary devices in the fuel cell and electrolyzer system (such as, filter, storage tank, compressor, separator, and purifier) were not modeled and are left for further investigation.

Development of a comprehensive but simplified model would allow a better understanding of long term performance of the wind-fuel cell system, ranging for months to years.

The use of a stand-by-battery might appear indispensable for pragmatic reasons such as, fuel cell start up, and electrolyzer corrosion prevention. Additionally, the overall efficiency of the system could be increased significantly by reusing the exhaust heat from these devices. Further research could aim at investigating these important issues.

A complete and comprehensive understanding of the reliability, performance and economics of a hybrid energy system could only be developed by experimentations. Since the cost of the system being considered is very high and associated logistical needs are huge, the modeling and simulation work presented in this thesis could be considered as an alternative scheme.

References

- [1] H. Graßl, J. Kokott, M. Kulesa, J. Luther, F. Nuscheler, R. Sauerborn, H., J. Schellnhuber, R. Schubert, E.-D. Schulze, “World in Transition-Towards Sustainable Energy Systems”, German Advisory Council on Global Change (WBGU), Secretariat Reichpietschufer 60-62, 8th Floor, D-10785 Berlin, Germany. 2003. ISBN: 1-84407-882-9.
URL: http://www.wbgu.de/wbgu_jg2003_engl.html/

- [2] Mark Malloch Brown, Nitin Desai, Gerald Doucet, “Energy and The Challenge of Sustainability”, World Energy Assessment, United Nations Development Programme (UNDP), Bureau for Development Policy, One United Nations Plaza, New York, NY 10017, 2000.
URL: <http://www.undp.org/seed/eap/activities/wea/drafts-frame.html/>

- [3] The Conference Board of Canada, “Renewable Energy in Canada”, Renewable portfolio standards (RPS) report to the Council of Energy Ministers (CEM), September 24, 2003. URL: <http://www.conferenceboard.ca/>

- [4] Martin Tampier, “Green Power Policies: A Look Across Borders”, Pollution Probe, 625 Church Street, Suite 402, Toronto, Ontario, Canada, M4Y 2G1, November 2002. URL: <http://www.pollutionprobe.org/Reports/greenpower.pdf>

- [5] American Wind Energy Association (AWEA), “Global Wind Energy Market Report”, AWEA, 122 C Street, NW, Suite 380, Washington, DC 20001. March 2004. URL: <http://www.awea.org/pubs/complimentary.html>
- [6] American Wind Energy Association (AWEA), “ROADMAP: A 20-year industry plan for small wind turbine technology”, AWEA, 122 C Street, NW, Suite 380, Washington, DC 20001. June 2002.
URL: <http://www.awea.org/smallwind/documents/31958.pdf>
- [7] Geoff Dutton, “Hydrogen Energy Technology”, Tyndall Working Paper No. 17, Energy Research Unit (ERU), CLRC Rutherford Appleton Laboratory, Chilton, Didcot, Oxon, OX11 0QX, April 2002.
- [8] United States Department of Energy (USDoE), “Hydrogen Posture Plan: An Integrated Research, Development, and Demonstration Plan”, Office of Energy Efficiency and Renewable Energy (EERE), Mail Stop EE-1, Washington, DC 20585, February 2004. URL: <http://www.eere.energy.gov/>
- [9] Jonathan W. Hurwitch, “DER Hybrid Systems Assessment Team: Findings and Recommendations”, 1st DOE DER Conference and Peer Review, Washington, DC, November 30, 2001.
URL: http://www.eere.energy.gov/de/pdfs/der_conf_01/hurwitch.pdf
- [10] K. Agbossou, R. Chahine, J. Hamelin, F. Laurencelle, A. Anouar, J. M. St. Arnaud, T. K. Bose, “Renewable Energy Systems Based on Hydrogen for Remote Applications”, Journal of Power Sources, Vol. 96, Issue 1, Page 168-172, 1 June 2001.

- [11] Kodjo Agbossou, Mohan Lal Kolhe, Jean Hamelin, Étienne Bernier, Tapan K. Bose, “Electrolytic Hydrogen Based Renewable Energy System with Oxygen Recovery and Re-Utilization”, *Renewable Energy*, Vol. 29, Issue 8, Page 1305-1318, July 2004.
- [12] M. Kolhe, K. Agbossou, J. Hamelin, T. K. Bose, “Analytical Model for Predicting the Performance of Photovoltaic Array Coupled with a Wind Turbine in a Stand-Alone Renewable Energy System Based on Hydrogen”, *Renewable Energy*, Vol. 28, Issue 5, Page 727-742, April 2003.
- [13] Kodjo Agbossou, Mohan Kolhe, Tapan K. Bose, “Operating Experience of Integrated Wind-Photovoltaic-Hydrogen Energy System”, *SESCI 2003*, Queen’s University, Kingston, Ontario, Canada, August 18-20, 2003.
- [14] A. G. Dutton, J. A. M. Bleijs, H. Dienhart, M. Falchetta, W. Hug, D. Prischich, A. J. Ruddell, “Experience in the Design, Sizing, Economics, and Implementation of Autonomous Wind-Powered Hydrogen Production Systems”, *International Journal of Hydrogen Energy*, Vol. 25, Issue 8, Page 705-722, August 1, 2000.
- [15] Wen-Jei Yang, Orhan Aydin, “Wind Energy-Hydrogen Storage Hybrid Power Generation”, *International Journal of Energy Research*, Vol. 25, Page 449-463, 2001.
- [16] Lars Nesje Grimsmo, Magnus Korpaas, Terje Gjengedal, Steffen Møller-Holst, “A Study of a Stand-alone Wind and Hydrogen System”, *Nordic Wind Power Conference*, Chalmers University of Technology, Sweden. March 2004.
- [17] Simonetta Palmas, Alfonso Damiano, Gianluca Gatto, Ignazio Marongiu, Anna, Maria Polcaro, Mariangela Usai, and Annalisa Vacca, “Modelling of Alkaline

Electrolysers for Wind-Powered System Optimisation”, H₂-age: When, Where, Why; Italian Association of Chemical Engineering, Pisa, May 16-19, 2004.

- [18] Lee Jay Fingersh, “Overview of Wind-H₂ Configuration & Control Model (WindSTORM)”, National Renewable Energy Laboratory (NREL), 617 Cole Boulevard, Golden, Colorado 80401-3393, September 9, 2003.

- [19] Øystein Ulleberg, “Stand-alone Power Systems for the Future: Optimal Design, Operation & Control of Solar-Hydrogen Energy System”, Ph.D. Dissertation, Norwegian University of Science and Technology, Trondheim, Norway. December 1998.

- [20] Lars Hedström, “Modelling and Evaluation of the Solar-Hydrogen-Fuel-Cell System in GlashusEtt”, Master's Theses, Chemical Engineering and Technology, Division of Energy Processes, Royal Institute of Technology, Stockholm, Sweden. 2003.

- [21] Wallmark, C., Alvfors, P., “Technical Design and Economic Evaluation of a Stand-alone PEFC System for Buildings in Sweden”, Journal of Power Sources, Vol. 118, Issues 1-2, Page 358-366, 2003.

- [22] Pierre Hollmuller, Jean-Marc Joubert, Bernard Lachal, Klaus Yvon, “Evaluation of a 5 KWp Photovoltaic Hydrogen Production and Storage Installation for a Residential Home in Switzerland”, International Journal of Hydrogen Energy, Vol. 25, Issue 2, Page 97-109, February 2000.

- [23] M. Santarelli, S. Macagno, “Hydrogen as an Energy Carrier in Stand-alone Applications Based on PV and PV–Micro-Hydro Systems”, Energy, Vol. 29, Issue 8, Page 1159-1182, June 2004.

- [24] Torres, L.A., Rodriguez, F.J., Sebastian, P.J., "Simulation of a Solar-Hydrogen-Fuel Cell System: Results for Different Locations in Mexico", International Journal of Hydrogen Energy, Vol. 23, Issue 11, Page 1005-1009, 1998.
- [25] J. Cotrell, W. Pratt, "Modeling the Feasibility of Using Fuel Cells and Hydrogen Internal Combustion Engines in Remote Renewable Energy Systems", National Renewable Energy Laboratory (NREL), 617 Cole Boulevard, Golden, Colorado 80401-3393, September 2003. URL: <http://www.osti.gov/bridge>
- [26] Vosen, S.R., Keller, J.O., "Hybrid Energy Storage Systems for Stand-alone Electric Power Systems: Optimization of System Performance and Cost Through Control Strategies", International Journal of Hydrogen Energy, Vol. 24, Issue 12, Page 1139-1156, 1999.
- [27] Bonanno, F., Consoli, A., Raciti, A., Morgana, B., Nocera, U., "Transient Analysis of Integrated Diesel-Wind-Photovoltaic Generation Systems", IEEE Transactions on Energy Conversion, Vol. 14, No. 2, June 1999.
- [28] Senjyu, T., Nakaji, T., Uezato, K., Funabashi, T., "A Hybrid Power System Using Alternative Energy Facilities in Isolated Island", IEEE/PES Transmission and Distribution Conference and Exhibition 2002, Asia Pacific, Vol. 2, 6-10 Oct. 2002.
- [29] HOMER V.2; National Renewable Energy Laboratory (NREL), 617 Cole Boulevard, Golden, Colorado 80401-3393. URL: <http://www.nrel.gov/homer/>
- [30] MATLAB-Simulink is a product of The MathWorks, 3 Apple Hill Drive, Natick, MA 01760-2098, USA. URL: <http://www.mathworks.com>

- [31] M. J. Khan, M. T. Iqbal, “Wind Energy Resource Map of Newfoundland”, *Renewable Energy*, Vol. 29, Issue 8, Page 1211-1419, July 2004.
- [32] M. Tariq Iqbal, “Energy Consumption Analysis of a Typical House in St. John’s, Newfoundland”, NECEC 2003, St. John’s, NL, November 12, 2003.
- [33] Natural Resources Canada (NRCan), “Photovoltaic Systems: A Buyer’s Guide”, Renewable and Electrical Energy Division, 580 Booth Street, 17th Floor, Ottawa, ON K1A 0E4, ISBN 0-662-31120-5.
- [34] Natural Resources Canada (NRCan), “RETScreen™ Database - Canadian Remote Communities Introduction”, RETScreen Customer Support, 1615 Lionel-Boulet, Blvd., P.O. Box 4800, Varennes, QC, CANADA J3X 1S6.
URL: <http://cetc-varennes.nrcan.gc.ca/e/412/retscreen/>
- [35] Natural Resources Canada (NRCan), “Case Study: Photovoltaic Project – Telecom (Genset/Battery), Newfoundland, Canada”, RETScreen Customer Support, 1615 Lionel-Boulet, Blvd., P.O. Box 4800, Varennes, QC, CANADA J3X 1S6. URL: <http://www.etscreen.net/>
- [36] Canada Mortgage and Housing Corporation (CMHC), “Energy Use Patterns in Off-Grid Houses”, Technical Series 01-103, CMHC, 700 Montreal Road, Ottawa, Ontario, K1A 0P7.
URL: <http://www.cmhc-schl.gc.ca/publications/en/rh-pr/tech/01-103-e.html>
- [37] Natural Resources Canada (NRCan), “Energy efficient new housing/R2000 homes”, Office of Energy Efficiency, Ottawa, ON.
URL: http://energy-publications.nrcan.gc.ca/index_e.cfm

- [38] Newfoundland and Labrador Hydro, Hydro Place, Columbus Drive, P.O. Box 12400, St. John's, NL A1B 4K7. URL: <http://www.nlh.nf.ca/Index.htm>
- [39] Canadian Climate Normals, Canadian Climate and Water Information, Environment Canada, 45 Alderney Drive, Dartmouth, Nova Scotia B2Y 2N6. URL: http://www.msc-smc.ec.gc.ca/climate/climate_normals_1990/
- [40] Homestead Technology, 822 NW Murray Blvd. #127, Portland, Oregon 97229. URL: <http://www.homesteadtechnology.com/>
- [41] Siemens Solar Panels, BULLNET, Unit D, Henfield Business Park, Henfield, Sussex, BN5 9SL. URL: <http://www.siemenssolar.co.uk/index.htm>
- [42] Bergey Wind Power Co., 2001 Priestley Ave., Norman, Ok 73069 USA, URL: <http://www.bergey.com>
- [43] Ballard Power Systems Inc, 4343 North Fraser Way, Burnaby, BC V5J 5J9, Canada, URL: <http://www.ballard.com/>
- [44] Plug Power Inc., 968 Albany-Shaker Road, Latham, New York 12110, URL: <http://www.plugpower.com/>
- [45] United States Department of Energy (US DoE), "Fuel Cell Report to Congress", ESECS EE-1973. Page 39, February 2003. URL: www.eere.energy.gov/hydrogenandfuelcells/pdfs/fc_report_congress_feb2003.pdf
- [46] Proton Energy Systems Inc., 10 Technology Drive, Wallingford CT 06492. URL: <http://www.protonenergy.com/>

- [47] Surrette Battery Engineering, P.O. Box 2020, 1 Station Road, Springhill, Nova Scotia, B0M 1X0, Canada. URL: <http://www.surrette.com/home.htm>
- [48] Patel M. R., "Wind and Solar Power Systems", CRC press LLC, Florida, USA. ISBN 0-8493-1605-7, 2000.
- [49] Pasqualetti M.J., Gipe P., Righter R.W.; "Wind Power in View - Energy Landscapes in a Crowded World", Academic Press, California, USA. ISBN 0125463340. February 2002.
- [50] Manwell J.F., McGowan J.G., Rogers A.L.; "Wind Energy Explained - Theory, Design and Applications", John Wiley & Sons Ltd, West Sussex, England. ISBN: 0-471-49972-2. June 2002.
- [51] T. Burton, D. Sharpe, N. Jenkins, and E. Bossanyi, "Wind Energy Handbook", John Wiley & Sons Ltd. ISBN 0-471-48997-2, 2001.
- [52] Mick Sagrillo, "Apples & Oranges '02: Choosing a Home-Sized Wind Generator", Home Power #90, Home Power magazine, August / September 2002. URL: <http://www.homepower.com>
- [53] Dunlite Wind Turbines, Victoria, Australia.
URL: <http://www3.telus.net/pearen/Reference/windmachines.htm>
- [54] C. Nichita, D. Luca , B. Dakyo, E. Ceanga, N. A. Cutululis, "Modelling Non-Stationary Wind Speed for Renewable Energy Systems Control", The annals of "Dunarea de Jos", University of Galati, Fascicle III. ISSN 1221-454X, 2000.

- [55] Harri Vihriälä, "Control of Variable Speed Wind Turbines", PhD. Thesis, Tampere University of Technology, Finland, June 2002.
- [56] Fitzgerald, A.E., Kingsley, Charles, Jr., Umans, Stephen D., "Electric Machinery", McGraw-Hill, 6th edition. ISBN 0071121935, 2002.
- [57] Ventzislav Valtchev, Alex Van den Bossche, Jozef Ghijselen, Jan Melkebeek, "Autonomous Renewable Energy Conversion System", Renewable Energy, Vol. 19, Issues 1-2, Page 259-275, January 2, 2000.
- [58] Marcelo Godoy Simões, Bimal K. Bose, Ronald J. Spiegel, "Design and Performance Evaluation of a Fuzzy-Logic-Based Variable-Speed Wind Generation System", IEEE Transactions on Industry Applications, Vol. 33, No. 4, July/August 1997.
- [59] Mohamed A., Eskander N., Ghale F., "Fuzzy Logic Based Maximum Power Tracing of a Wind Energy System", Renewable Energy, Vol. 23, No. 2, Page 235-245, 2001.
- [60] Chedid R., Mrad F. Basma M., "Intelligent control of a class of wind energy conversion systems", IEEE transactions of Energy Conversion; Vol. 14, Issue 4, Page 1597-1604, December 1999.
- [61] Delarue P., Bouscayrol A., Tounzi A., Guillaud X., Lancigu G., "Modeling, control and simulation of an overall wind energy conversion system", Renewable Energy, Vol. 28, No. 8, Page 1169-1185, July 2003.
- [62] M. T. Iqbal, A. H. Coonick, L. L. Freris, "Dynamic Control of a Stand-alone Wind Turbine", BWEA-16 annual conference, 1994.

- [63] A. Tomlinson, J. Quaiocoe, R. Gosine, M. Hinchey, N. Bose, "Application of a Static VAR compensator to an Autonomous Wind-Diesel System", *Wind Engineering*, Vol. 22, No. 3, Page 131-142, 1998.
- [64] L. A. Zadeh, "Fuzzy Sets", *Information and Control*, Vol. 8., Academic Press, New York, Page 338-353, 1965.
- [65] René Jager, "Fuzzy Logic in Control", Ph.D. Thesis, Delft University of Technology, Department of Electrical Engineering, Control laboratory, Delft, The Netherlands. ISBN 90-9008318-9, 1995.
URL: <http://users.pandora.be/jati/renej/phd/rjphd.pdf>
- [66] National Energy Technology Laboratory (NETL), "Fuel Cell Handbook (Sixth Edition)", DOE/NETL-2002/1179, November 2002.
- [67] J. Larminie, A Dicks, "Fuel Cell Systems Explained", John Wiley & Sons Ltd, West Sussex, England. ISBN 0-471-49026-1, 2001.
- [68] Amphlett J.C., Baumert R.M., Mann R.F., Peppley B.A., Roberge P.R., "Performance Modeling of the Ballard Mark IV Solid Polymer Electrolyte Fuel Cell (I-Mechanistic Model Development)", *Journal of the Electrochemical Society*, Vol. 142, No. 1, August 1995.
- [69] Amphlett J.C., Baumert R.M., Mann R.F., Peppley B.A., Roberge P.R., "Performance Modeling of the Ballard Mark IV Solid Polymer Electrolyte Fuel Cell (II-Empirical Model Development)", *Journal of the Electrochemical Society*, Vol. 142, No. 1, August 1995.

- [70] Kim J., Lee S., Srinivasan S., "Modeling of Proton Exchange Membrane Fuel Cell performance with an Empirical Equation", *Journal of the Electrochemical Society*, Vol. 142, No. 8, August 1995.
- [71] Marr C., Li X., "An Engineering Model of Proton Exchange Membrane Fuel Cell Performance", Springer-Verlag, ARI (1998) 50, Page 190-200, 1998.
- [72] Ceraolo M., Miulli C., Pozio A., "Modeling Static and Dynamic Behaviour of Proton Exchange Membrane Fuel Cells on the Basis of Electro-chemical Description", *Journal of Power Sources*, Vol. 113, Page: 131-144, 2003.
- [73] Wagner N., "Characterization of Membrane Electrode Assemblies in Polymer Electrolyte Fuel Cells Using a.c. Impedance Spectroscopy", *Journal of Applied Electrochemistry*, Vol. 32, Page: 589-563, 2002.
- [74] Wohr M., Bolwin K., Schnurnberger W., Fischer M., Neubrand W., Eig G., "Dynamic Modelling and Simulation of a Polymer Membrane Fuel Cell Including Mass Transport Limitations", *International Journal of Hydrogen Energy*, Vol. 23, No. 3, Page 213-218, 1998.
- [75] Ronald F. Mann, John C. Amphlett, Michael A. I. Hooper, Heidi M. Jensen, Brant A. Peppley, Pierre R. Roberge, "Development and Application of a Generalised Steady-state Electrochemical Model for a PEM Fuel Cell", *Journal of Power Sources*, Vol. 86, Issues 1-2, Page 173-180, March 2000.
- [76] J. C. Amphlett, R. F. Mann, B. A. Peppley, P. R. Roberge, A. Rodrigues, "A Model Predicting Transient Responses of Proton Exchange Membrane Fuel Cells", *Journal of Power Sources*, Vol. 61, Issue 1-2, Page 183-188, July-Aug 1996.

- [77] John C. Amphlett, Erick H. de Oliveira, Ronald F. Mann, Pierre R. Roberge, Aida Rodrigues, John P. Salvador, “Dynamic Interaction of a Proton Exchange Membrane Fuel Cell and a Lead-Acid Battery”, *Journal of Power Sources*, Vol. 65, Issues 1-2, Page 173 -178, March 4, 1997.
- [78] Hamelin, J., Agbossou, K., Laperriere, A., “Dynamic Behavior of a PEM Fuel Cell, Stack for Stationary Applications”, *International Journal of Hydrogen Energy*, Vol. 26, No.6, Page 625-629, June 2001.
- [79] F. Laurencelle, R. Chahine, K. Agbossou, “Characterization of a Ballard MK5-E PEM Fuel Cell Stack”, *Fuel Cells-from Fundamentals to Systems*, Vol. 1, No. 1., 2001.
- [80] Gemmen R.S, “Analysis for the Effect of Inverter Ripple Current on Fuel Cell Operating Conditions”, 2001 ASME International Mechanical Engineering Congress and Expositions, NY, November 11-16, 2001.
- [81] Farmouri, P.; Gemmen, R.S., “Electrochemical Circuit Model of a PEM Fuel Cell”, 2003 IEEE Power Engineering Society General Meeting, Vol. 3, Page 1436 – 1440, July 13-17, 2003.
- [82] Srinivasan, P., Sneckenberger, J.E., Feliachi, A., “Dynamic Heat Transfer Model Analysis of the Power Generation Characteristics for a Proton Exchange Membrane Fuel Cell Stack”, *Proceedings of the 35th Southeastern Symposium on System Theory*, Page 252 – 258, March 16-18, 2003.
- [83] Correa, J.M., Farret, F.A., Canha, L.N., “An Analysis of the Dynamic Performance of Proton Exchange Membrane Fuel Cells Using an Electrochemical

Model”, IECON '01, The 27th Annual Conference of the IEEE Industrial Electronics Society, Vol. 1, Page 141 – 146, Nov. 29-Dec. 2, 2001.

- [84] Lu-Ying Chiu, Diong, B.M., “An Improved Small-Signal Model of the Dynamic Behavior of PEM Fuel Cells”, The 38th IAS Annual Meeting, Industry Applications Conference-2003, Vol. 2, Page 709 – 715, Oct 12-16, 2003.
- [85] Yerramalla, S., Davari, A., Feliachi, A., “Dynamic Modeling and Analysis of Polymer Electrolyte Fuel Cell”, 2002 IEEE Power Engineering Society Summer Meeting, Vol. 1, Page 82 – 86, July 21-25, 2002.
- [86] Boettner D.D., Paganelli G., Guezennec Y.G., Rizzoni G., Moran M.J., “Proton Exchange Membrane Fuel Cell System Model for Automotive Vehicle Simulation and Control”, Transactions of the ASME, Vol. 124, March 2002.
- [87] Macdonald J.R., “Impedance Spectroscopy-Emphasizing Solid Materials and Systems”, John Wiley & Sons Inc, NY, USA. ISBN 0471-83122-0, 1987.
- [88] Øystein Ulleberg, “Modeling of Advanced Alkaline Electrolyzers: a System Simulation Approach”, International Journal of Hydrogen Energy, Vol. 28, Page 21-33, 2003.
- [89] Rodatz, P., Paganelli, G., Guzzella, L., “Optimizing Air Supply Control of a PEM Fuel Cell System”, American Control Conference, 2003, Vol. 3, Page 2043-2048, June 4-6, 2003.
- [90] Pukrushpan. J. T., Stefanopoulou. A.G., Peng. H., “Modeling and Control for PEM Fuel Cell Stack System”, American Control Conference, Vol. 4, May 8-10, 2002.

- [91] Pukrushpan. J. T., Stefanopoulou. A.G., Peng. H., "Simulation and Analysis of Transient Fuel Cell System Performance Based on a Dynamic Reactant Flow Model", 2002 ASME International Mechanical Engineering Congress and Expositions, New Orleans, Louisiana, USA. November 17-22, 2002.
- [92] Ballard Power Systems Inc., 4343 North Fraser Way, Burnaby, BC V5J 5J9, Canada. URL: <http://www.ballard.com/>
- [93] Incropera, F. P., Dewitt D. P., "Fundamentals of Heat and Mass Transfer", 3rd edition, Wiley. ISBN 0471612464, 1990.
- [94] Kuo B. C., "Automatic Control Systems", 7th edition, Prentice Hall Inc. ISBN 8120309685,1995.
- [95] M. J. Khan, M. T. Iqbal, "Modeling and Analysis of Electrochemical, Thermal and Reactant Flow Dynamics for a PEM Fuel Cell System", submitted for publication in the Fuel Cells, Wiley, May 2004.
- [96] Frano Barbir, "The Potential for Electrolyzers in Renewable Energy Based Stand-alone Power Systems", H-SAPS Workshop, EHEC 2003, European Energy Conference, Grenoble, France, September 4, 2003.
- [97] Matt Kauffman, "Electrolytic Hydrogen Production", USDoE, Office of Energy Efficiency and Renewable Energy (EERE), Mail Stop EE-1, Washington, DC 20585, February 2004. URL: <http://www.eere.energy.gov/>

- [98] Johanna Ivy, “Summary of Electrolytic Hydrogen Production: Milestone Completion Report”, National Renewable Energy Laboratory (NREL), 1617 Cole Boulevard, Golden, Colorado 80401-3393. URL: [http:// www.nrel.gov/](http://www.nrel.gov/)
- [99] Robert H. Williams, “Alternative Technologies and Strategies for Hydrogen Production”, Princeton Environmental Institute, Princeton University Workshop on Future Energy Issues – Future Energy Resources, National Defense University, Washington, DC 20329-5066, May 9, 2003.
- [100] B.K. Bose, “Energy, Environment, and Advances in Power Electronics”, IEEE Transactions on Power Electronics, Vol. 15, No. 4, July 2000.
- [101] Mohan N., Undeland T. M., Robbins W.P., “Power Electronics: Converters, Applications, and Design”, John Wiley & Sons Inc., Canada. ISBN 0-471-58408-8, 1989.
- [102] R. Naik, N. Moham, M. Rogers, A. Bulawka, “A Novel Grid Interface, Optimized for Utility-Scale Applications of Photovoltaic, Wind-electric, and Fuel-Cell Systems”, IEEE Transactions of Power Delivery, Vol. 10, No. 4, October 1995.
- [103] L.E. Lesster, “Fuel cell power electronics: Managing a variable-voltage DC source in a fixed-voltage AC world”, SatCon Technology Center, 161, First Street, Cambridge, MA 02142, USA. URL: <http://www.satcon.com/>

Appendix A

MATLAB-Simulink[®] Subsystem Blocks

In this Appendix, MATLAB-Simulink[®] block diagrams for the subsystems (SS) described in Chapter 4 are given. Most of the blocks and parameters are symbolized with similar notations as found in Chapter 3. Parameter units are indicated mostly at the subsystem inputs and outputs.

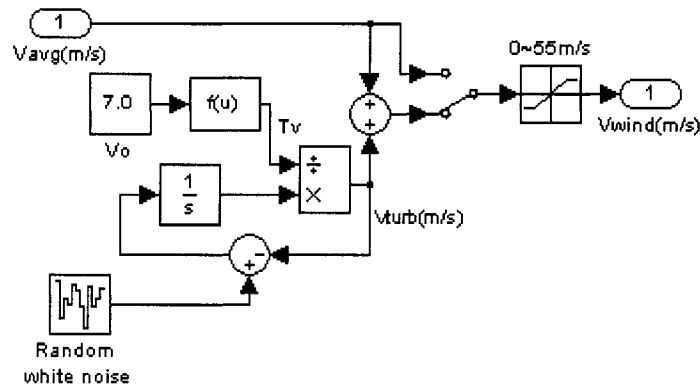


Figure A.1: Subsystem 'SS: Wind Field'

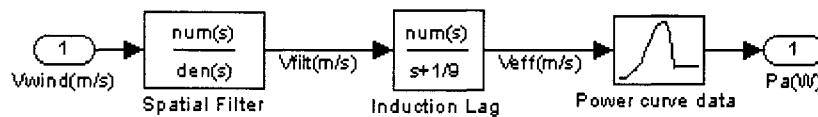


Figure A.2: Subsystem 'SS: Aerodynamics'

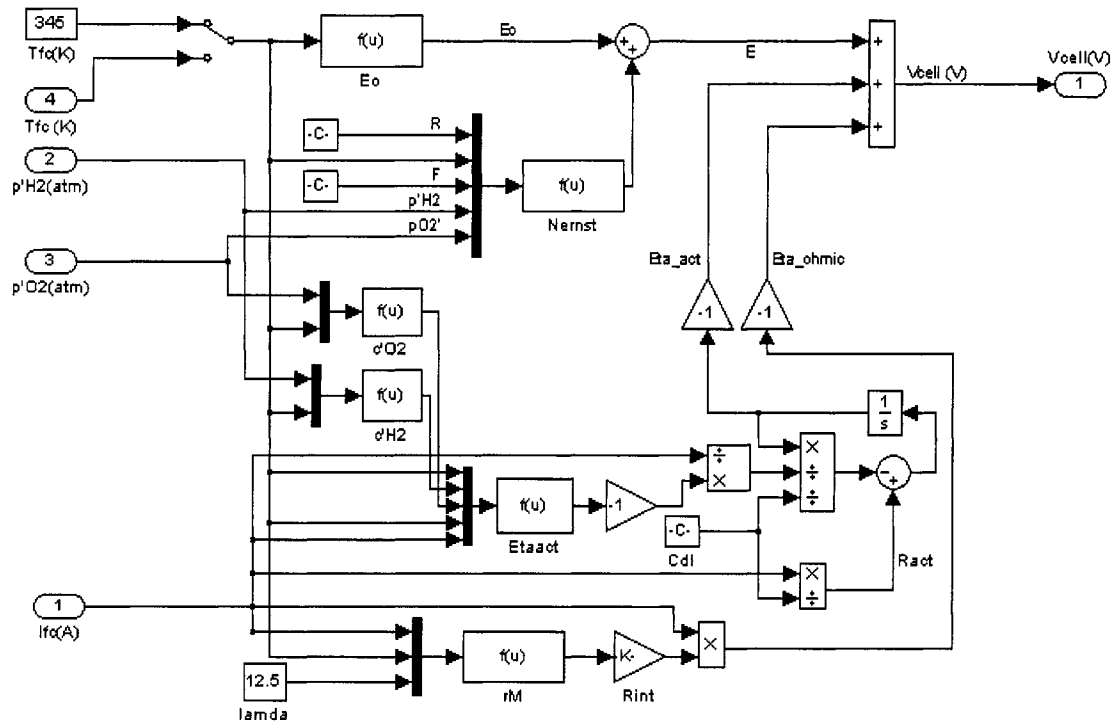


Figure A.5: Subsystem 'SS: Fuel Cell'

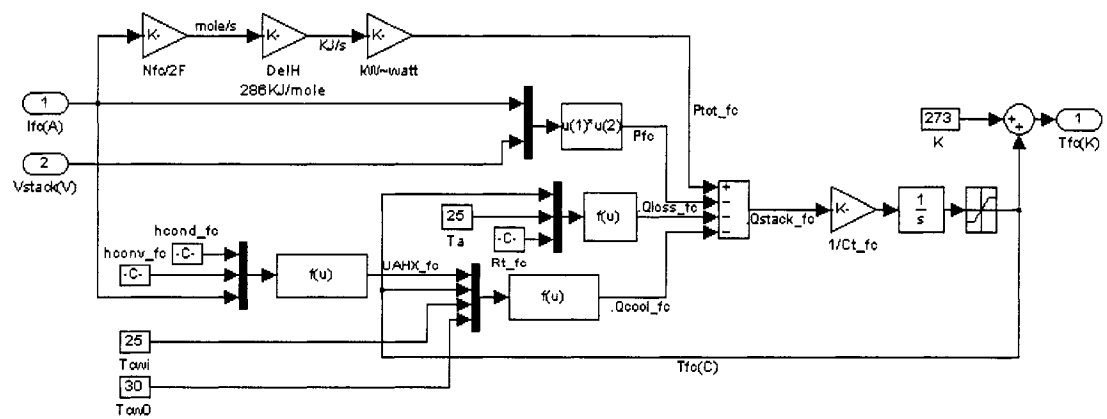


Figure A.6: Subsystem 'SS: Fuel Cell Energy Balance'

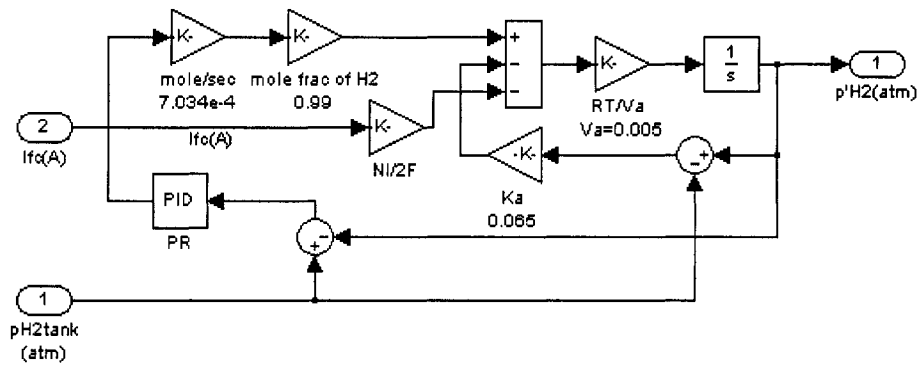


Figure A.7: Subsystem 'SS: Anode H2 Flow'

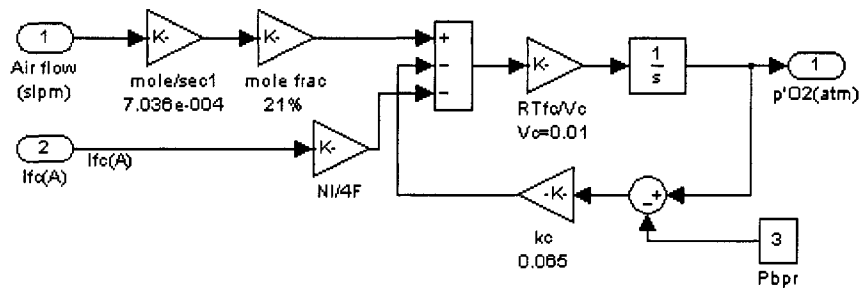


Figure A.8: Subsystem 'SS: Cathode O2 Flow'

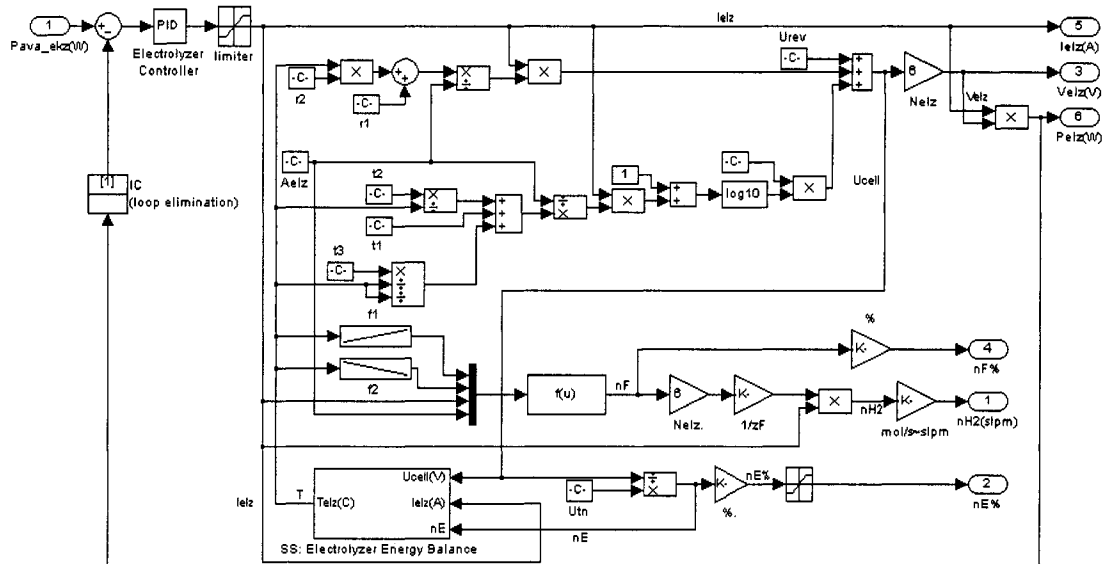


Figure A.9: Subsystem 'SS: Electrolyzer'

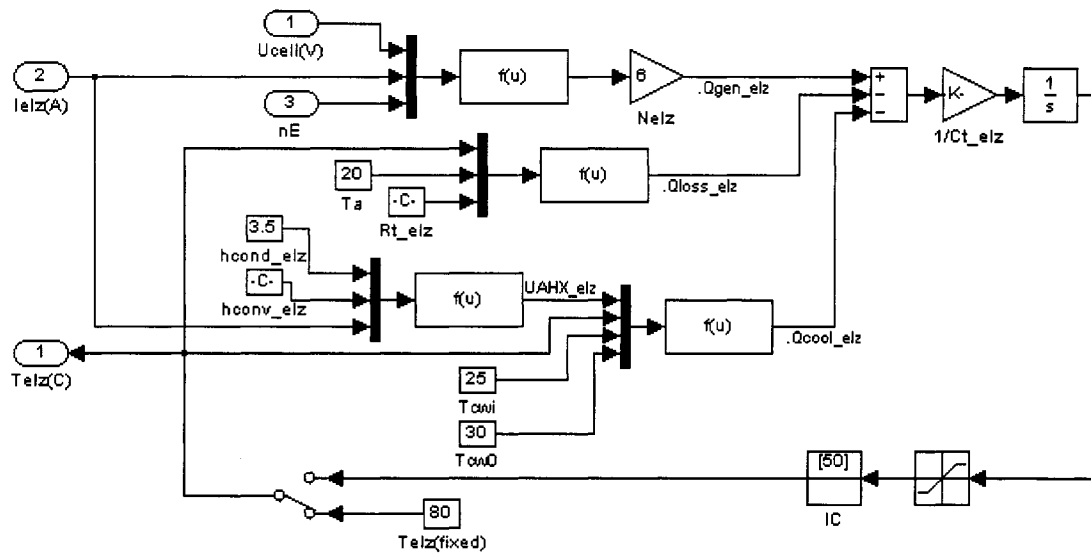


Figure A.10: Subsystem 'SS: Electrolyzer Energy Balance'

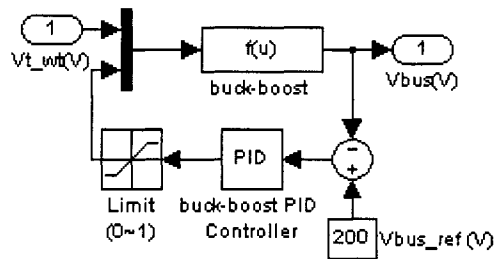


Figure A.11: Subsystem 'SS: Buck-boost'

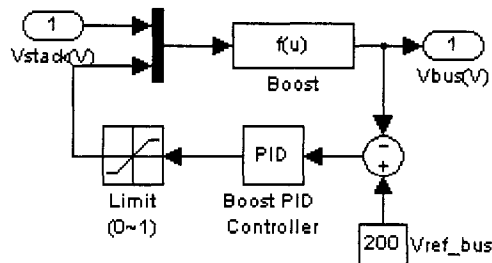


Figure A.12: Subsystem 'SS: Boost'

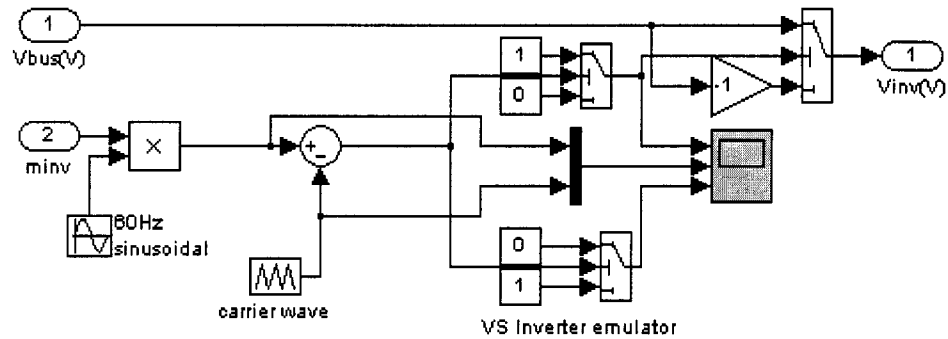


Figure A.13: Subsystem 'SS: PWM Inverter'

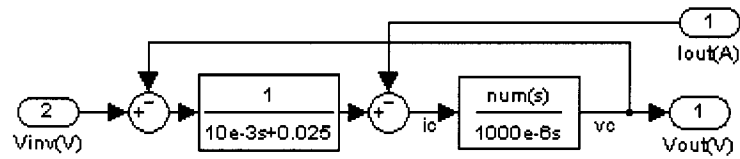


Figure A.14: Subsystem 'SS: LC Filter'

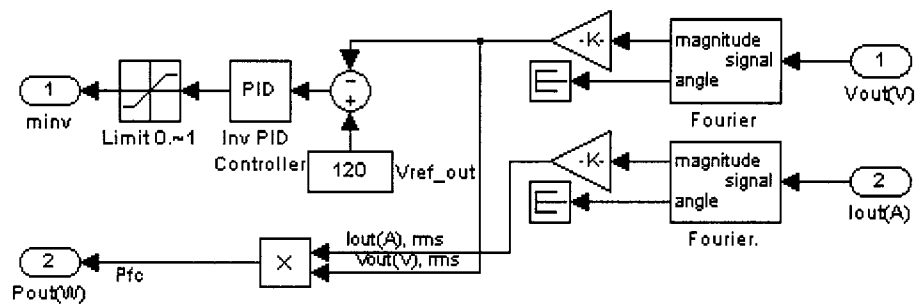


Figure A.15: Subsystem 'SS: Inverter Controller'

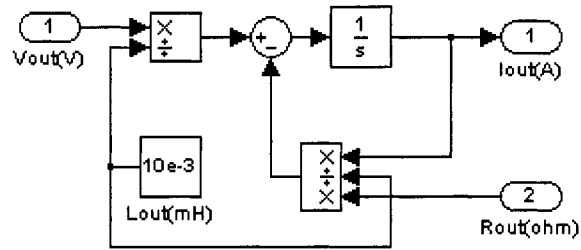


Figure A.16: Subsystem 'SS: R-L Load'

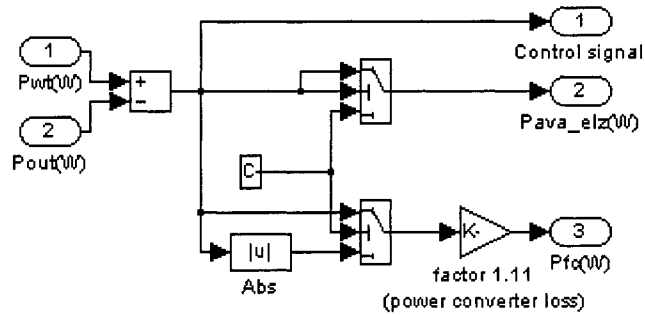


Figure A.17: Subsystem 'SS: Power Controller'

Appendix B

List of Research Papers Based on this Research

In this Appendix, a list of journal/conference papers that originated during the course of this work is given. There is a significant level of overlap between the contents of this thesis and some of the articles. However, a greater understanding of the proposed models and their validity could be gained from these publications. The author is the lead investigator in most of the works. The submitted/reviewed papers are expected to appear in the corresponding journals in due time.

(Journals)

Paper 1

M. J. Khan, M. T. Iqbal, "Pre-feasibility Study of Stand-alone Hybrid Energy Systems for Applications in Newfoundland", Submitted for publication in *Renewable Energy*, May 2004.

Paper 2

M. J. Khan, M. T. Iqbal, "Modeling and Analysis of Electrochemical, Thermal and Reactant Flow Dynamics for a PEM Fuel Cell System", submitted for publication in *Fuel Cells-from Fundamentals to Systems*, Wiley, May 2004.

Paper 3

P. Jewer, M. T. Iqbal, M. J. Khan, “Wind Energy Resource Map of Labrador”, Submitted for publication in *Renewable Energy*, April 2004.

Paper 4

M. J. Khan, M. T. Iqbal, “Dynamic Modeling and Simulation of a Small Wind Fuel Cell Hybrid Energy System” to appear in *Renewable Energy*.

Paper 5

M. J. Khan, M. T. Iqbal, “Dynamic Modeling and Simulation of a Fuel Cell Generator”, invited paper to appear in *Fuel Cells-from Fundamentals to Systems*, Wiley.

Paper 6

M. J. Khan, M. T. Iqbal, “Wind Energy Resource Map of Newfoundland”, *Renewable Energy*, Vol. 29, Issue 8, July 2004.

Paper 7

M. J. Khan, M. T. Iqbal and S. Mahboob, “A Wind Map of Bangladesh”, *Renewable Energy*, Vol. 29, Issue 5, April 2004.

(Conference and Workshop Presentations)

Paper 8

M. J. Khan, M. T. Iqbal, “Dynamic Modeling, Simulation and Control of a Small Wind Energy Conversion System”, presented at ICME, December 26, 2003 Dhaka, Bangladesh.

Paper 9

M. J. Khan, M. T. Iqbal, “Stand-alone Power Generation: an Essential Part of Remote Internet Communications” presented at IWIER January 1, 2004 Dhaka, Bangladesh.

Paper 10

M. J. Khan, M. T. Iqbal, “Simulation and Performance Analysis of a Grid Connected Fuel Cell System”, presented at IEEE 13th, NECEC conference, St. John’s NL, 2003.

Paper 11

M. J. Khan, M. T. Iqbal, “Wind Energy Resource Map of Newfoundland”, presented at IEEE 13th, NECEC conference, St. John’s NL, 2003.

Paper 12

M. J. Khan, M. T. Iqbal, ‘Dynamic Modeling and Simulation of a Small Wind Fuel Cell Hybrid Energy System,’ Presented at SESCOI 2003, Queen’s University, Kingston, Ontario, Canada, August 18 - 20, 2003.



